DESIGN OF A MODULAR ORTHOPEDIC IMPLANT

A THESIS SUBMITTED TO
THE GRADUATE SCHOOL OF NATURAL AND APPLIED SCIENCES
OF
MIDDLE EAST TECHNICAL UNIVERSITY

BY
ONUR MERT ERKAN

IN PARTIAL FULFILLMENT OF THE REQUIREMENTS
FOR
THE DEGREE OF MASTER OF SCIENCE
IN
MECHANICAL ENGINEERING

AUGUST 2015

Approval of the thesis:

DESIGN OF A MODULAR ORTHOPEDIC IMPLANT

submitted by **ONUR MERT ERKAN** in partial fulfillment of the requirements for the degree of **Master of Science in Mechanical Engineering Department, Middle East Technical University** by,

Prof. Dr. Gülbin Dural Ünver _____

Director, Graduate School of **Natural and Applied Sciences**

Prof. Dr. Tuna Balkan _____

Head of Department, **Mechanical Engineering**

Asst. Prof. Dr. Ergin Tönük _____

Supervisor, **Mechanical Engineering Department, METU**

Examining Committee Members:

Prof. Dr. Orhan Yıldırım _____

Mechanical Engineering Department, METU

Asst. Prof. Dr. Ergin Tönük _____

Mechanical Engineering Department, METU

Prof. Dr. Erbil Oğuz _____

Orthopedics and Traumatology, GATA

Asst. Prof. Dr. Buğra Koku _____

Mechanical Engineering Department, METU

Asst. Prof. Dr. Kıvanç Azgın _____

Mechanical Engineering Department, METU

Date: 27.08.2015

I hereby declare that all information in this document has been obtained and presented in accordance with academic rules and ethical conduct. I also declare that, as required by these rules and conduct, I have fully cited and referenced all material and results that are not original to this work.

Name: Onur Mert Erkan

Signature:

ABSTRACT

DESIGN OF A MODULAR ORTHOPEDIC IMPLANT

Erkan, Onur Mert

M.S., Mechanical Engineering Department

Supervisor: Asst. Prof. Dr. Ergin Tönük

August 2015, 123 Pages

Bone fracture due to trauma and bone defects by birth are very common in orthopedics, making their treatment crucial. In this study, a novel design to treat upper arm fractures is introduced and assessed mechanically. The design offers medical doctors longitudinal and angular flexibility when compared to widely used orthopedic plates. Hence the new design covers a variety of fracture types. Earlier conceptual designs are reviewed to demonstrate the progress of design. Mechanical performance of the final design is evaluated using analytic methods, finite element analysis and physical experiments. Assessment was based on a safe axial external load of 15 kgf suggested by the medical doctors and focused on the rigidity problems caused by modularity, along with strength concerns. It is proven in this study that the novel design can fix the fracture successfully, even under the aforementioned external load.

Keywords: modular, orthopedic implant, fracture fixation

ÖZ

MODÜLER ORTOPEDİK İMPLANT TASARIMI

Erkan, Onur Mert

Yüksek Lisans: Makina Mühendisliği Bölümü

Tez Yöneticisi: Yard. Doç. Dr. Ergin Tönük

Ağustos 2015, 123 sayfa

Travmaya bağlı kemik kırıkları ve doğuştan kemik bozukluklarına ortopedide sıkça rastlanmakta olup bu durum tedavileri çok önemli kılmaktadır. Bu çalışmada üst kol kırıklarını tedavi etmekte kullanılacak özgün bir implant tasarımı tanıtılmış ve mekanik olarak incelenmiştir. Yeni tasarım yaygın biçimde kullanılan ortopedik plaklara nazaran tıp doktorlarına boylamsal ve açısal serbestlik sağlamaktadır. Böylece farklı tiplerde kırıklar kapsanmıştır. Kavramsal tasarımlar değerlendirilip tasarım süreci gösterilmiştir. Nihai tasarım analitik yöntemler, sonlu elemanlar analizi ve fiziksel deneylerle mekanik açıdan değerlendirilmiştir. Değerlendirme doktorlar tarafından önerilen 15 kgf eksenel dış yükü temel alıp mukavemetin yanı sıra modüler tasarıma bağlı rijidite problemlerine odaklanmıştır. Çalışmada özgün tasarımın bahsedilen dış yüke maruz kaldığında dahi kırığı başarıyla sabitlediği kanıtlanmıştır.

Anahtar Kelimeler: modüler, ortopedik implant, kırık sabitleme

ACKNOWLEDGEMENTS

The author wishes to express deepest, sincere gratitude to his supervisor Dr. Ergin Tönük for his guidance, advice, criticism, encouragement and insight throughout this study.

The author also would like to thank Erbil Oğuz, MD and Cemil Yıldız, MD for their medical feedback and help having manufactured the prototypes for experimentation.

The contribution of Çağrı Yenigün is also sincerely appreciated.

The help of Cihan Keskin and Ömer Pektaş especially in obtaining the equipment for the experiments is gratefully acknowledged.

The author also would like to thank Hipokrat Tıbbi Malzemeler İmalat ve Pazarlama A. Ş. for having manufactured the prototypes of the design in this study.

This study was supported by TÜBİTAK and conducted as a part of a 1003 project.

TABLE OF CONTENTS

LIST OF FIGURES

FIGURES

LIST OF TABLES

TABLES

LIST OF EQUATIONS

NOMENCLATURE

C_α: Coefficient relating external force to frictional moment in ball and socket joint

δ: Radial interference

μ: Coefficient of friction

σ: Normal stress

τ: Shear stress

A: Cross sectional area

d: Major diameter

d_r: Root diameter

E: Young's modulus

F_f: Friction force

I: Second moment of area

K: Torque coefficient

p: Pressure distribution

R: Nominal radius

r_i: Inner radius

r_o: Outer radius

V: Shear force

CHAPTER 1

INTRODUCTION

1.1 Human Bone

1.1.1. Cellular Structure of Human Bone

Movement, form, support and stability of the human body are provided by musculoskeletal system. As the name suggests skeleton, which is made up of bones is a main part of this system. Three fundamental types of bones in terms of materials are woven bone, cortical bone and cancellous bone. Woven bone is present in embryonic stage, at the time of fracture healing and in some pathological cases. Normally, it is substituted by cortical or cancellous bones. Cortical bone is remodeled by the woven bone and it establishes the internal and external tables of flat bones and the external surfaces of long bones. Cancellous bone is located between cortical bone surfaces. The trabeculae within the cancellous bone lie perpendicular to external forces to provide structural support. Continuous remodeling takes place in cancellous bone on the internal endosteal surfaces. From a histological point of view, bones consist of osteogenic precursor cells, osteoblasts, osteoclasts, osteocytes, and the hematopoietic elements of bone marrow. Osteogenic precursor cells form the deep layer of the periosteum, which invests the outer surface of bone, and the endosteum, that covers the internal medullary surfaces. The periosteum is a resilient, vascular layer of connective tissue that covers the bone except the joint surfaces. The thick outer layer is called fibrous layer and it is made up of irregular, dense connective tissue. Osteogenic layer is the inner layer and contains osteogenic cells. The endosteum is a single layer of osteogenic cells missing a fibrous component. Osteoblasts are mature, metabolically active, cells which form the bone. Approaching the end of their bone

forming activity, some osteoblasts are transformed into osteocytes while the rest stay on the periosteal or endosteal surfaces of bone as lining cells. Osteocytes are mature osteoblasts in the bone matrix. Extracellular concentration of calcium and phosphorus, in addition to adaptive remodeling behavior via cell-to-cell interactions in response to local environment are controlled by osteocytes. Osteoclasts, controlled by hormonal and cellular mechanisms, are multinucleated, bone-resorbing cells. These cells function in groups, attaching to bare bone surfaces, dissolve the inorganic and organic matrices of bone and calcified cartilage by delivering hydrolytic enzymes. (Kalfas, 2001)

1.1.2. Bone Fracture and Classification

Bone fracture is defined formally as a medical condition in which there is a break in the continuity of the bone. (Marshall & Browner, 2012) Main causes of the fractures are listed as trauma, pathology (e.g. bone cancer), medical or design errors in prosthesis and overuse. Although many categorizations of the fractures are available, OTA (Orthopedic Trauma Association) classification is the most organized one, classifying the fractures with a number indicating which bone is broken (e.g. 1 for Humerus); another number indicating the location of the fracture (e.g. 1 for Diaphyseal); then a group (Type A1, etc.) and a subgroup (Simple, Complex, etc.) both indicating the geometry of the fracture. (Cannada, 2011) Further detail of the classification is more of a medical area than an engineering one, hence out of the scope of the present study.

1.1.3. Fracture Healing

After the fracture occurs, bone healing process starts, which consists of three stages: early inflammatory stage, repair stage and late remodeling stage. In the inflammatory stage, a hematoma develops within the fracture site during the first few hours and days. Inflammatory cells and fibroblasts infiltrate the bone under prostaglandin mediation,

which leads to the formation of granulation tissue, ingrowth of vascular tissue, and migration of mesenchymal cells. The primary nutrient and oxygen source of this early process is provided by the exposed cancellous bone and muscle. During the repair stage, fibroblasts begin to lay down a stroma, connective tissue cell that helps support vascular ingrowth. During vascular ingrowth, a collagen matrix is formed while osteoid is secreted and subsequently mineralized, which leads to the formation of a soft callus around the repair site. This callus is feeble regarding resistance to movement in the first 4 to 6 weeks of the healing process, so adequate fixation is essential. Eventually, the callus ossifies, forming a bridge of woven bone between the fracture fragments. Alternatively, if proper fixation is not employed, ossification of the callus may not occur, and an unstable fibrous union may develop instead, leading to longer healing time. (Kalfas, 2001) In this stage, if the fracture site is properly fixed and space between bone fragments is less than or equal to 0.1 mm, the process is called primary healing; otherwise the process is called secondary healing. Experiments showed that primary healing leads to 100% improvement on healing time. (Şen, Çakmak , Seyhan, Göğüş, & Taşer, 1991) Healing bone is restored to its original shape, structure, and mechanical strength and fracture healing is completed during the remodeling stage. Remodeling of the bone occurs slowly over months to years and is promoted by mechanical stress placed on the bone. As the fracture site is exposed to an axial loading force, bone is generally laid down where it is needed and resorbed from where it is not needed. Thus, appropriate amount of load should be applied on the bone, to avoid stress shielding effect. Satisfactory mechanical properties are typically obtained in 3 to 6 months (Kalfas, 2001).

1.2 Fracture Fixation

1.2.1. History

Groundwork of the modern treatment techniques of bone and joint injuries were laid in the first half of the 19th century. (Bartonicek, 2010) However, the focus of the treatment was avoiding surgery and immobilizing the injured limb, due to pain and infections associated with surgery. In 1846, inhaling ether vapor as anesthetic was put

forward. In the second half of the century, use of antiseptics and other means to improve surgical hygiene were suggested and started to be widely used. Also, the invention of x-ray imaging in 1896 made surgery planning and result evaluation possible. All these developments led to operative treatment becoming more popular.

Surgical techniques were made possible by the scientific advances, however the production of implants were still lacking. Therefore doctors had to develop their own implants in late 19th and early 20th centuries. Search for suitable material was also a serious concern. The oldest implants for internal fixation of fractures were made from mainly ivory, bone and metals such as bronze, lead, gold, copper, silver, brass, steel and aluminum. Ivory and bone pegs were used for intramedullary fixation; silver was used for cerclage wires, plates and intramedullary pins. The first plates were made from nickel coated sheet steel and later from silver, high carbon steel, vanadium steel, aluminum or brass. For the metals corrosion was a major problem during this period. The use of stainless steel as implant material solved this problem.

1.2.1.1. Cerclage

Wire cerclage was one of the earliest methods of internal fixation. Improvement of this technique was published in 1912 by Robert Milne as cerclage using flexible threaded pins. In 1914 Vittorio Putti presented cerclage with a narrow metal band. In 1916 a similar method was published by Frederick William Parham and the implant spread world-wide under the name Putti-Parham bands whose various modifications are still occasionally used today (Bartonicek, 2010).

1.2.1.2. Plates

Carl Hansmann was the first to publish his experience with fracture fixation using a plate in 1886. Hansmann used plates from nickel coated sheet steel, which is demonstrated in Figure 1, in 20 different cases. Part of the plate and the shanks of the screws that fixed it to the bone protruded from the wound and therefore could be

removed percutaneously. The wound was kept strictly aseptic for 4-8 weeks and then the plates were removed upon healing. No complications were reported in the study.

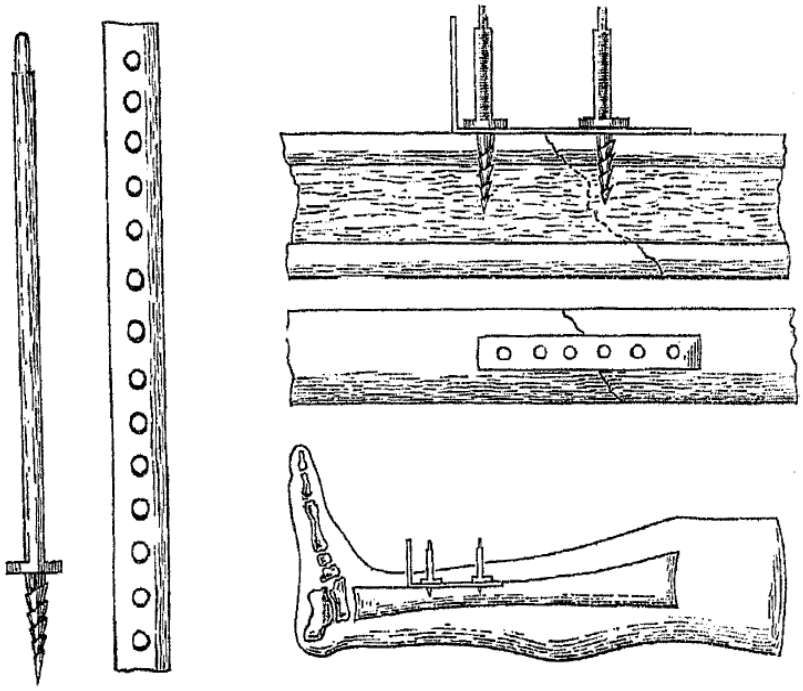

Figure 1: Hansmann Plate (Bartonicek, 2010)

Lewis W. Steinbach in 1900 used a silver plate of his design, fixed to the bone fragments by two steel screws in four cases. It was the first study to document the injury, the plate fixation and the final outcome with radiography. Martin in 1906 also used radiographs to document his study in which plates and monocortical screws in addition to Ashhurst's study with bicortical screws in 1899. William Lawrence Estes in 1912 used a plate made of nickel plated soft steel to treat the fractures and his design is reported to have good results. Joseph Augustus Blake published his work of seven years in 1912, reporting the treatment of 106 cases with his plate design made mostly of silver and occasionally brass or steel. Also in 1912, for the first time a radiograph of a fracture of the medial malleolus fixed with a plate was published by Emil H. Beckman. William O'Neil Sherman, working for Carnegie Steel Company had the chance of experimenting with both material and design of the plates. His sophisticated

plates designed on the basis of mechanical principles were made of vanadium steel using self-tapping monocortical screws. He published his results in 1912 as well. In 1914, the first angled blade plate for osteosynthesis of femoral neck fractures was designed by Miller Edwin Preston. However, he was unable to use the design in many cases. In the meantime, in Europe Albin Lambotte presented his work of seven years in 1907. He treated various diaphyseal fractures with plates made of aluminum which were fixed by self-tapping monocortical screws. In 1913 he published three different types of plates, one of which was contoured. In 1907, William Arbuthnot Lane published a successful fixation of diaphyseal femur fracture using a pair of plates. Carbon steel plates of his design were fixed to the bone with monocortical screws. Their disadvantage was their flimsiness and the necessity to immobilize postoperatively the limbs with external splints. Henry S. Souttar published his work in 1913 with a new design of plate fixed with a finely threaded screw. He considered the invasion of the plate on the bone and tried to reduce its "footprint" to avoid negative effects on healing. Ernest William Hey Groves included animal experiments in his study. He designed curved plates and plates with T-shaped ends. Moreover, comparison of Lane and Lambotte plates as well as wood and metal screws were his contributions to development of the plates. The efforts of all the aforementioned researchers, plates became the most frequently used implant for internal fixation at the beginning of the 20th century. (Bartonicek, 2010)

Research on the bone plates led to development of compression plate (CP) in 1949. Solving some problems of the earlier plates such as insufficient stability, requirement of additional splinting, corrosion and infections; compression plate was not widely used due to structural weakness. An improvement over compression plate, dynamic compression plate (DCP) was introduced in 1969. Superiority of dynamic compression plate was due to increased stability of the fixation and removal of the external immobilization. This plate included holes for axial compression, which was achieved with eccentric screw insertion. However dynamic compression plate delayed mating, caused cortical bone loss under the plate and microscopic gaps on the bone upon removal of the plate. Moreover it acted like a stress concentrator leading to increase in likelihood of re-fracture. To overcome the problem of disturbance of the periosteal blood circulation in dynamic compression plate, limited-contact dynamic compression

plate (LC-DCP) was developed. The contact surface was reduced by more than 50%. Yet the principle of plate osteosynthesis with compressive forces acting against the bone was still present. To eradicate the ill-effects, point contact fixator (PC-Fix) was introduced. This plate was the first version of plate fixators in which angular stability was accomplished by a conical connection between screw heads and screw holes. Additionally, the use of unicortical self-tapping screws appeared as equally effective as external fixation in obtaining stability. During healing, the head of a screw had produced a nearly "cold-forged" connection between the screw head and the screw hole which made the removal of the plate problematic. Hence, less invasive stabilization system (LISS) was developed with a new thread connection between the screw head and screw hole. The plate is implanted through the skin and locked to the bone with unicortical screws. To lock the plate tightly, locking head screws are used. Unlike the compression screw, this screw-plate assembly does not need friction between the plate and the underlying bone for stabilization. Hence the plate does not have to have the geometry adapted exactly to the shape of the bone. In year 2000, locking compression plate (LCP) was released, which was based on a combination of the anchorage technologies of PC-Fix and LISS in one implant. Today, almost all plate shapes have been equipped with the new locked compression plate hole which permits the use of either conventional cortex screws or angular-stable screws. Moreover, LCP can be applied in three manners depending on the approach of the surgery: conventional LCP, pure internal fixator (PIF) or a combination of both. Despite the advantages of LCP, there was still room for improvement and pre-shaped LCP was introduced in 2001. This plate allows all screws to be centrally anchored in the bone fixed laterally and is useful in fracture fixation of various anatomical regions. Pre-shaped LCPs are widely used today especially in corrective surgery of the bone when the fracture is close to joints. However it is still not ideal since it is non-biodegradable and removal of the implant requires surgery. Aforementioned plates can be seen in Figure 2 (Malekani, Schmutz, Gu, Schuetz, & Yarlagadda, 2012).

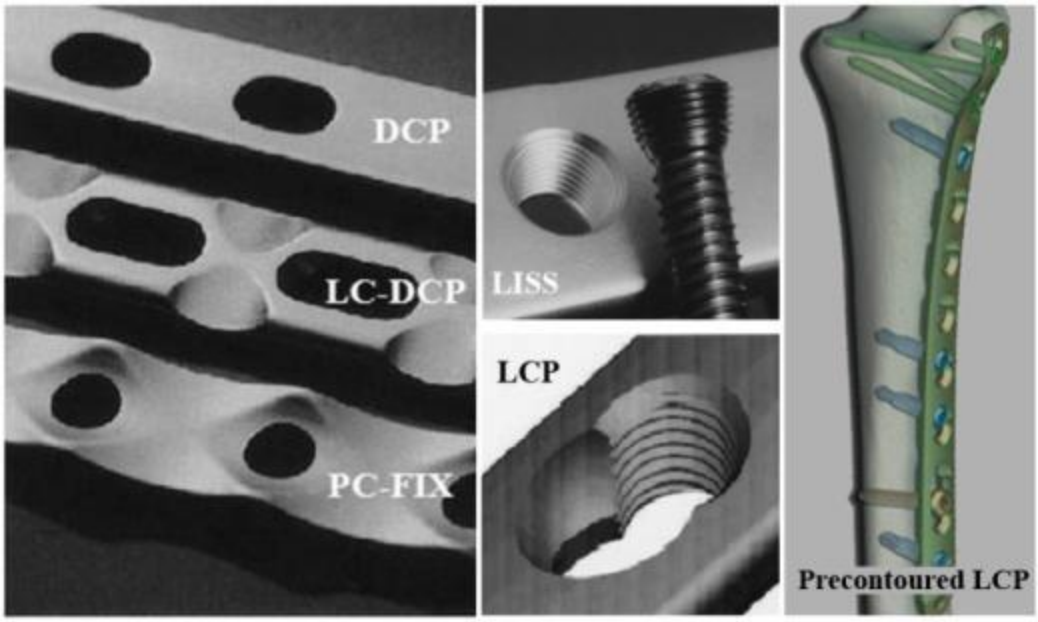

Figure 2: Different Types of Plates (Bartonicek, 2010)

1.2.1.3. External Fixation

Earliest external fixation evidence was found in the writings of Hippocrates, who lived before Christ. More modern designs were seen in the 19th century, however in the first half of the century, published work on external fixators were unsuccessful, mainly due to infections. In 1872, Heine used an external fixator of his design which consisted of two ivory pins inserted transversely through both cortices of each fragment and a bar to which pins were connected. He had good results in humerus, however his fixator was seen to be inadequate for femur or other high load bearing bones. External fixation as we know it today, started to develop in the 20th century. In the USA, in 1897-1898 Clayton Parkhill designed external fixation clamps and used them for different types of fractures. Parkhill's design can be seen in Figure 3. In 1911, Freeman improved his work and introduced the "turnbuckle" to facilitate reduction, which was a highly sophisticated precursor of the AO (Arbeitsgemeinschaft für Osteosynthesefragen) femoral distractor. In Europe, Albin Lambotte was the pioneer of external fixation. He developed his own external fixator independently of his American colleagues and his sophisticated design was similar to current AO tubular fixator. (Bartonicek, 2010)

Researchers like Stader, Lewis, Breidenback, Herzberg, Klap and Illizarov all modified and improved the design of Parkhill throughout the 20th century (Apley & Noorden, 2000).

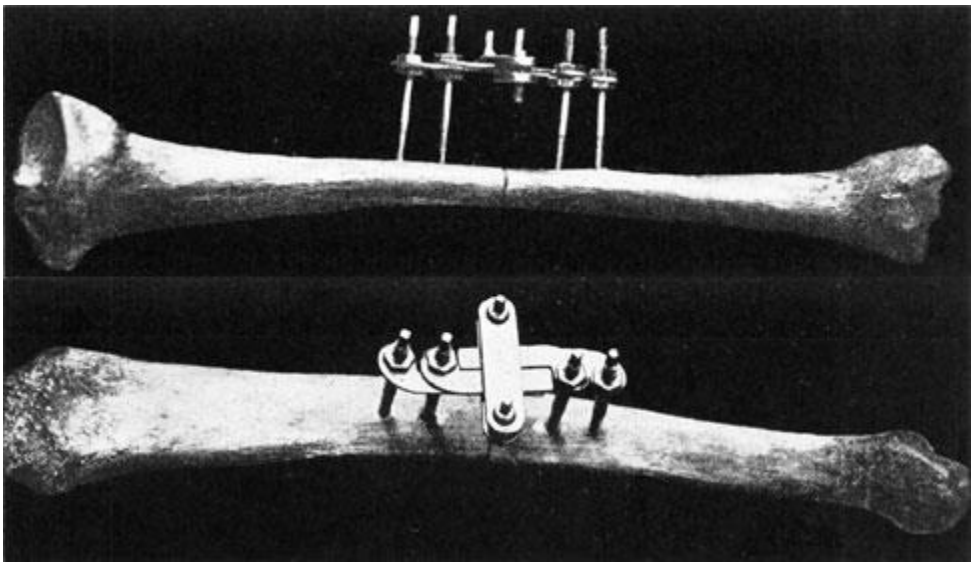

Figure 3: Parkhill's External Fixator (Bartonicek, 2010)

1.2.1.4. Intramedullary Nailing

Intramedullary (IM) nails in 18th and early 19th centuries were made by ivory. They acted more like biological stimulators instead of mechanical fixators. The nail was attacked by the patient's body so they had to be removed in 1 to 3 weeks, still helping the healing process. Metallic nails were originally used to fix fractures of the articular ends of bones, specifically in fractures of the femoral neck. The first operation was performed by Langenbeck in 1858. Paul Niehans in 1904 published treatment of a supracondylar humeral fracture in a child. The author performed open reduction and nailing in six cases. The first successful "close" nailing of a diaphyseal fracture was described by Georg Schöne in 1913. Under fluoroscopic control, seven diaphyseal fractures of the ulna and radius were treated with silver nails inserted percutaneously.

Hey Groves conducted a series of experiments to evaluate the performance of nails made of bone, ivory and metals. In 1918 he treated two cases of gunshot fracture with steel nails (Bartonicek, 2010). In 1940 Gerhard Küntscher developed his famous cloverleaf nail, whose modifications are still in use. An example of Küntscher nail can be seen in Figure 4. Throughout the World War 2, Küntscher treated many wounded soldiers with his design. After the war ended, Küntscher nail was known and started being used worldwide. In the second half of 20th century, as previously mentioned, there were rapid advances in plate technology and plates were the most popular treatment technique. Therefore there were no ground breaking advances in the design of IM nails after Küntscher (Bong, Koval, & Egol, 2006).

Figure 4: Küntscher Nail in Femur (Christensen, 1973)

1.2.2. Modern Bone Plates

Bone plates can be defined formally as implantable fracture fixation devices attached to bone fragments with screws to bridge the fracture gap and shield the fracture site from stress as bone heals (Universal Medical Device Nomenclature System, 1999). Today, using biocompatible and mechanically fit materials, bone plates provide a good solution and they are used either internally or externally. As mentioned earlier, bone

plates dominate the field when compared to alternative treatment techniques such as IM nails, external fixators and wires in the last 30 years. Non-surgical technique casting, also having its own advantages like, obviously, absence of surgery and invasion (leading to better nourishment of the bone), cannot provide as much fixation as the surgical techniques do. Hence, the bone plates are of main concern in this study.

Some of the major orthopedic plate manufacturers are Johnson& Johnson, Stryker, Zimmer, Biomet and Medtronic. Figure 5 illustrates an osteotomy set (consisting of bone plates, screws and hand tools) from a major plate manufacturer from Turkey, TST.

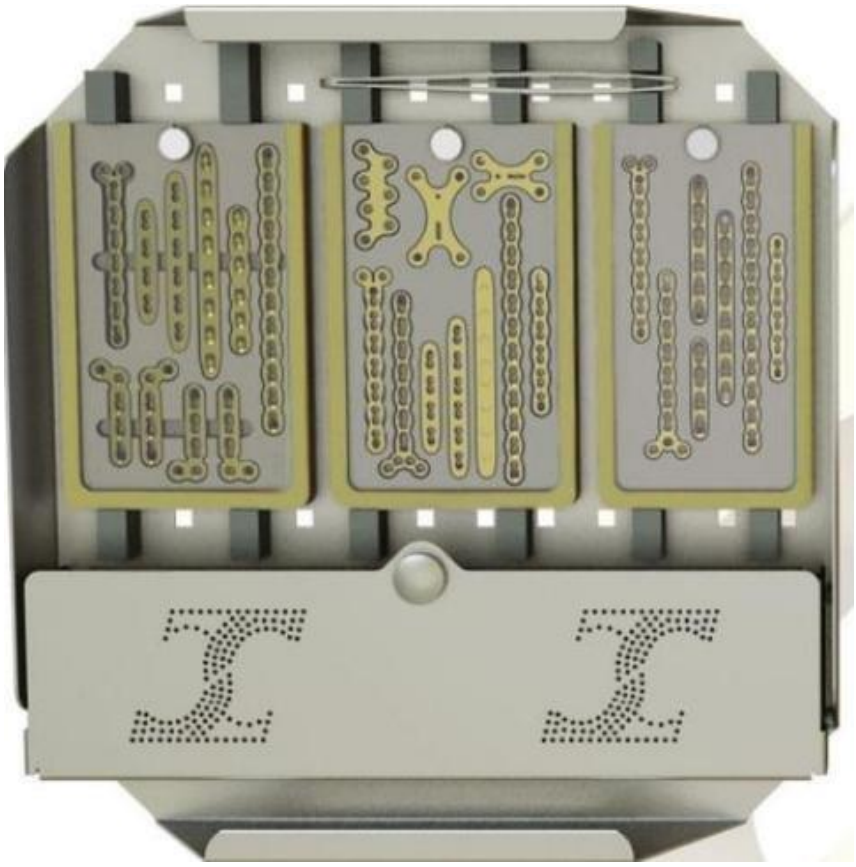

Figure 5: Osteotomy Set Example (TST, 2015)

A drawback of the bone plates today is that they are sold as huge sets consisting of many plates (like the one shown in Figure 5), to cover various types of bone fractures

and bone properties, which change with patient age, habits and environment. The sets need to be carried to the surgery rooms and sterilized. Afterwards the suitable plate for the patient is chosen by the medical doctor. Even with a set, all cases still cannot be covered, since the plates offer predetermined locations and angles for the bone screws. There are plates with multi-axial and poly-axial screws, but these solutions offer a limited angular degree of freedom and the screw locations are predetermined. Some plate examples are shown in Figure 6, Figure 7 and Figure 8.

Figure 6: Distal Radius Plate (Zimmer, 2015)

Figure 7: Proximal Femur Plate (Stryker, 2015)

Figure 8: Proximal Humerus Plate (Biomet, 2015)

1.3 Design Problem and Motivation

As previously mentioned, the main criticism to the osteotomy sets in this study is the lack of freedom they offer to the surgeon in terms of position and orientation of the fixation, despite the number of plates they include. So the aim in this study is designing a novel internal implant providing more flexibility and decreasing the number of parts necessary to fix the bone. For this purpose, an engineering problem definition document is prepared in addition to medical doctors' explanations about the issue. Due to lack of quantitative data available, objective target values are not specified.

Requirements:

- Successful fixation of the bone
- Improvement on weight, volume and number of parts of the osteotomy sets (mobility)
- Ability to be used in diaphyseal area of humerus (upper arm)

- Biocompatibility
- Minimal invasion of periosteum
- Ease of use: Satisfactory pre-operative and operation times
- Satisfactory post-operative time (recovery time of the patient)
- Comfort of the patient: The implant geometry and weight should not cause discomfort

It should be stated that the initial aim of this study was designing an implant to work on all human long bones, which would be the only way the new design can replace the osteotomy sets as a commercial product. However, the study evolved into only focusing on humerus, still proving the concept works. The current design should be extensively improved to supplant the osteotomy sets.

CHAPTER 2

LITERATURE REVIEW

2.1 Introduction

The aim of this study is offering a new alternative to the osteotomy sets by designing a modular orthopedic implant, which can be used internally and externally to treat a variety of fractures and defects. Moreover, the novel design in this study is inspired by the pedicle screws used in spinal trauma, applying the idea to long bones. Hence the literature review in this study concentrates on modular designs and studies on them, in addition to spinal treatment techniques. Subsequently, materials used in bone fixation, both commercially used and more innovative ones, are reviewed.

2.2 Plates

As previously mentioned, bone plates are the most commonly used treatment technique for the bone fractures today. Since this study focuses on assessment of a novel design to be an alternative treatment technique, bone plates are reviewed. More specifically, the attention is centered on studies on modular designs. It should be noted that not all of the following studies uses the term “modular” as flexibility for different cases. In some studies the term is used to define an assembly. Nevertheless, these studies are still worthy of interest, since one of the main problems in modularity (also assembly) is the loss of rigidity when compared to solid materials.

An experimental study was conducted (Sakellariou, et al., 2012) to compare four types of surgical treatment techniques on human humerus (upper arm) The techniques compared can be seen in Figure 9:

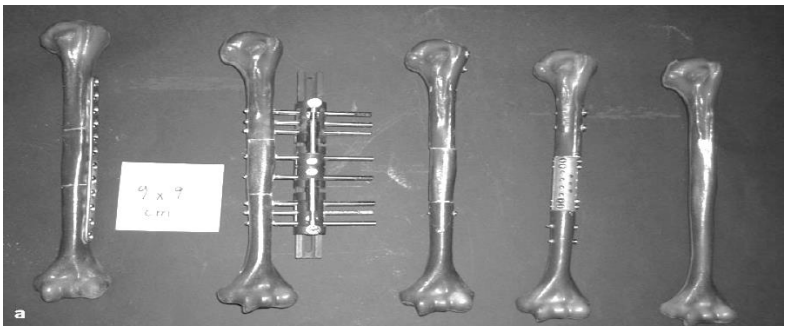

Figure 9: Left to Right: 12 Hole Locking Plate, Monolateral External Fixator, Intramedullary Nail, Modular Segmental Fixation Implant, Intact Model (Sakellariou, et al., 2012)

Four different methods were applied to fourth generation bone composite models, one model was left intact. Axial compression, four-point bending and torsion tests were conducted on these five models, in that order. The loads applied were within the linear elastic region at the sub-yield level, as determined by preliminary pilot tests. Axial compression was determined as the slope of load versus displacement curve. Flexural rigidity is by definition elastic modulus (E) multiplied with second moment of area (I) and indicates the resistance material can offer against bending loads. In this study loads were controlled, deflection was measured and flexural rigidity was calculated using the deflection formulae. Likewise, for the torsional rigidity torque was controlled and angle of twist was measured. Mean value results are presented in Table 1:

Table 1: Mean Values of Test Results, Compression Stiffness, Flexural and Torsional Rigidity (Sakellariou, et al., 2012)

	Intact	Modular Segmental Implant	IM Nail	Locking Plate	External Fixator
Axial Compression (N)	973	919	816	758	619
Four Point Bending (N)	835	629	320	597	651
Internal Torsion (N×m)	2.66	1.37	0.84	0.778	1.44
External Torsion (N×m)	2.59	1.268	0.73	0.788	1.438
Compression Stiffness (N/μm)	0.97	0.92	0.816	0.758	0.62
Flexural Rigidity ($N \times m^2$)	44.37	33.32	16.93	31.67	34.51
Internal Torsional Rigidity ($N \times m^2/deg$)	0.77	0.418	0.208	0.22	0.418
External Torsional Rigidity ($N \times m^2/deg$)	0.75	0.388	0.24	0.22	0.418

Using the results, the researchers ranked these four reconstructive methods with respect to stiffness, flexural rigidity and torsional rigidity. These rankings are given in Table 2: (Lower ranks indicates better values)

Table 2: Rankings of Four Reconstructive Methods (Sakellariou, et al., 2012)

Compression Stiffness		Flexural Rigidity		Torsional Rigidity	
Intact	1	Intact	1	Intact	1
Modular Implant	2	Modular Implant	2	Modular Implant	2
IM Nail	2	External Fixator	2	External Fixator	2
Locking Plate	3	Locking Plate	2	Locking Plate	3
External Fixator	4	IM Nail	3	IM Nail	3

According to these rankings, the researchers scored each reconstructive method, reaching the conclusion that modular segmental implant and monolateral external fixator have significantly better mechanical behavior, proving their initial hypothesis. In another study researchers used finite element analysis to assess fatigue properties of commercially available hip implants, which can be considered modular design due to assembly of several parts. The results of the study indicated the modular design was successful, even under the worst loading case of jogging (Dickinson, Browne, Roques, & Taylor, 2013). Another design focused on mandibular (jaw) fractures, achieving modularity of the bone plate by deformation. There was a deformable region on the plate helping the doctor to align the plate for better fixation. Experiments were conducted using the static loading case, whose results showed that the designed plate can withstand the average human bite force (Cervantes , Slocum Jr, & Seldin, 2011). Another study focused on modular femoral implants, observing patient recovery after the application of the implant to the patients with various bone defects. An example of the femoral stem part can be seen in Figure 10. Femoral stem was assembled with a spherical part called acetabular cup, which replaces the hip joint.

Figure 10: Femoral Stems (Cervantes , Slocum Jr, & Seldin, 2011)

The authors stated that overall; the operations were a success with 96.9% survival at 5 years. The advantages of modular implants were listed as: intraoperative versatility; minimized proximal stress shielding due to porous coating; variety of stem and neck length and offset. The disadvantage of modular implants was high stress at taper junction, hence the need of thorough mechanical design. The study showed that modular femoral implant surgeries have high success rate, but bone defect type should be carefully considered planning for surgery. For instance, the authors refer to the work of Mccarthy and Lee, in which success rates were high for Paprosky types 1, while 9% failure was observed in Paprosky type 3A and 4 (McCarthy & Lee, 2007). However, in their study, with careful surgical planning, no significant difference in success rate between defect types was observed (Desai, et al., 2012).

High success rates of bone plates are common knowledge, therefore studies on non-modular plates are excluded. Furthermore, aforementioned studies indicate that modular plates or treatment devices consisting of assembly of several parts are also successful, hence encouraging the success of the novel design in this study.

2.3 Pedicle Screws

Treatment of spinal trauma or deformities requires angular degree of freedom for the surgeon, due to the shape of human spine. A commonly used device, pedicle screw can be seen in Figure 11:

Figure 11: Sequoia Pedicle Screw System (Zimmer, 2015)

In this system, assembly heads are free to rotate and translate on the rod, which comes in varying shapes and diameters for different cases. Polyaxial screw heads provide additional angular degree of freedom. Upon achieving desired configuration, the surgeon locks the system using the locknut part. Axial force of the locknut part causes friction force, securing the orientation of polyaxial screw; location and orientation of the head assembly. A study was conducted to investigate the effect of depth and diameter of the bone screw on pull-out strength (Talu, Kaya, Dikici, & Şar, 2000). Five groups were formed with pedilen rigid foam as the model of lumbar vertebrae. In the first group 6.5 mm diameter and 40 mm long screws were used to obtain reference values. The following groups consisted of after application and removal of 6.5 mm × 40 mm screws, application of screws: of the same size; 6.5 mm × 45 mm; 7 mm × 40 mm; 7 mm × 45 mm. Ten different pull-out tests were performed for each group.

Results are shown in Table 3. As can be seen, substituting a pedicle screw with another screw of the same size results in drastic reduction in pull-out strength of the pedicle screw. It is obvious from these results that if a second surgery is to take place for some reason, the surgeon should choose a screw larger in diameter and length.

Table 3: Results of the Pull-out Test (Talu, Kaya, Dikici, & Şar, 2000)

	Number of Experiments	Pull-out Strength (Average) (N)
Group 1	10	2033.0
Group 2	10	1508.6
Group 3	10	2332.4
Group 4	10	2707.7
Group 5	10	3023.3

Another study focused on the effect of rod reduction technique on pull-out strength of the pedicle screw (Kang, et al., 2014). Rod reduction is deforming the rod when it is misaligned with the spine. The researchers contemplated that undertaking this procedure might pull the pedicle screw head, rather than pushing the rod, hence leading to damage in screw-bone interface. To test their hypothesis, thoracic Ponte osteotomies were performed on 3 thoracic levels in 15 cadaveric specimens and pedicle screw systems were applied. Left rod was perfectly aligned while the rod was reduced. A sample specimen that was used can be seen in Figure 12.

Figure 12: Left Side Control Rod and Right Side Reduced Rod (Kang, et al., 2014)

Afterwards the pull-out strength was measured using tensile test machine. Rod reduction resulted in 40% decrease in pull-out strength of the screws: 419 N in reduced rod versus 708 N in the control rod; meaning rod reduction procedure should be carried out with caution. A comparative study was conducted to evaluate performances of pedicle screws and spinous process screws in C2 vertebra (Liu, Mao, Xu, & Ma, 2014). Spinous process screws are easier to insert in C2 vertebra due to its size and shape. The researchers aimed to compare the mechanical properties. Eight fresh human cadaveric cervical spine specimens were harvested and screws were inserted in pairs. Results showed that the pull-out strength of the spinous process screw is comparable to the pedicle screw, an average of 387 N and 465 N respectively. The researchers concluded, from a medical stand point spinous process screw may provide an alternative to pedicle screw. Another study was conducted to compare anterior lumbar screw-plate fixation and posterior lumbar pedicle screw fixation (Liu, et al., 2014). Twelve fresh human cadaveric lumbar specimens (L4-L5) were divided into four groups: anterior lumbar interbody fusion+pedicle screw fixation; anterior lumbar interbody fixation+anterior lumbar locked screw plate (both fixed); anterior lumbar interbody fixation and untreated control (both non-fixed). Axial compression, flexion, extension, left and right lateral bending and rotation tests were applied to the specimens, in that order. Specimens can be seen in Figure 13 and Figure 14.

Figure 13: Anterior Lumbar Interbody Fusion+Anterior Lumbar Locked Screw Plate Specimen in Axial Compression Test (Liu, et al., 2014)

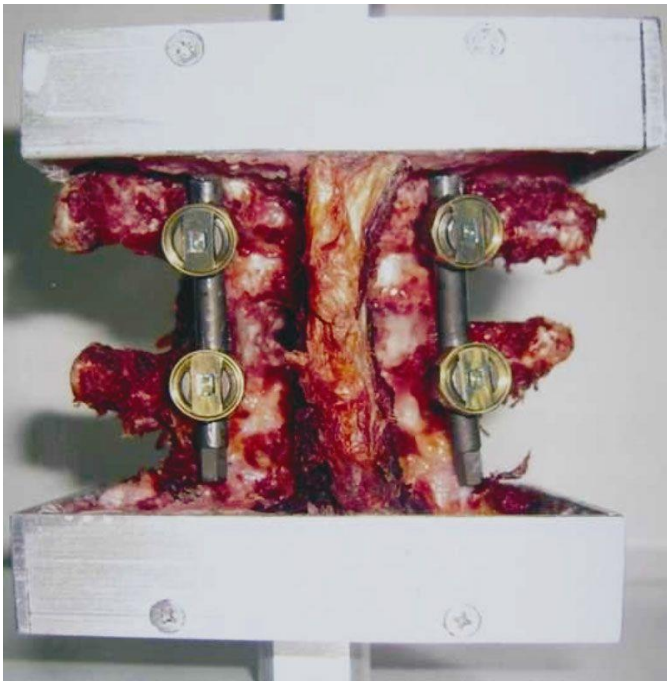

Figure 14: Anterior Lumbar Interbody Fusion+Pedicle Screw Fixation Specimen in Axial Compression Test (Liu, et al., 2014)

The tested loads for axial compression were 400, 600, 800, 1000 and 1200 N at the loading speed of 5mm/min. The loads for flexion, extension, left and right lateral bending and rotation tests were 100, 200, 300, 400 and 500 N, respectively. In the axial compression test, axial stiffness of the specimens were compared. Control and anterior lumbar interbody fusion groups had significantly lower axial stiffness than the two fixed groups. Anterior lumbar interbody fusion+anterior lumbar locked screw plate group had the highest axial stiffness. In the flexion test, angular displacement in specimens were compared and similar results were obtained; two fixed groups performed noticeably better. However, no significant difference was observed between the two. In the extension test, anterior lumbar interbody fusion+pedicle screw fixation specimen had the lowest linear displacement. This specimen also had the lowest angular displacement in the left and right lateral bending tests. In the rotation test however, the anterior lumbar interbody fusion+anterior lumbar locked screw plate specimen had the lowest angular displacement values. To sum up, this study proves that the stability of the anterior lumbar interbody fusion treatment can be increased considerably with the use of pedicle screws or locked plates. In another study, reliability of the pedicle screw fixation was assessed (Yalnız, Çiftdemir, Eşkin, & Dülger, 2009). 144 patients who had posterior thoracic pedicle screw implanted were retrospectively reviewed. A total of 827 thoracic pedicle screws were inserted to the patients by the same spine surgeon using the free-hand technique. Screw containment was evaluated by three independent reviewers on post-operative plain radio-graphs and thin-slice computed tomography scans for the cases necessary. 780 of the screws (94.3%) were observed to accurately fix the thoracic spine. Slightly more than half of the faulty screws (%51.1) were encountered in scoliosis patients. No symptoms or complications took place related to faulty screw placement. To sum up, the researchers concluded that pedicle screw fixation has a high success rate and is a safe method for thoracic spine treatment.

The novel design in this study, which will be presented in the upcoming sections, is inspired by the design of pedicle screws. Hence their comparative performance was worthy of interest. Aforementioned studies show that the performance is satisfactory, supporting the novel design.

2.4 Materials

From a material science point of view, medical grade stainless steels and titanium alloys are most commonly used in implants. During this research, medical grade stainless steels and titanium alloys are evaluated considering mechanical properties, cost and market availability. Steel has an elastic modulus of around 200 GPa, whereas titanium has an elastic modulus of around 100 GPa, which is closer to the elastic modulus of the bone, which is in the order of 10 GPa. Closer elastic modulus leads to reduction of stress shielding effect. Stress shielding can be described as the implant carrying too much of the compressive load, therefore fracture site not carrying enough of it. As a result bone loses strength according to Wolff's Law (Samiezadeh, Avval, Fawaz, & Bougherara, 2014). In addition to elastic modulus, titanium alloys are advantageous in terms of yield strength. Medical grade stainless steels have a yield strength in the order of 200 MPa whereas medical titanium alloys have yield strength within the range of 170 to 895 MPa, as can be seen in Table 4. The combination of elastic modulus closer to the bone and higher yield strength makes Ti6Al4V mechanically superior to stainless steels. Moreover, titanium alloys offer the chance of using magnetic resonance imaging, unlike the steel which is magnetic. Considering all these factors an agreement on Ti6Al4V (also known as Grade 5 Titanium) alloy is reached, just like the current common knowledge in the field.

Table 4: Comparison of Medical Titanium Alloys

	Grade 1	Grade 2	Ti6Al4V	Ti6Al7Nb
Density (g/cm^3)	4.51	4.51	4.42	4.51
Tensile Strength, Ultimate (MPa)	240	344	890	995
Tensile Strength, Yield (MPa)	170 - 310	275 - 410	820	895
Elongation at Break	24 %	20 %	14%	12%
Reduction of Area	35 %	35 %	25%	35%
Modulus of Elasticity (GPa)	105	105	114	100

In spite of the popularity of Ti6Al4V, in their previously mentioned study Samiezadeh et al. showed that composite bone plates were promising. In another study, the authors designed a polyetheretherketone (PEEK) spinal fixation device for rats. The experiments on rats were a success. Although loads on a human's long bones and rat's spine cannot even be compared, the study is worthy of interest since the current materials have aforementioned flaws, while the suggested material has the potential to overcome these. (Shahrokni, Zhu, Liu, Tetzlaff, & Oxland, 2012) In the final study reviewed on innovative materials for bone fixation, the authors used interchangeable titanium or stainless steel plates, connected with staples made of Nitinol (Nickel Titanium Naval Ordinance Laboratory). Shape memory property of Nitinol allowed the adjustability of compressive force on the fracture site. Naturally the staples were heat treated so that maximum compressive force was obtained at 37°C. (Tarnita, Tarnita , Tarnita , Berceanu, & Cismaru, 2010) Development of new materials grows more and more important due to recent claims and studies on metal ion release from Ti6Al4V, whose significance on patient health is not yet agreed on. A study on dental implants showed that metal ion release was significantly more in human saliva (in vivo group) than in buffered saline solution (in vitro group). However metallic ions released were still within the physiological limit of trace elements in the human body. (El Sawy & Shaarawy, 2013)

2.5 Conclusion

Throughout the literature review comprehensive information on design, assessment and performance of bone plates, pedicle screws and some other fixation techniques as measures of comparison. Particular weaknesses of the treatment techniques are presented. Since this study is focused on analysis of a certain fracture fixation device, knowing the competition and being familiar to evaluation techniques such as analytical methods, finite element method and experiments are the keys. Moreover, biomaterials in use today and the ones still being developed are reviewed. Mechanical properties of titanium alloys are presented. To sum up, literature review enlightened the path to accurately assess the present design.

CHAPTER 3

CONCEPTUAL DESIGNS

Design is an iterative process by nature. After the conceptual design phase, detailed design is conducted to see the performance of the concept. After that, optimization follows to reach the best design. Likewise, in this study, several conceptual designs were eliminated due to mechanical or medical deficiencies. These preliminary designs will be presented and discussed from mechanical and medical stand points. There are five types to present as preliminary designs, Type 2 having three revisions, so a total of seven designs will be introduced. It should be noted that these designs are conceptual and analyses are based on educated guesses, when available information and analytical methods are insufficient. 3D models are drawn using Solidworks software.

3.1 Type 1

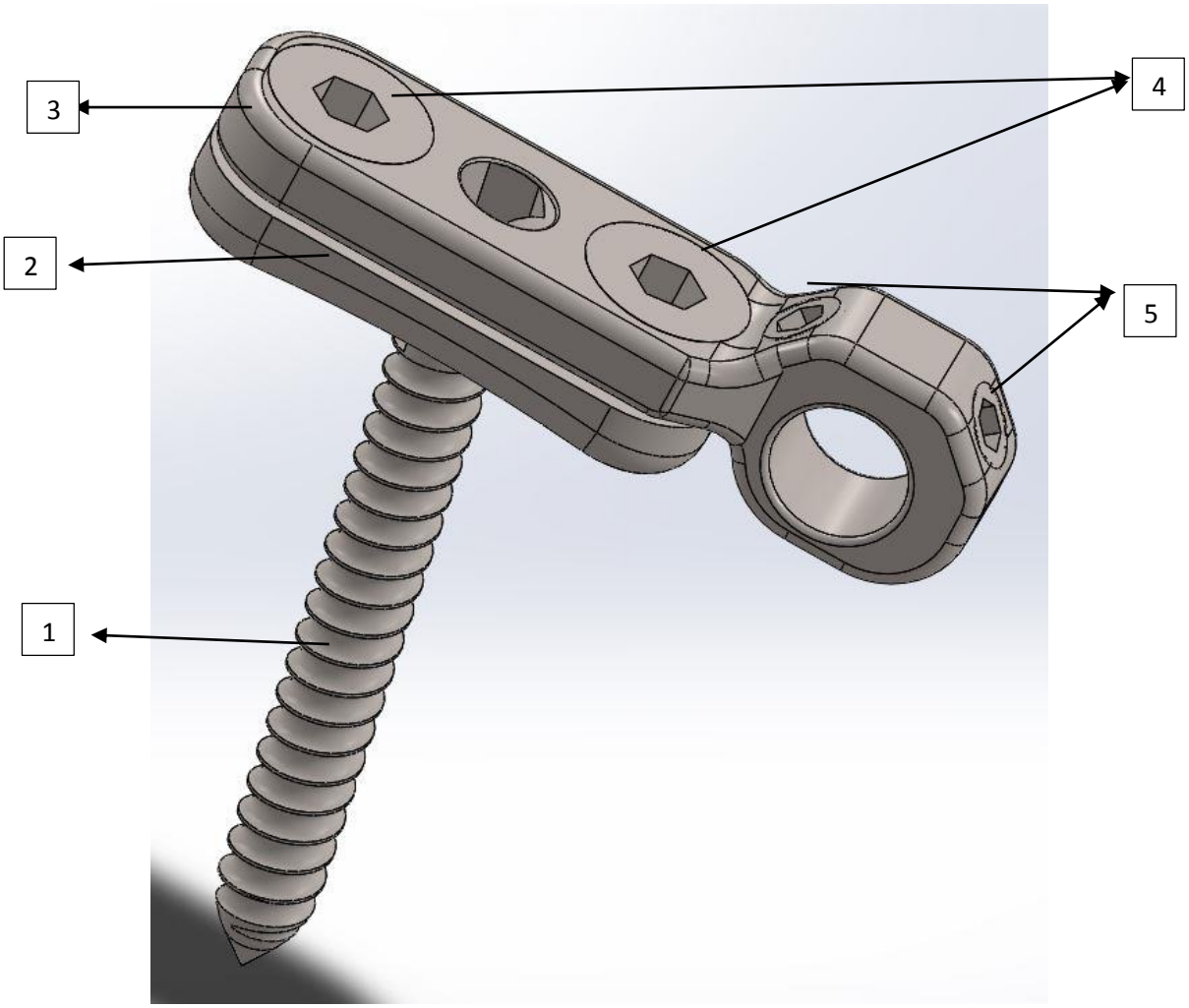

Figure 15: Type 1 3D Model (1: Bone Screw, 2: Base Bottom Part, 3: Base Top Part, 4: Clamping Screws, 5: Set Screws)

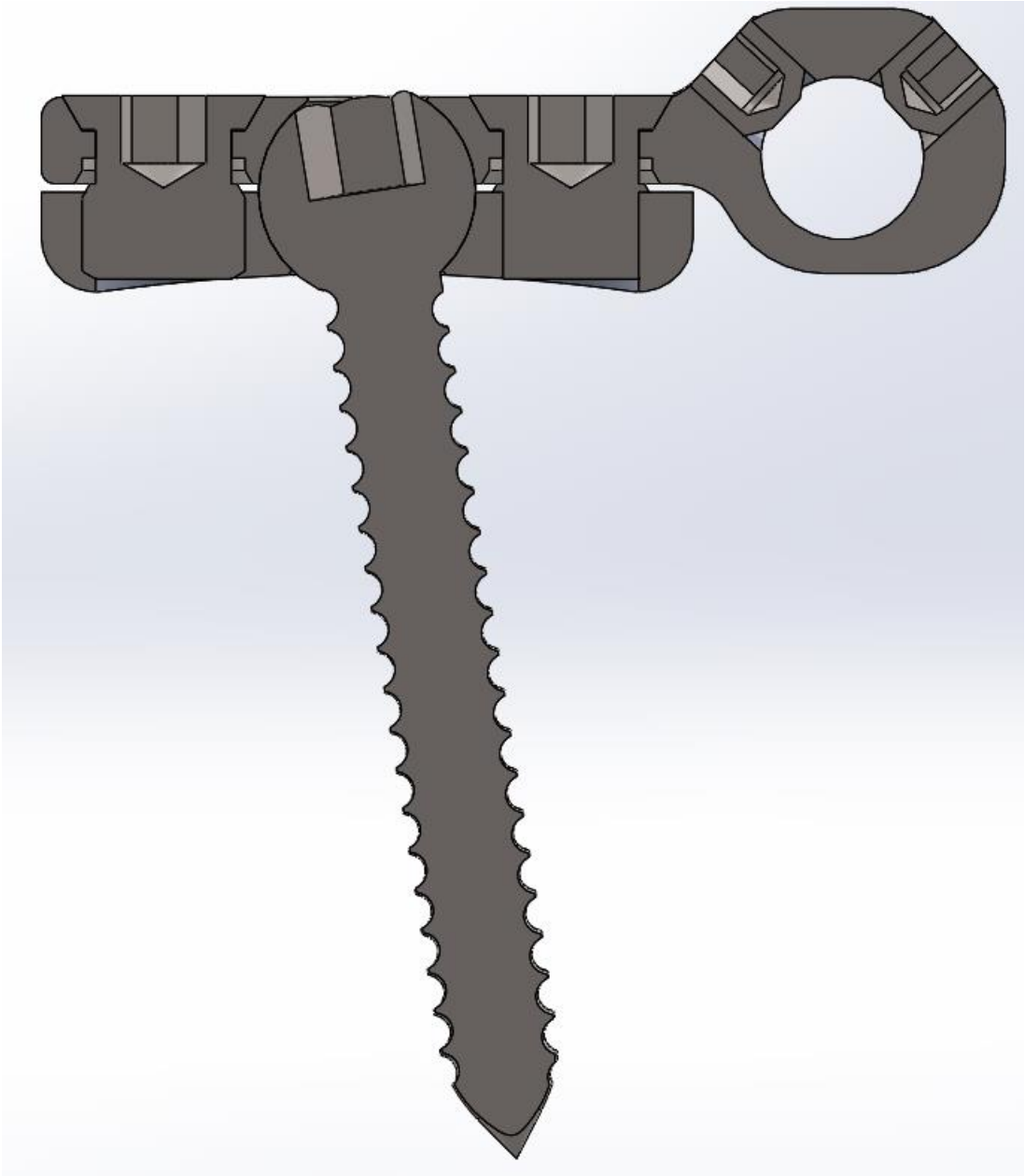

Figure 16: Type 1 3D Model Section View

This design consists of 5 different parts and a rod which is not drawn in Figure 15. Part 1 is polyaxial bone screw, threaded portion is placed into the bone and spherical head is constrained between parts 2 and 3, with the help of screws 4. The assembly is placed

on a rod through the hole in part 3. Set screws 5 are used to lock the assembly with the frictional force on the rod. More than one assembly will be placed anywhere on the rod, providing freedom for location of the screws. The fact that the assembly can rotate on the rod before being fixed with set screws, offers the surgeon angular degree of freedom. Additionally, polyaxial screw, as the name suggests, increases angular degree of freedom since the axis of the screw can be adjusted before fixing with screws 4.

One of the mechanical concerns in the design is whether or not the screws 4 are able to fix the spherical head of the bone screw. A study on frictional moment in spherical ball and socket joints (Faraz & Payandeh, 2001) stated that frictional moment can be estimated by the equation:

$$M = FRC_{\alpha}\frac{\mu}{\sqrt{1+\mu^2}} \qquad (3.1)$$

Where:

F: External load on the spherical joint (Force applied by screws 4 in this case)

R: Radius of the spherical head, 4 mm

C_{α}: A coefficient regarding the geometry of the joint. Suggested as $3\pi/8$ for the full contact spherical joint in the study.

μ: Coefficient of friction, 0.3

To calculate frictional moment, force applied by screws 4 should be estimated first. For this purpose equation 8.27 from Shigley's Mechanical Engineering Design (Budynas & Nisbett, 2008) is used:

$$T = KFd \qquad (3.2)$$

Where:

T: Torque applied to the screw

d: Major diameter

K: Torque coefficient, tabulated for steel and can be calculated as: (equation 8.26 from Shigley's Mechanical Engineering Design)

$$K = \left(\frac{d_m}{2d}\right)\left(\frac{tan\lambda + f\,sec\alpha}{1 - f\,tan\lambda\,sec\alpha}\right) + 0.625 f_c \qquad (3.3)$$

Where:

$$d_m = \frac{d + d_r}{2}$$

$$tan\lambda = \frac{l}{\pi\, d_m}$$

In this case values are:

$$d = 6\ mm$$
$$d_r = 5\ mm$$
$$l = 5.5\ mm$$
$$f_c = 0$$
$$f = 0.3$$
$$\alpha = 30°$$

Note that f_c is collar friction coefficient and the collar does not exist in the design. α is half the thread angle and its value is standardized. Using these values in Equation 3.3:

$$K = 0.342$$

To obtain F using Equation 3.2, a torque value should be assumed. This assumption is made as 40 N force applied using an equipment with 50 mm moment arm, hence:

$$T = 40 \times 50 = 2000\ N \cdot mm$$

Using the diameter 6 mm:

$$F = \frac{T}{Kd} = 973\ N$$

Now that the force is decided, it can be used in Equation 3.1 to get frictional moment on the spherical head of the bone screw. Note that there are two screws applying this force, so twice the value will be used.

$$M_f = 2FRC_\alpha \frac{\mu}{\sqrt{1+\mu^2}} = 2636\ N \cdot mm$$

Now the moment load on the bone screw will be calculated. The portion of the bone screw in the bone is 30 mm long, and the load suggested by the medical doctors, 147.15 N is assumed to be uniformly distributed on the screw. Hence the moment load is:

$$M_l = 147.15 \times 15 = 2207\ N \cdot mm$$

Since the screw head is spherical, frictional moment calculated is valid for every direction. Frictional moment exceeds the moment caused by the loading, therefore the bone screw is fixed successfully. One final remark about this issue is that Faraz and Payandeh stated that for the full contact spherical joint, their work has 15% error. Considering the worst case in this calculation, 85% of frictional moment is 2241 N·mm and still exceeds the loading moment.

A preliminary mechanical analysis is conducted for this design using ANSYS Software. Boundary conditions can be seen in Figure 17:

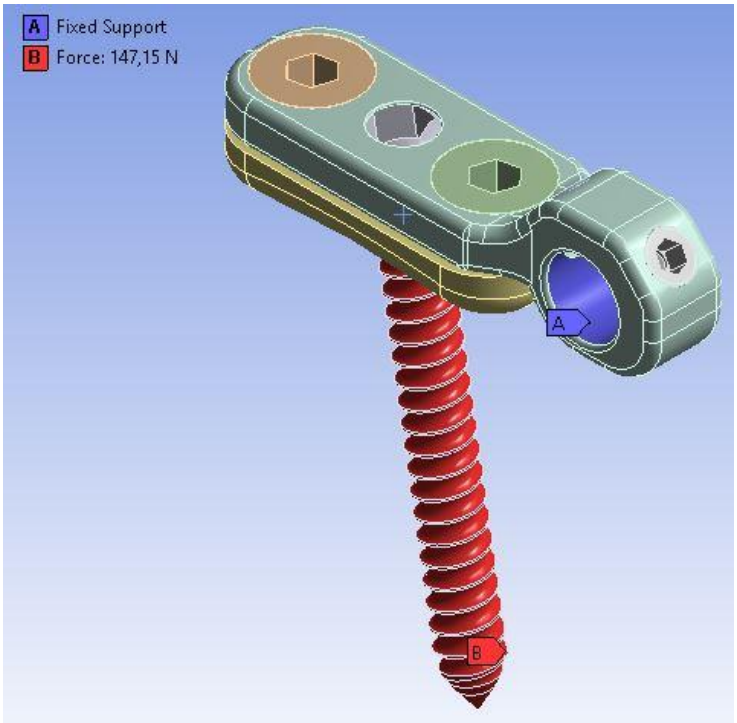

Figure 17: Type 1 Finite Element Analysis Boundary Conditions

As can be seen, the assembly is assumed to be perfectly fixed on the rod. The other boundary condition is that, 147.15 N force (equivalent to 15 kgf, which is the load suggested by the medical doctors for the humerus) is applied on the bone screw. Note that by elementary mechanics, this force is also applied to the rod. From Shigley's Mechanical Engineering Design Table 7.4 (Budynas & Nisbett, 2008) for #8 (4.166 mm diameter) alloy steel set screw against steel shaft, holding power is 1713 N. It should be noted that holding power is actually a force, but curiously named as such in the source provided. To avoid misunderstanding, the term "holding force" will be used from now on. Since the working principle of the set screw is based on friction force; assuming a linear friction model, titanium against titanium holding force value can be obtained by multiplying the holding force with the fraction of coefficients of friction, which are 0.3 for titanium-titanium and 0.8 for medical grade steel-steel:

$$F_{holding} = 1713 \times \frac{0.3}{0.8} = 642\ N$$

With the aforementioned assumptions, holding force of the set screw is found as 642 N in both axial and tangential directions. In this case axial force is important and it is found to be well above 147.15 N, hence the first boundary condition of fixed support is justified. Note that the diameter and length of the set screw are 4 and 3.3 mm, respectively. The dimensions also satisfy the suggestion in Shigley's Mechanical Engineering Design that the set screw length should be at least half of the rod diameter, which is 6 mm in the design. Using the two boundary conditions and bonded contacts, equivalent Von-Mises stress results are obtained.

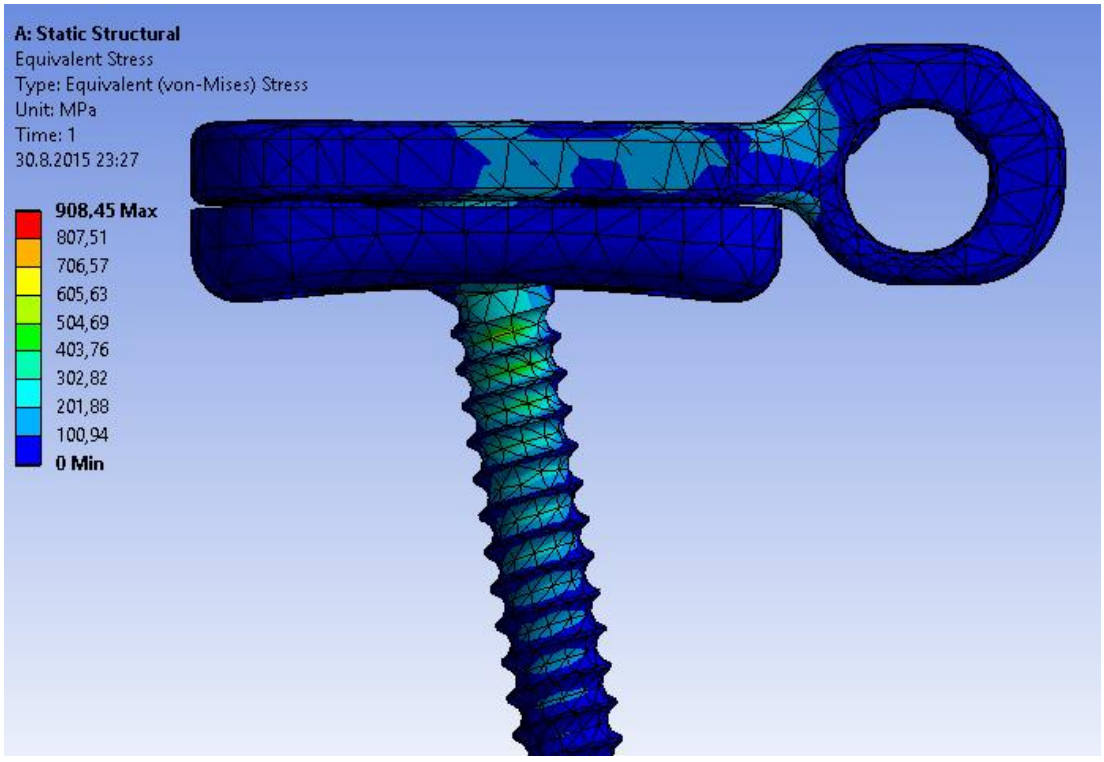

Figure 18: Type 1 Equivalent Stress Results

It can be seen from Figure 18 that maximum stress is dangerously close to the yield strength of Ti6Al4V, however, these high stress regions are very local suggesting that stress concentration is observed. It should be noted that the assembly is planned to work in at least pairs (connected to different fracture fragments) so one assembly carrying the whole load is actually a worst case scenario. One other concern of this

design (and similar designs that will follow) is that the polyaxial screw should be rigidly fixed by the screws 4. The axial clamping force of the screws is related to torque applied by the surgeon. For this purpose, for the final design (not the preliminary ones) experiments will be presented in this study and a safe torque value to use the design will be suggested. To sum up, obviously not being perfect, the design is mechanically promising and worthy of interest. However, the difficulties in assembly, especially in the messy environment of the human body, caused this design to be eliminated, instead of improved. There are four small screws in the design. More importantly, one of the set screws will be facing away from the medical doctor during the surgery, making it problematic to be tightened. Finite element details can be seen in Table 5.

Table 5: Mesh Statistics for Type 1 FEA

Nodes	37299
Elements	20015
Mesh Metric	Element Quality
Min	7.0158E-04
Max	0.9999
Average	0.6581
Standard Deviation	0.2072
Element Type	10 Noded Tetrahedral

Element quality will be used as a mesh metric in the rest of the study so it should be explained. It is a geometric quantity for which a value of 1 indicates a perfect 3D element (for instance, a perfect cube) while a value of 0 indicates the element has zero volume (ANSYS Inc, 2013). The element quality is defined as:

$$Quality = C\left(\frac{volume}{\sqrt{\sum(Edgelength^2)^3}}\right)$$

C is a constant whose values are presented in Table 6.

Table 6: Values of C for Various Element Geometries

Triangle	6.928
Quadrangle	4.0
Tetrahedron	124.7
Hexagon	41.57
Wedge	62.35
Pyramid	96

Ten noded tetrahedral element is also used throughout the study. The element shape and the locations of the nodes are presented in Figure 19.

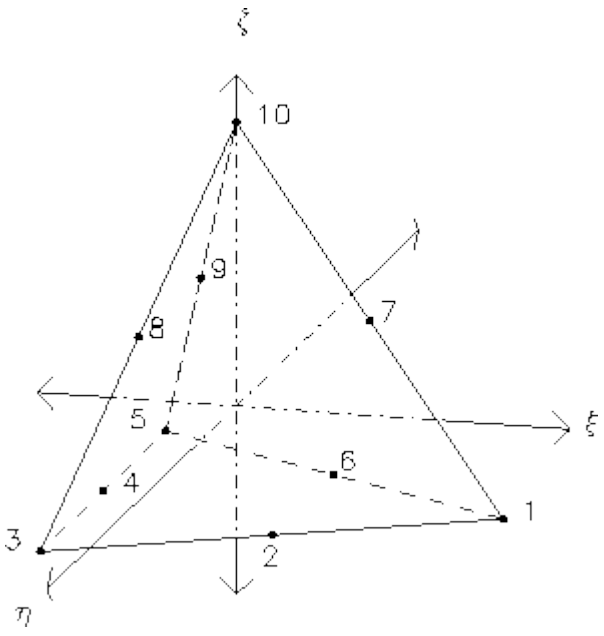

Figure 19: Sample 10 Noded Element (Greenough, 2000)

3.2 Type 2 Revision 1

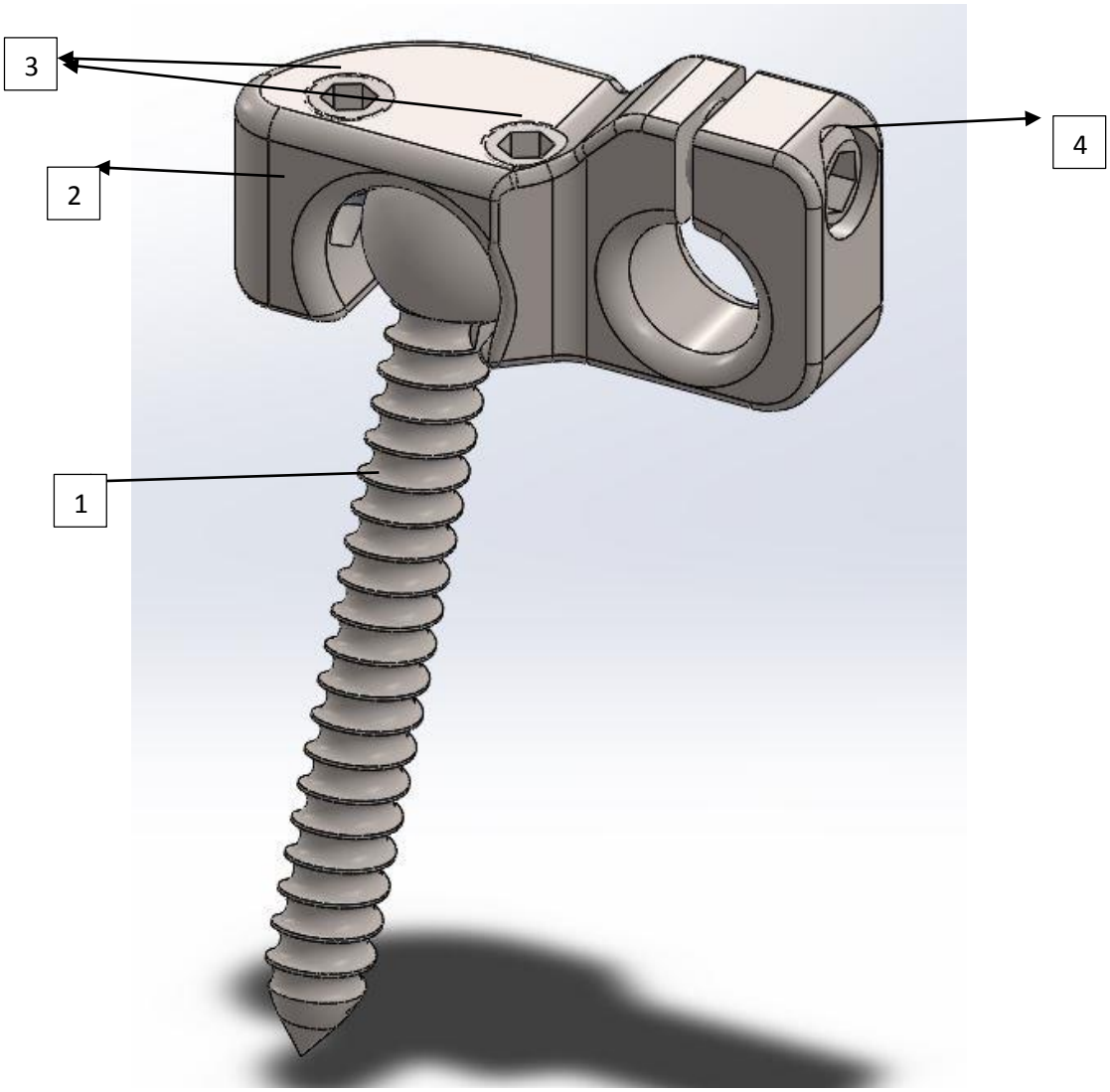

Figure 20: Type 2 Revision 1 3D Model (1: Bone Screw, 2: Base, 3: Set Screws, 4: Clamping Screw)

In this design bone screw 1 is similar to the one in Type 1. Set screws 3 are tightened on plate 2 to fix the bone screw. To fix the assembly on the rod, plate 2 is deformed by screw 4. Since set screws are discussed earlier, one of the main concerns for this design is fixing the assembly on the rod. First, the clamping force provided by screw 4 should be decided. For this purpose, Equation 3.2 will be used again with the same torque assumption of 2000 N·mm. Equation 3.3 also should be used to determine K for this screw. Everything except the geometry is the same, dimensions are:

$$d = 4.5\ mm$$
$$d_r = 3.1\ mm$$
$$l = 7.5\ mm$$

With these dimensions K, torque coefficient and F, force applied by the screw are:

$$K = 0.526$$
$$F = 1001\ N$$

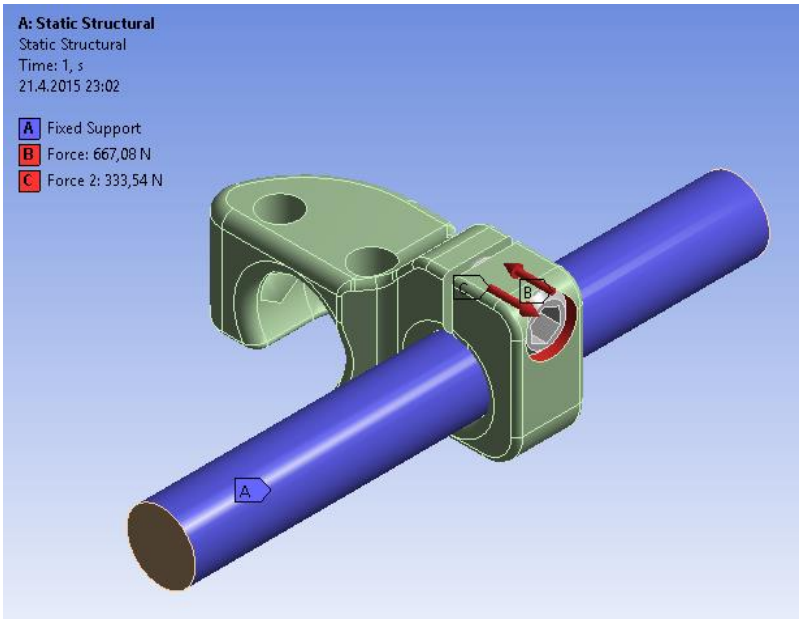

Figure 21: Type 2 Revision 1 Clamping Force Analysis Boundary Conditions

As can be seen, rod is also added and assumed fixed. Total clamping force of 1001 N is divided to three contact surfaces of the screw which are two threaded surfaces and the counterbore surface. Bone screw and set screws are excluded to save computational time.

The force reaction directly from the finite element analysis will be used to obtain friction force. Obviously, friction force should be obtained from normal force whereas the force reaction is not exactly normal, but it will be assumed so.

Total force reaction on the rod is computed as 341 N and detailed information on the mesh can be seen in Table 7. To calculate the axial fixing force of the assembly on the rod, this force should be multiplied with the friction coefficient of 0.3.

$$F_f = 341 \times 0.3 = 102\ N$$

The axial friction force, 102 N is less than the load suggested by the medical doctors, 147.15 N. As in Type 1, this is a worst case scenario but this design is not safe in terms of fixation of the assembly on the rod, hence the design is eliminated and no further analysis is done. Mesh statistics of the finite element analysis can be seen in Table 7.

Table 7: Type 2 Revision 1 FEA Mesh Statistics

Nodes	88789
Elements	35790
Mesh Metric	Element Quality
Min	3.079E-02
Max	0.9995
Average	0.8138
Standard Deviation	0.1253
Element Type	10 Noded Tetrahedral

3.3 Type 2 Revision 2

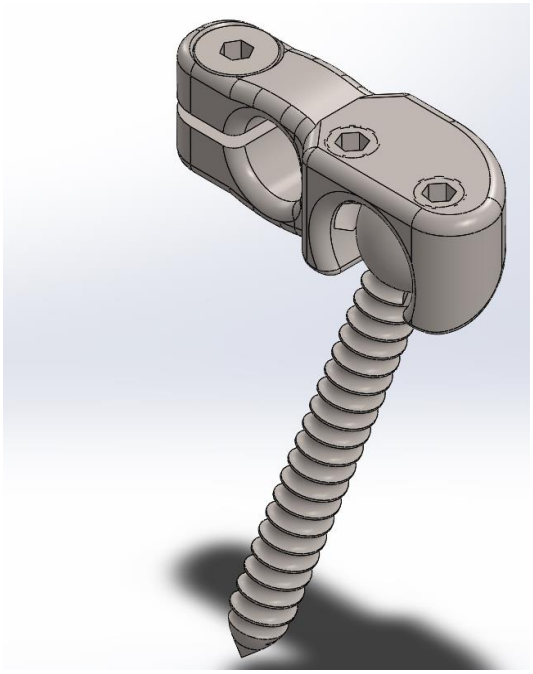

Figure 22: Type 2 Revision 2 3D Model

This design is very similar to Type 2 Revision 1, only difference being the fixation mechanism of the assembly and the rod. Hence, the mechanical concerns are similar

and fixation on the rod will be checked first. Equations 3.2 and 3.3 will be used with the following screw dimensions:

$$d = 4\ mm$$
$$d_r = 3.2\ mm$$
$$l = 7.3\ mm$$

Leading to K and F values of:

$$K = 0.575$$
$$F = 966\ N$$

To decide the force applied on the rod, finite element analysis will be used. Boundary conditions can be seen in Figure 23.

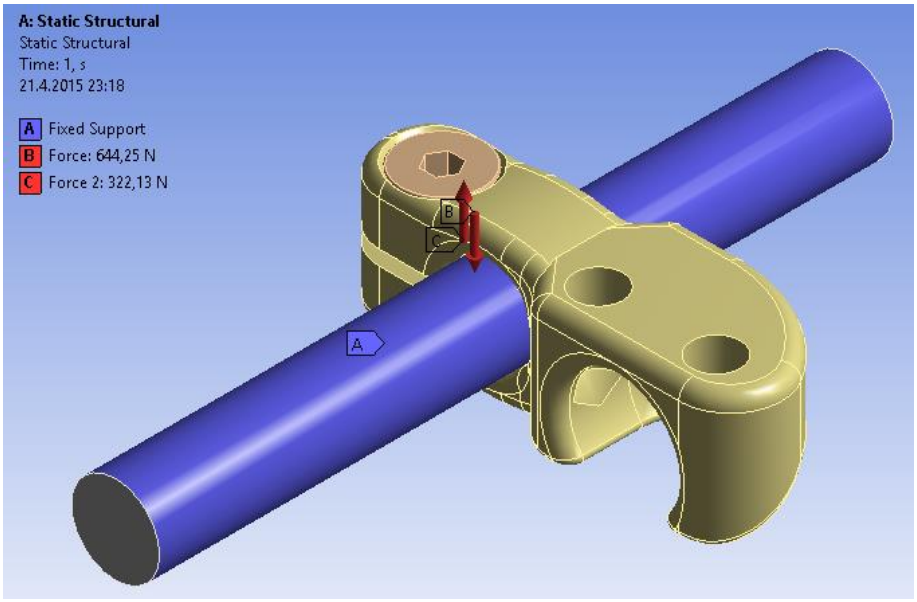

Figure 23: Type 2 Revision 2 Clamping Force Analysis Boundary Conditions

Boundary conditions are naturally similar to the ones in Type 2 Revision 1 analysis. Rod is fixed and clamping force is distributed to three contact surfaces. Force reaction on the rod will be assumed as normal force. Force on the rod is computed to be 323 N. To calculate the friction force:

$$F_f = 323 \times 0.3 = 97\ N$$

Hence this design does not offer any improvements on fixation of the assembly on the rod, in fact friction force is slightly less. To sum up, the design is eliminated and no further analysis will be conducted. The details of the mesh can be seen in Table 8.

Table 8: Type 2 Revision 2 FEA Mesh Statistics

Nodes	54875
Elements	23545
Mesh Metric	Element Quality
Min	7.3580E-02
Max	0.9999
Average	0.7865
Standard Deviation	0.1433
Element Type	10 Noded Tetrahedral

3.4 Type 2 Revision 3

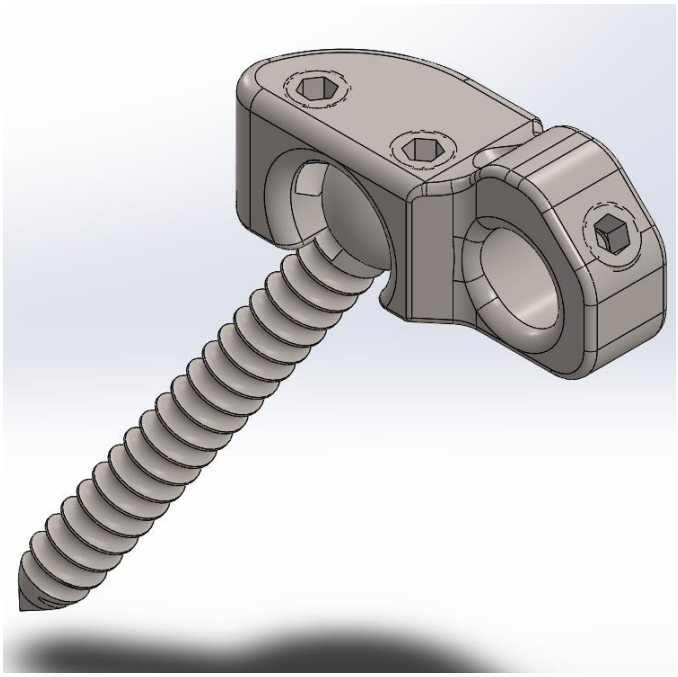

Figure 24: Type 2 Revision 3 3D Model

In this revision fixation on the rod system is changed from deformation to two 4 mm diameter set screws. Such set screws are discussed earlier in Type 1 and shown to be successfully fixing the assembly on the rod. Another major mechanical concern is fixation of the spherical bone screw head, which is done by set screws in this design. Note that the holding force that was calculated earlier in the analysis of Type 1 , 642 N apply to both axial holding force for resisting thrust and tangential holding force for resisting torsion, hence the same amount of force acts on the spherical head by each set screw (Budynas & Nisbett, 2008). Since two set screws are present, a total force of 1285 N will be used in Equation 3.1. Another value that is different from earlier analysis is C_α since the spherical head is not in full contact in this design. In the aforementioned study (Faraz & Payandeh, 2001) a range of 1.01 to 1.17 is suggested for partial contact; to be on the safe side, 1.01 will be used in the analysis. Spherical head radius, R and coefficient of friction μ remain unchanged; 4 mm and 0.3 respectively. Using these values

$$M_f = 1491\ N \cdot mm$$

Which is less than the loading moment of 2207 N·mm, hence the set screws cannot fix the bone screw successfully. Therefore this design too, is eliminated.

3.5 Type 3

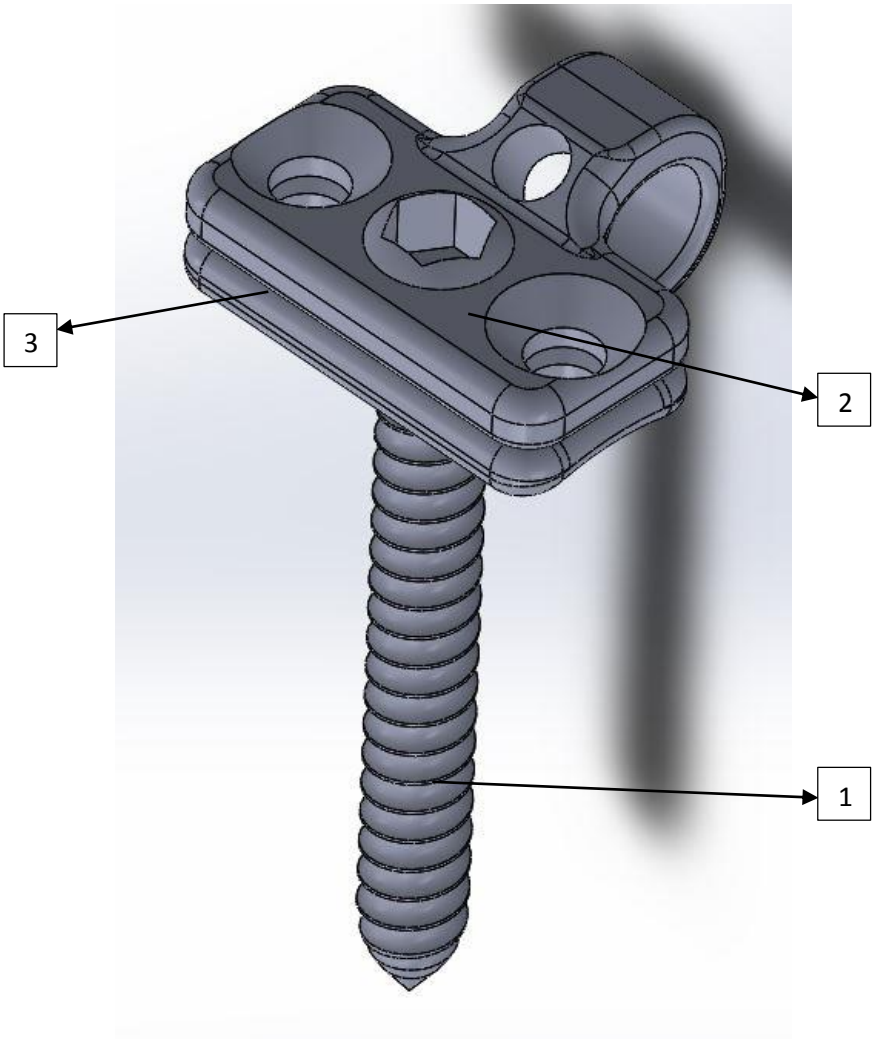

Figure 25: Type 3 3D Model (1: Bone Screw, 2: Base Top Part, 3: Base Bottom Part)

In this design, bone screw 1 is the same as the other designs. Spherical bone screw head is fixed between parts 2 and 3, which are pressed together with two screws. The

assembly is fixed on the rod using a set screw. Rod and screws are excluded in the assembly.

A procedure similar to Type 1 and Type 2 designs will be followed for the analysis. First the fixation of the assembly on the rod will be checked. Set screw diameter in this design is 3.3 mm. Referring to Table 7.4 from Shigley's Mechanical Engineering Design (Budynas & Nisbett, 2008) again, for #5 (3.17 mm diameter) steel set screw, holding force is 890 N. With the Coulomb dry friction model assumption, in titanium the holding force will be:

$$F_{holding} = 890 \times \frac{0.3}{0.8} = 334\ N$$

Which exceeds the load suggested by the medical doctors, 147.15 N so the assembly will not slide on the rod.

Another aspect of mechanical importance is the fixation of the bone screw. Equations 3.1, 3.2 and 3.3 will be used again, with the values:

$$d = 3.3\ mm$$
$$d_r = 3.3\ mm$$
$$l = 4.65\ mm$$
$$C_\alpha = 1.01$$

The screw has a uniform diameter hence the same values. Furthermore, the spherical joint is not in full contact, so the safe value of 1.01 is used for C_α. Same torque assumption of 2000 N·mm is applied and the results for K, F (for each screw) and M (total frictional moment) are:

$$K = 0.471$$
$$F = 1288\ N$$
$$M_f = 2990\ \ N \cdot mm$$

Since the total frictional moment exceeds the loading moment of 2207 N·mm, it can be said that the screws successfully fix the spherical head of the bone screw.

It is shown that the assembly will be rigidly fixed, now the stress under the loading conditions in the body will be evaluated using finite element analysis.

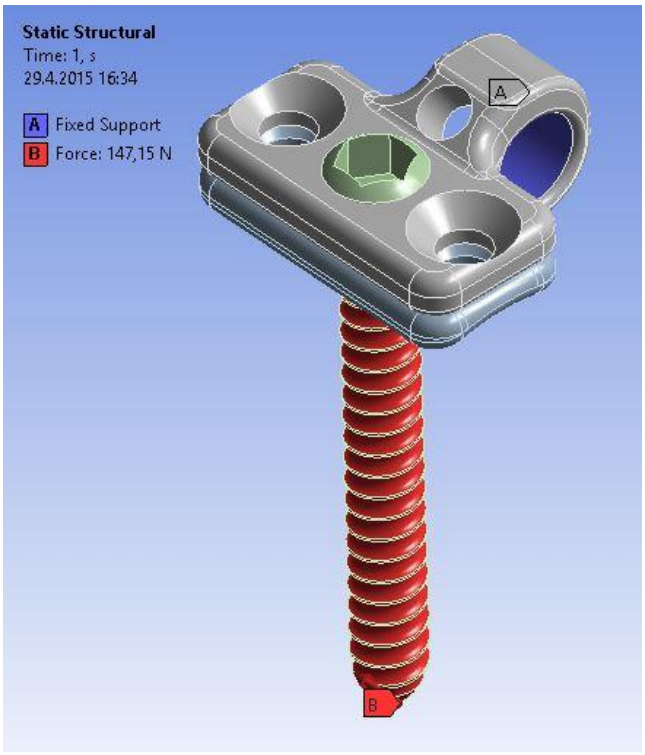

Figure 26: Type 3 Finite Element Analysis Boundary Conditions

As seen in Figure 26, the assembly is assumed fixed on the rod and the load is applied on the bone screw in the direction of the rod.

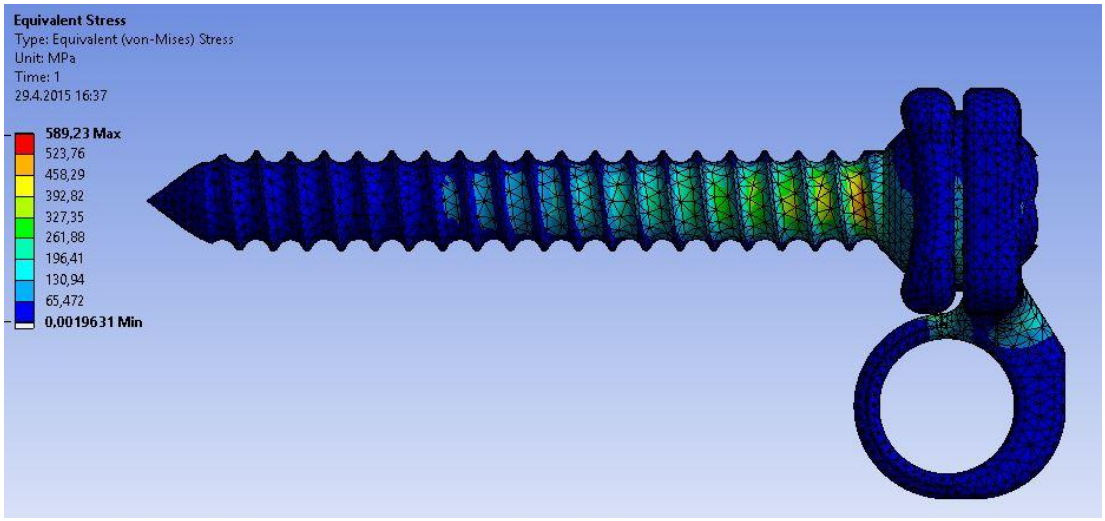

Figure 27: Type 3 Equivalent Stress Results

Figure 27 shows the finite element analysis results. Maximum stress is 589 MPa, near the head of the bone screw, expectedly. Design is safe hence similar design alternatives will follow. Details of the finite element analysis can be seen in Table 9.

Table 9: Type 3 FEA Mesh Statistics

Nodes	82177
Elements	48270
Mesh Metric	Element Quality
Min	1.1411E-03
Max	1
Average	0.7596
Standard Deviation	0.1454
Element Type	10 Noded Tetrahedral

3.6 Type 4

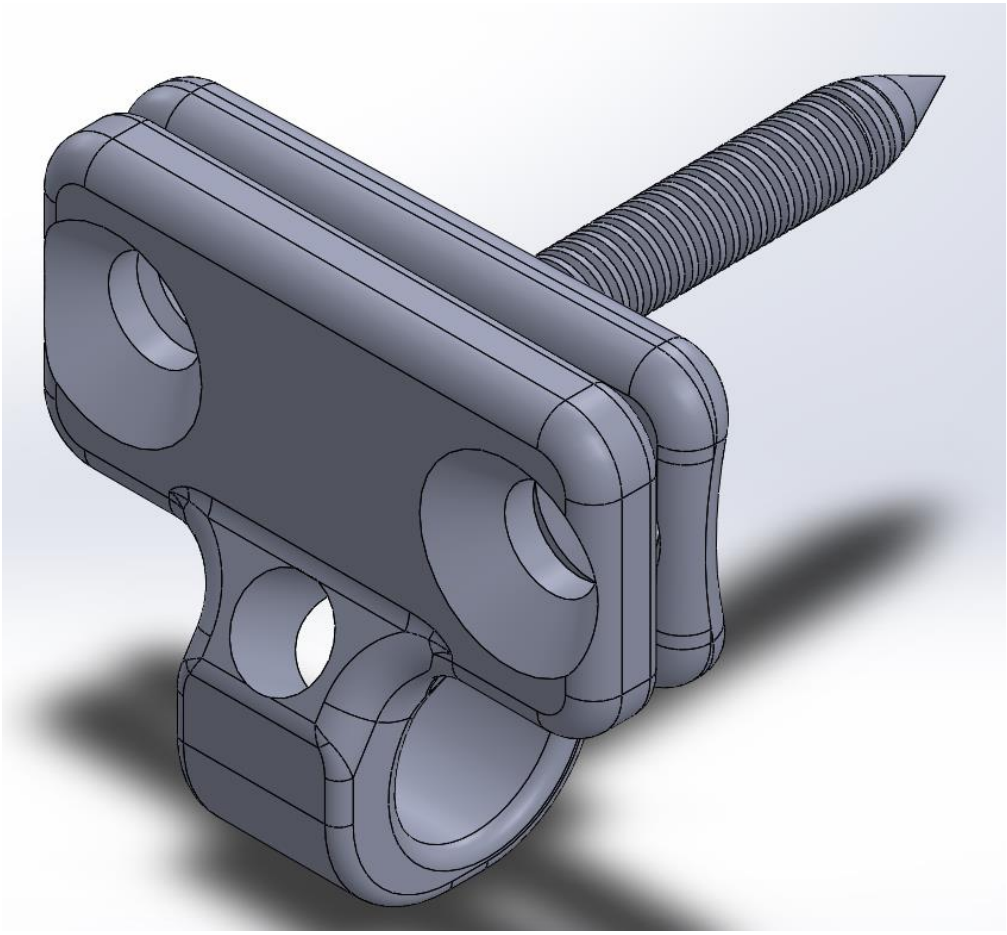

Figure 28: Type 4 3D Model

Type 4 is very similar to Type 3, only differences being the full coverage of the spherical screw head and some dimensional differences, which will be presented later. An increase in fixation of the screw head and a decrease in the open space in the body (hence less tissue formation and probability of infection) are presumed.

Length of the screws is decreased to 4.5 mm, which was 4.65 mm in Type 3. Additionally, C_α is increased to $3\pi/8$ according to aforementioned study (Faraz & Payandeh, 2001). The radius of the spherical bone head is decreased to 2.75 mm. The rest of the geometry remains the same with Type 3. With smaller dimensions, comfort

of the patient can be increased. With these values, using Equations 3.1, 3.2 and 3.3 the results are:

$$K = 0.459$$
$$F = 1320\ N$$
$$M_f = 2457\ \ N \cdot mm$$

As can be seen, force of each screw increases slightly due to decreased length of the screw, however even with the increased force and increased contact in the joint, the frictional moment decreases due to decrease in its radius. Still, the frictional moment exceeds the loading moment, hence the design is safe regarding rotational degree of freedom of the bone screw.

Fixation of the assembly on the rod is the same as Type 3 both geometrically and as a method, therefore the same performance is expected. Since fixation of the design is justified, stresses in the body will be analyzed using finite element method.

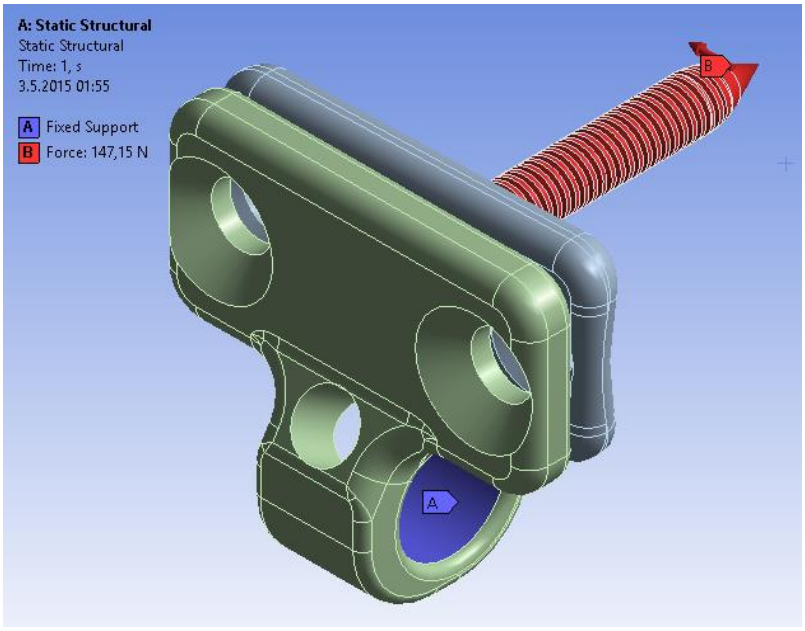

Figure 29: Type 4 Finite Element Analysis Boundary Conditions

Boundary conditions for the finite element analysis can be seen in Figure 29. Similar to the analysis of previous types, the assembly is assumed fixed on the rod and evenly distributed load of 147.15 N is applied on the bone screw.

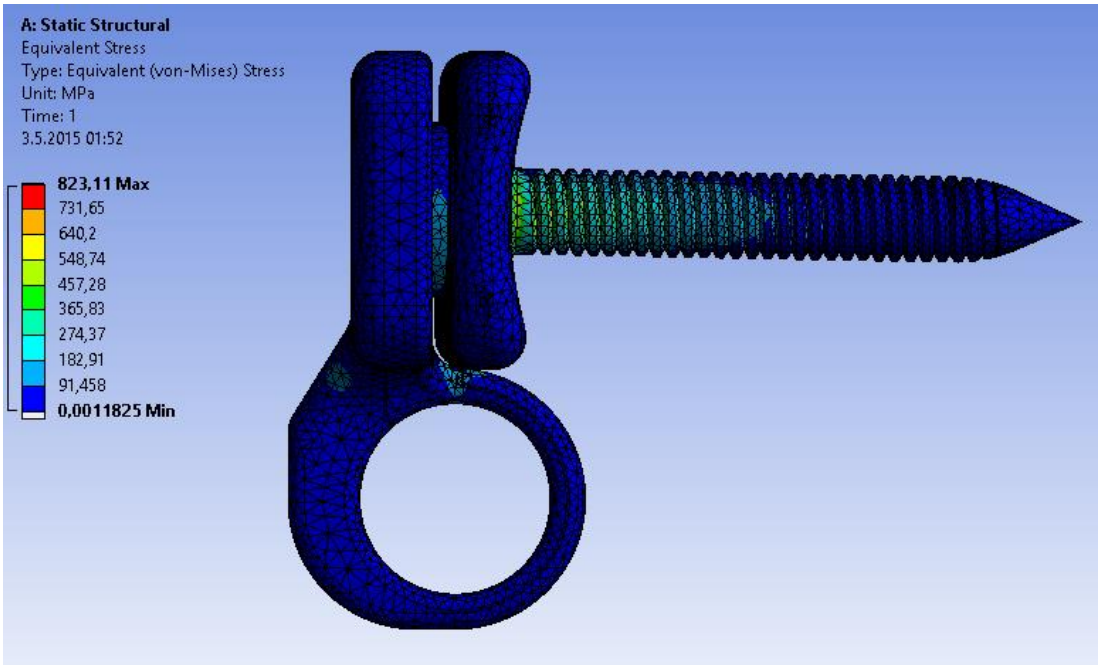

Figure 30: Type 4 Equivalent Stress Results

Equivalent stress results of the assembly can be seen in Figure 30. Expectedly, maximum stress occurs near the spherical head of the screw. On the other hand, still being less than yield strength of Ti6Al4V, maximum stress increased compared to Type 3, due to dimensions getting smaller. An obvious drawback of the system is the assembly. Since the spherical head of the bone screw cannot be reached from above, the surgeon must place the bottom part, then fix the bone screw, finally fix the top part of the assembly. To sum up, having satisfactory mechanical properties, the design should be improved further. Details of the mesh used in finite element analysis can be seen in Table 10.

Table 10: Type 4 FEA Mesh Statistics

Nodes	127446
Elements	76158
Mesh Metric	Element Quality
Min	1.7659E-03
Max	1
Average	0.7818
Standard Deviation	0.1231
Element Type	10 Noded Tetrahedral

3.7 Type 5

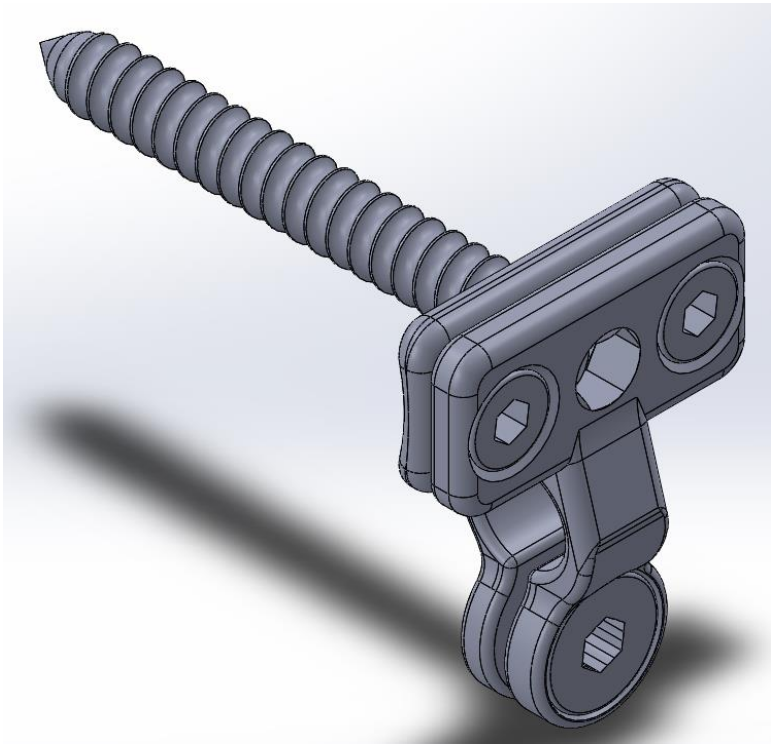

Figure 31: Type 5 3D Model

In this design full contact spherical joint concept from Type 4 is abandoned and spherical head of the bone screw is reachable by the surgeon, like in Type 3. Additionally, the mechanism of fixation on the screw is changed from set screw to deformation of the assembly. There are also geometrical changes, which will be presented in the related analyses.

First of all, fixation of the assembly on the rod will be examined, since the concept was problematic in Type 2. Using Equations 3.2 and 3.3 with the assumed torque of 2000 N·mm and following screw geometry:

$$d = 5\ mm$$
$$d_r = 5\ mm$$
$$l = 5.5\ mm$$

Leading to results:

$$K = 0.396$$

$$F = 1009\ N$$

This force will be used in finite element analysis to obtain the force exerted on the rod, which will then be used to obtain friction force resisting sliding on the rod.

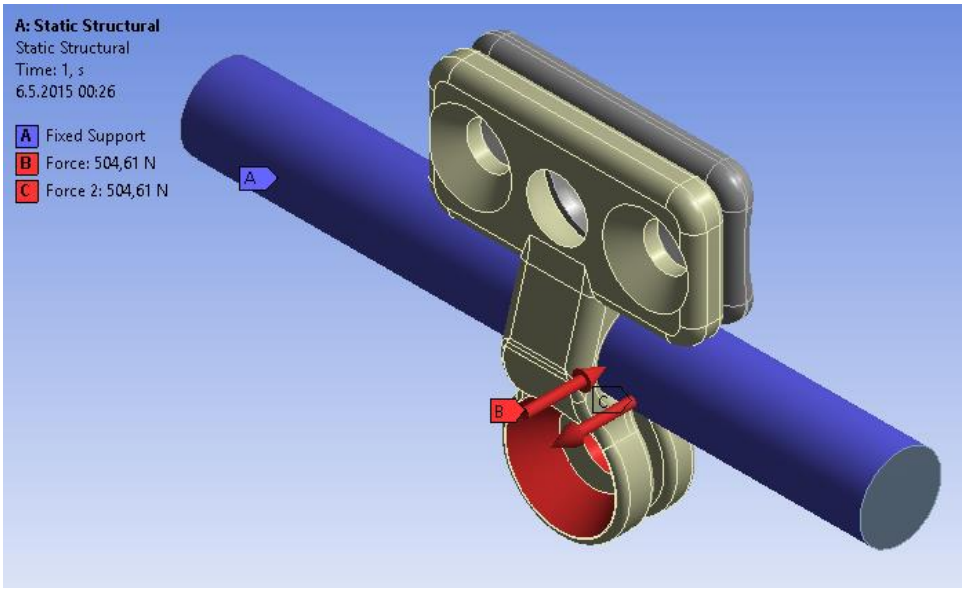

Figure 32: Type 5 Clamping Force Analysis Boundary Conditions

As can be seen in Figure 32, rod is assumed fixed and the force of the screw is distributed to two surfaces. Total reaction force obtained from finite element analysis will be used. Total reaction force on the rod is computed as 692 N and the mesh details on the analysis can be found in Table 11.

Table 11: Type 5 Clamping FEA Mesh Statistics

Nodes	41287	
Elements	15182	
Mesh Metric	Element Quality	
Min	0.02882	
Max	0.9998	
Average	0.7605	
Standard Deviation	0.1732	
Element Type	Rod	20 Noded Hexahedral (Dominant) and 15 Noded Wedge
	Base	10 Noded Tetrahedral

20 noded hexahedral and 15 noded wedge sample elements are presented in Figure 33 and Figure 34 respectively.

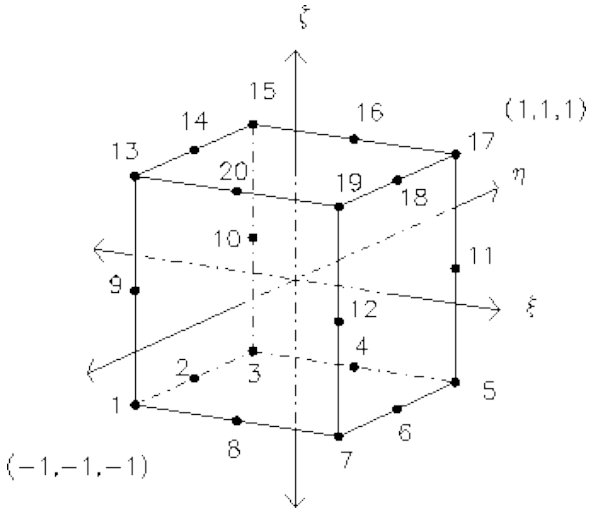

Figure 33: Sample 20 Noded Hexahedral Element (Greenough, 2000)

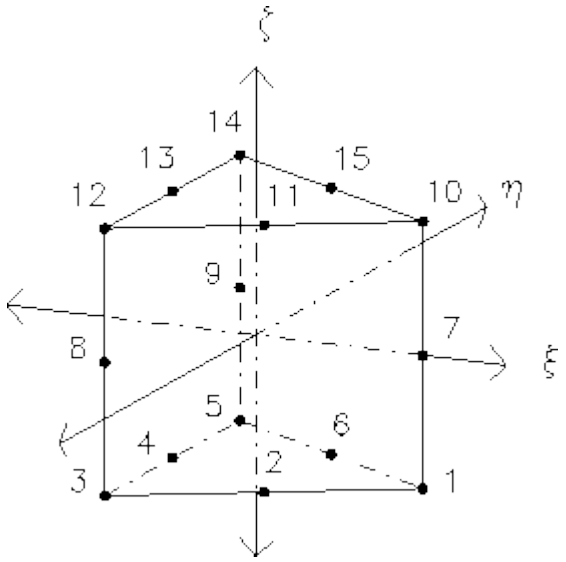

Figure 34: Sample 15 Noded Wedge Element (Greenough, 2000)

To obtain the friction force, friction coefficient will be multiplied with the force from the finite element analysis:

$$F_f = 692 \times 0.3 = 208\ N$$

Which exceeds 147.15 N, indicating that the assembly is successfully fixed on the rod and will not slide. Analysis on the fixation of spherical bone screw head will be examined, once again using Equations 3.1, 3.2 and 3.3 with the values:

$$d = 3\ mm$$
$$d_r = 4\ mm$$
$$l = 4.75\ mm$$
$$C_\alpha = 1.01$$

Note that for C_α safe value of 1.01 is used again since the spherical joint is in partial contact in this design. Results are:

$$K = 0.400$$
$$F = 1426\ N$$
$$M_f = 2456\ \ N \cdot mm$$

Since frictional moment exceeds the loading moment of 2207 N·mm the rotational degree of freedom of the spherical bone head is constrained successfully by two screws. Now that the fixation of the assembly is justified, stresses in the design will be examined using finite element analysis.

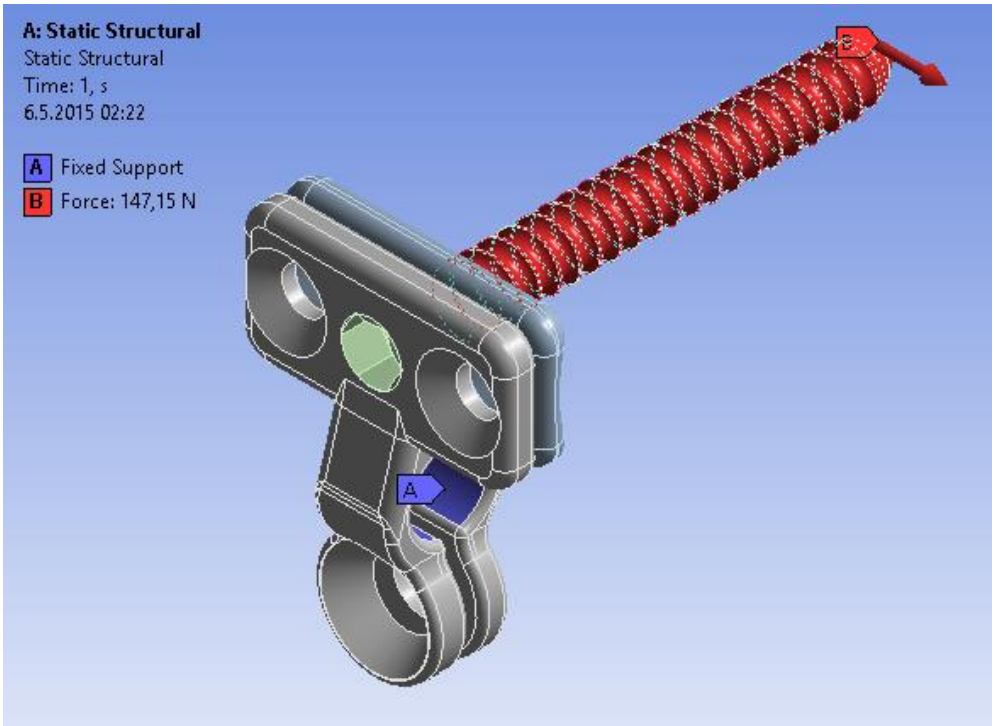

Figure 35: Type 5 Stress Analysis Boundary Conditions

The assembly is assumed fixed on the rod, which was justified earlier. 147.15 N load is applied on the bone screw uniformly. The other screws and the rod are excluded to save computational time.

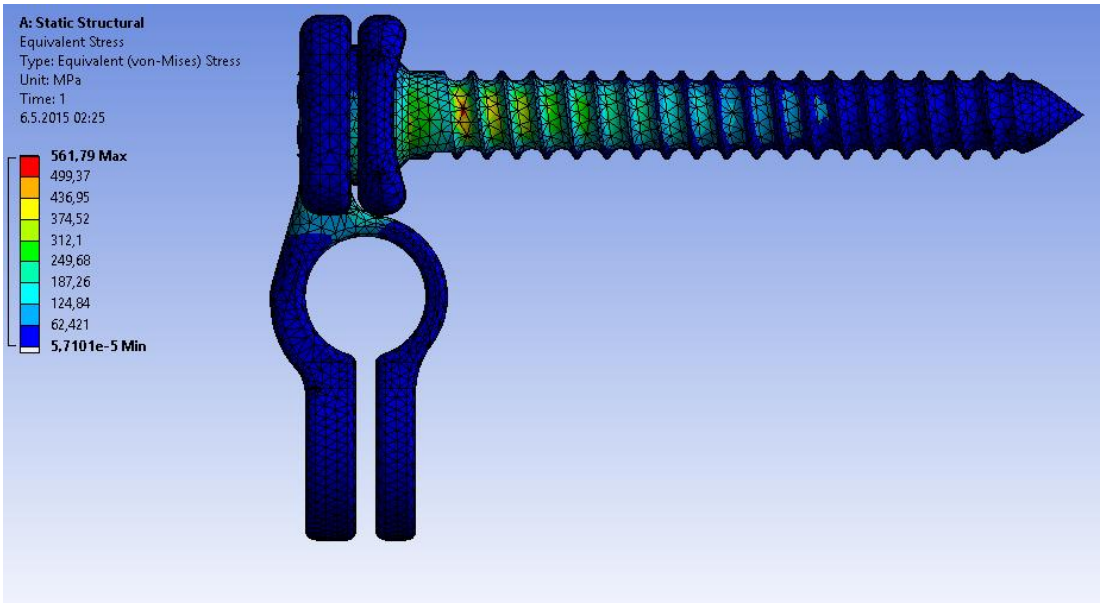

Figure 36: Type 5 Equivalent Stress Results

As can be seen in Figure 36 maximum stress on the assembly is 562 MPa. Results are satisfactory and the design can be considered to be mechanically competent. No apparent medical inadequacies or assembly problems are present. However the effort to make the design more compact to increase patient comfort continues. Mesh details of the analysis can be seen in Table 12.

Table 12: Type 5 FEA Mesh Statistics

Nodes	76871
Elements	44469
Mesh Metric	Element Quality
Min	4.3897E-02
Max	1
Average	0.7576
Standard Deviation	0.1473
Element Type	10 Noded Tetrahedral

CHAPTER 4

FINAL DESIGN

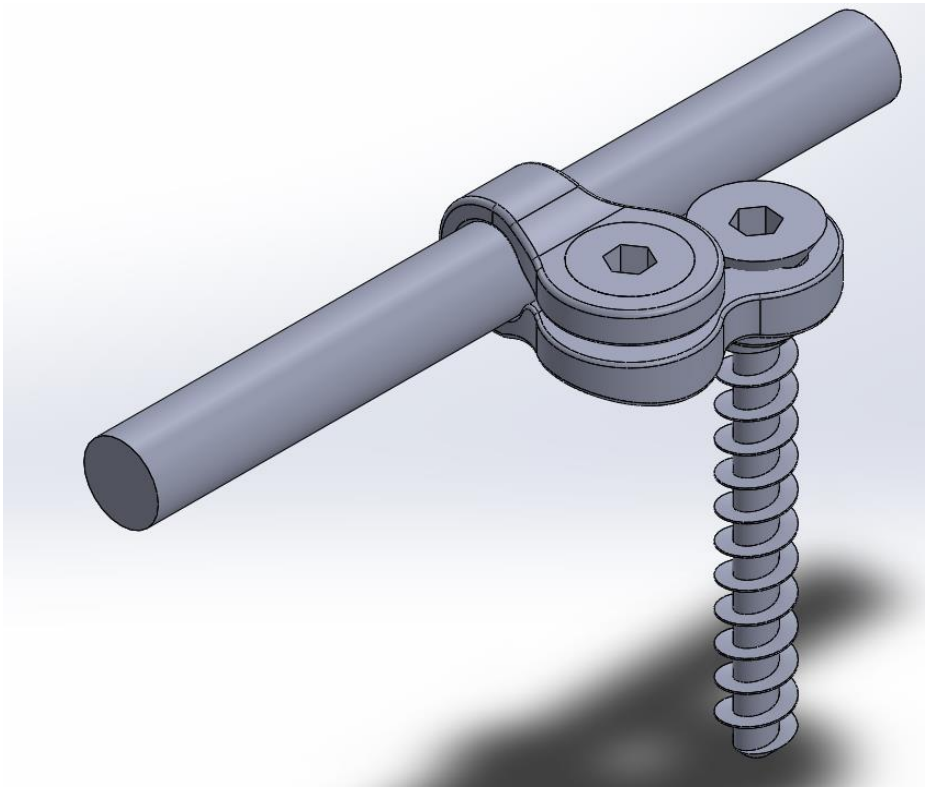

Figure 37: Final Design 3D Model

Final design uses the concept of compression by a screw to fix the base on the rod, similar to some of the early designs. Due to decision of medical doctors, multi-axial screw instead of poly-axial screw is used. Base part has 4 slots for the bone screw to be fixed to, providing the medical doctors angular freedom with certain increments whereas a poly-axial screw has a spherical head, so some of the degree of freedom is lost compared to conceptual designs. Self-tapping design of the bone screw is another important feature of the bone screw. Additionally, the face of the base part that is in contact with the bone is shaped with a relatively large radius to reduce contact on the bone, hence decreasing the negative effects on the nourishment of the bone during

healing. 3D models of each part are presented separately in Figure 38, Figure 39 and Figure 40. The technical drawings can be seen in Appendix B.

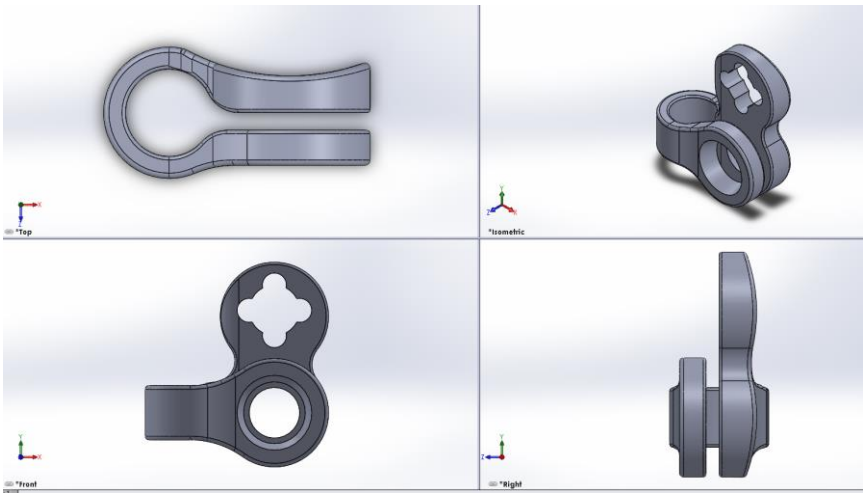

Figure 38: Final Design Base 3D Model

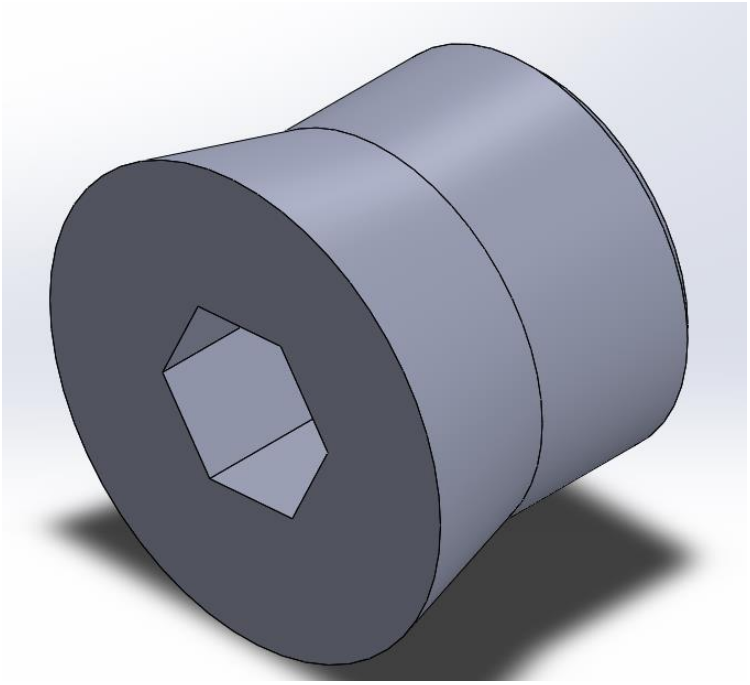

Figure 39: Final Design Screw 3D Model

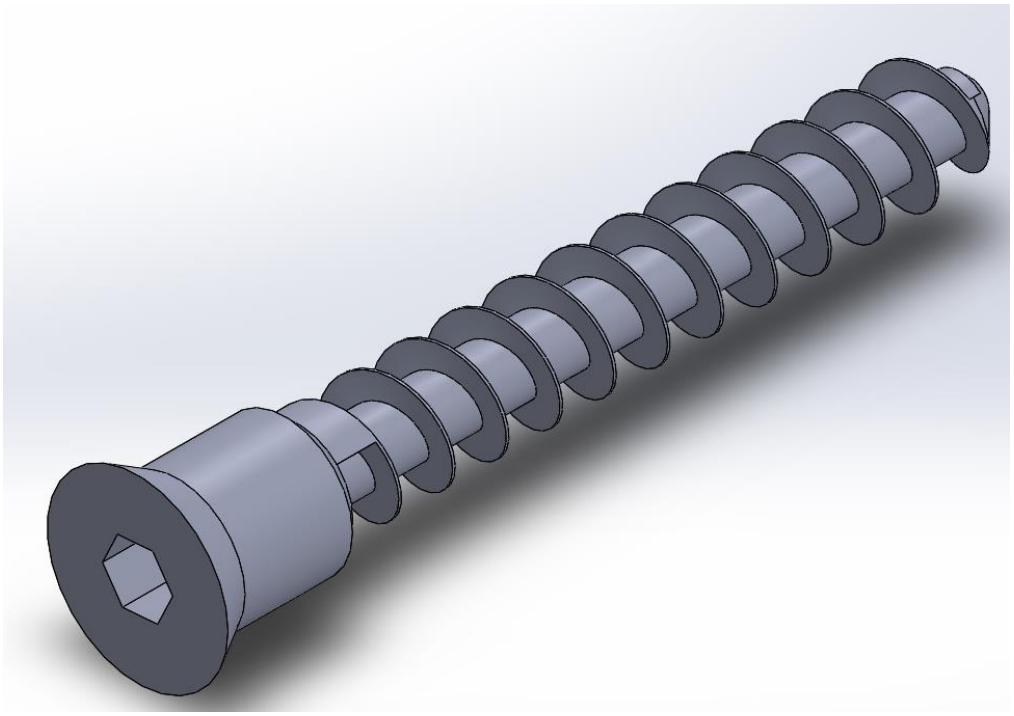

Figure 40: Final Design Bone Screw 3D Model

4.1 Analysis

4.1.1. Worst Case Loading Analysis

Even though the medical doctors suggested a purely axial 147.15 N loading as a design criteria, to find the worst loading case a 360° rotation of the humerus around the shoulder is investigated. A 147.15 N load constantly towards the ground, i.e. weight, is assumed at the hand of the patient as a very conservative approximation. Obviously some interval of this weight carrying is very unnatural for a human being, none the less whole rotation is examined for the sake of completion. The patients are strongly recommended to avoid swift moves so inertia effects are disregarded. Moreover, weight of the bones is calculated to be 0.15 kg, negligible when compared to external load of 15 kg, so it is excluded in the analysis. Finally, humerus is assumed to be a

perfect hollow cylinder with 18 mm and 14 mm outer and inner diameters, respectively. (Lokanadham, Khaleel, & Raj, 2013) (Ma, 1992)

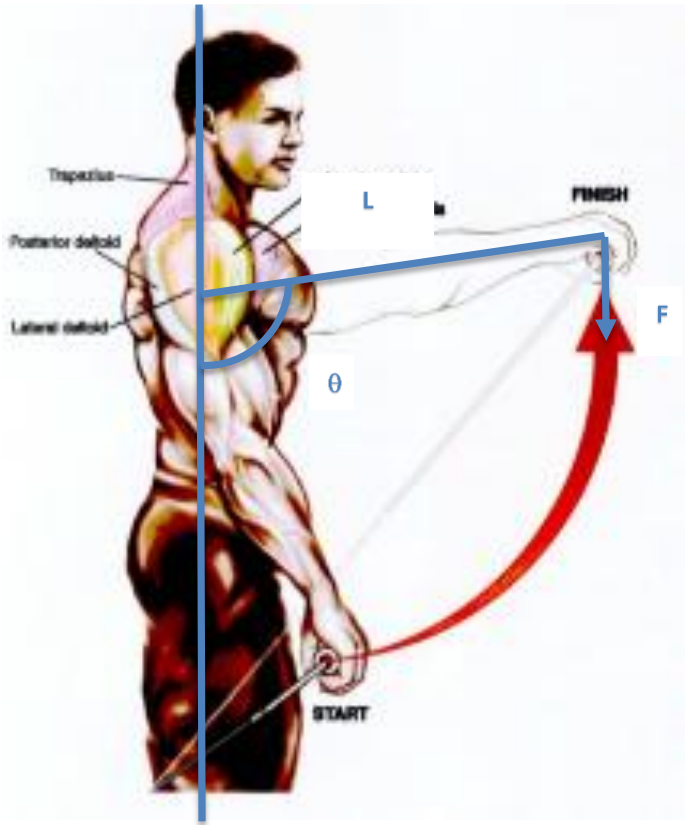

Figure 41: Representative Drawing for Worst Case Analysis (Piero, 2013)

From Figure 41:

$$F = 147.15\ N\ (Constantly\ vertical)$$

$$L = 300 + 270 = 570\ mm\ (Humerus + Forearm)$$

$$\theta: 0\ to\ 360°$$

$$F_{axial} = F \cdot \cos(\theta)$$

$$F_{bending} = F \cdot \sin(\theta)$$

$$A_{cs} = \pi \frac{d_{outer}^2 - d_{inner}^2}{4}\ (Cross\ sectional\ area\ of\ humerus)$$

$$\sigma_{axial} = \frac{F_{axial}}{A_{cs}}$$

$$I_{humerus} = \pi \frac{d_{outer}^4 - d_{inner}^4}{64}$$

$$M = F_{bending} \cdot L$$

$$c = \frac{d_{outer}}{2} = 9\ mm$$

$$\sigma_{bending} = \frac{Mc}{I_{humerus}}$$

Maximum normal stress due to axial load on the humerus obviously occurs when the arm is vertical and the calculated value is 1.47 MPa whereas maximum normal stress due to bending occurs when the arm is horizontal and its calculated value is 231 MPa. This value is too much even for a healthy person since average yield strength of human long bone is about 130 MPa. A daily observation alone would be sufficient to realize excluding soft tissue from bending analysis causes unrealistic stress results on the bone, so from now on the suggestion of medical doctors, purely axial 147.15 N will be considered as the design criteria. As a final remark, even though the analysis results are erroneous, the patients should still be advised to avoid lifting heavy loads, especially in ways leading to bending loads.

4.1.2. Load Sharing Analysis

In this part, the portion of the load that is carried by the humerus will be decided. Excessive loading of the fractured bone will lead to pain for the patient and even fracture again while insufficient loading may lead to so called stress shielding. Stress shielding effect is the implant carrying too much load while the bone carrying less than necessary, leading to weakening of the bone. To see how the rod and the bone shares the load, an analogy with springs in parallel connection is made. Stiffness of the humerus is calculated while the stiffness of bone screw-base-rod assembly is decided with the help of finite element analysis. The humerus is assumed as a perfect hollow cylinder. Since there is no Young's modulus data available for the stages during healing, the analysis will be performed on a healthy humerus first, then the results for several lower moduli of the bone will be presented to model load sharing for the stages

during healing. Moreover, bone is assumed isotropic, since the load is purely axial. A load of 147.15 N is applied in compression and finally load on each part is calculated. Representation of the analogy can be seen in Figure 42. Note that length of a human humerus is 300 mm, while rod is 130 mm. In the analysis, the portion of the humerus which is connected to the rod is used since only 130 mm of it will contribute to the stiffness.

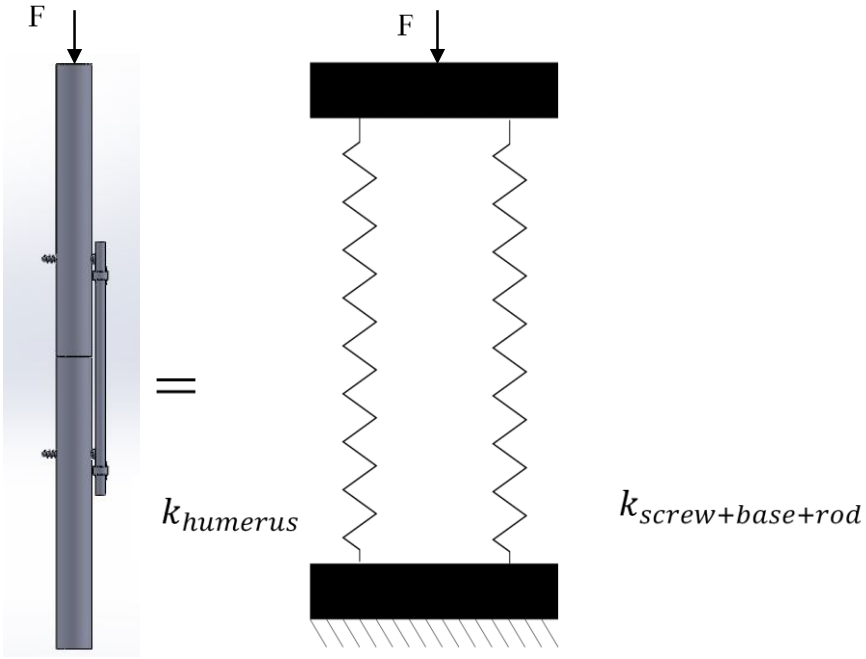

Figure 42: Representation of the Analogy (Left: 3D Model, Right: Springs in Parallel Connection)

Stiffness of the humerus will be calculated first.

$$k = \frac{AE}{L}$$

$$A_{humerus} = \pi \frac{d_{outer}^2 - d_{inner}^2}{4} = \pi \frac{18^2 - 14^2}{4} = 101\ mm^2$$

$$E_{humerus} = 10\ GPa$$

$$L_{humerus} = 130\ mm$$

$$k_{humerus} = \frac{A_{humerus}E_{humerus}}{L_{humerus}} = 7733\ \frac{kN}{m}$$

The screw-base-rod assembly is used in finite element analysis for which the boundary conditions are presented in Figure 43. Applied force is increased for five steps, eventually reaching 147.15 N.

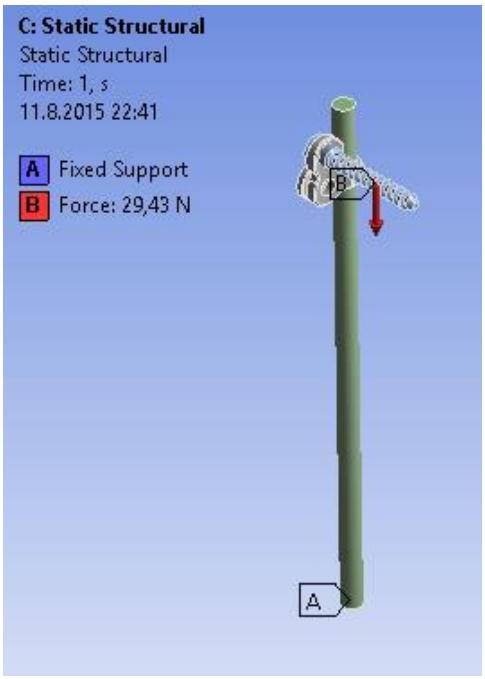

Figure 43: Boundary Conditions for Load Sharing Analysis

Force-deflection curve of the assembly is used to obtain stiffness value which can be seen in Figure 44.

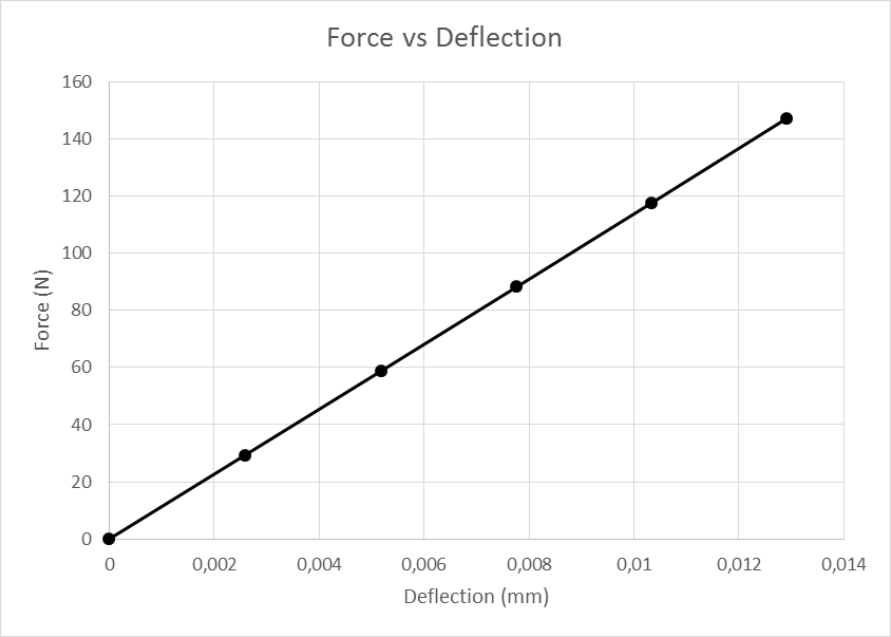

Figure 44: Force vs Deflection for the Assembly

The slope of the line is the stiffness value necessary and is obtained as:

$$k_{screw+base+rod} = 11403\ \frac{kN}{m}$$

The mesh statistics of the analysis is presented in Table 13.

Table 13: Mesh Statistics for Load Sharing Analysis

Nodes	16822
Elements	4851
Mesh Metric	Element Quality
Min	0
Max	0.9998
Average	0.6983
Standard Deviation	0.2459
Element Type	10 Noded Tetrahedral+20 Noded Hexahedral+6 Noded Triangle+8 Noded Quadrilateral

Sample six noded triangle and eight noded quadrilateral elements are presented in Figure 45 and Figure 46, respectively.

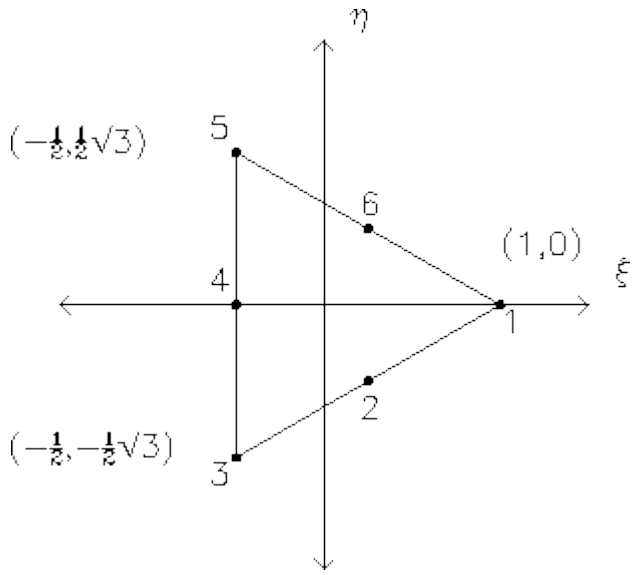

Figure 45: Sample Six Noded Triangle Element (Greenough, 2000)

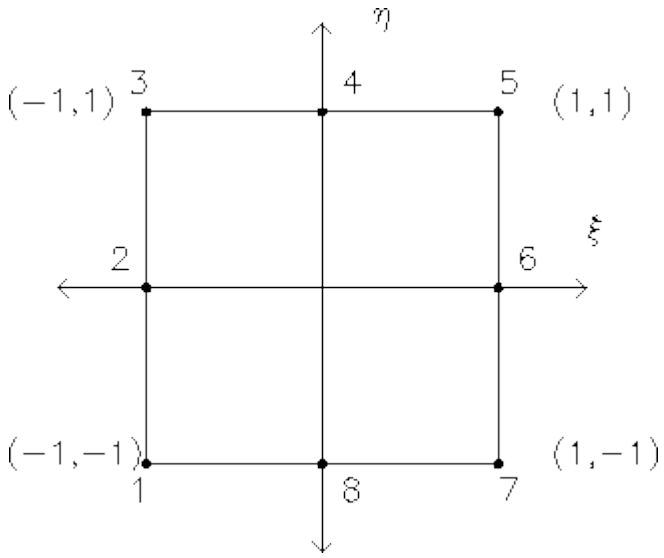

Figure 46: Sample 8 Noded Quadrilateral Element (Greenough, 2000)

$$k_{equivalent} = k_{humerus} + k_{screw+base+rod} = 19136\ \frac{kN}{m}$$

Since the equation $F = kx$ is linear, humerus and rod will share the axial load proportional to their stiffness.

$$F = 147.15\ N$$

$$F_{humerus} = F\frac{k_{humerus}}{k_{equivalent}} = 59.5\ N$$

$$F_{rod} = F\frac{k_{rod}}{k_{equivalent}} = 87.7\ N$$

It should be noted that soft tissue is not included in the analysis. The results for increasing elastic moduli of the bone, modeling the behavior during healing, are presented in Table 14.

Table 14: Load Sharing Results for Changing Bone Elastic Moduli

$E_{humerus}\ (GPa)$	$k_{humerus}\ (kN/m)$	$k_{equivalent}\ (kN/m)$	$F_{humerus}\ (N)$	% of Force on Humerus
1	773	12176	9.4	6.4
2	1547	12950	17.6	11.9
3	2320	13723	24.9	16.9
4	3093	14496	31.4	21.3
5	3867	15270	37.3	25.3
6	4640	16043	42.6	28.9
7	5413	16816	47.4	32.2
8	6187	17590	51.9	35.2
9	6960	18363	55.8	37.9
10	7733	19136	59.5	40.4

Unfortunately, whether or not the force is enough to avoid stress shielding remains unknown, since there is no literature indicating the minimum load a fractured bone

should carry. Interpretation of the analysis regarding the stress shielding will therefore be left for the experience of the medical doctors.

4.1.3. Stress Analysis of Bone Screw

Stress analysis on bone screw will be conducted using analytical methods first, then finite element analysis will be performed to compare the results. Upon suggestion of the medical doctors, six bone screws and six base parts will be assumed to be on the rod. Moreover, these six screws will be assumed to share the load of 147.15 N equally, leading to 24.5 N load on one screw. Analysis will be performed statically, hence the screw is assumed to be rigidly fixed to the base. This assumption cannot be checked using analytical or numerical methods accurately, so experiments are necessary to observe the fixation of the bone screw to the base. In the analytical method, the bone screw is modeled as a beam with the root diameter of the screw. Root diameter will provide a good estimate for the critical cross section of the screw. However, one drawback of this approach is lack of attention to stress concentration. Provided that the results of two approaches agree, the assumptions can be considered valid. Free body diagram of the bone screw can be seen in Figure 47.

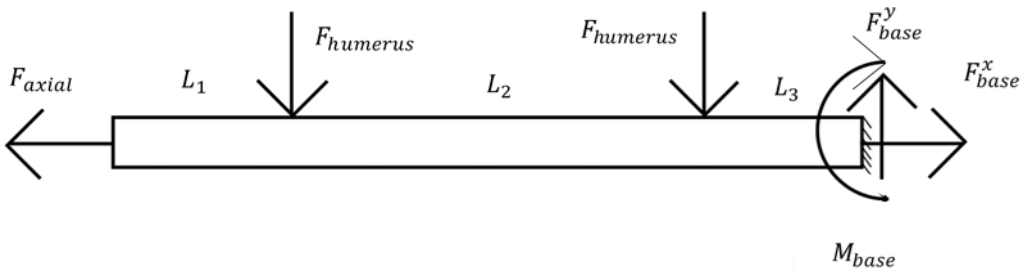

Figure 47: Free Body Diagram of Bone Screw

$$L_1 = 7\ mm$$
$$L_2 = 16\ mm$$

$$L_3 = 8\ mm$$

$$F_{humerus} = \frac{24.5}{2} = 12.25\ N$$

Axial force due to torque applied to the bone F_{axial} will be calculated using equations 3.2 and 3.3 with assumed torque of 2000 N·mm and following geometry:

$$d = 4\ mm$$
$$d_r = 2\ mm$$
$$l = 8\ mm$$

Note that only 8 mm of the screw is gripped, so whole length is not used. The results are:

$$K = 0.633$$
$$F_{axial} = 1020\ N$$

Support reactions $F_{base}^x, F_{base}^y, M_{base}$ will be calculated using equilibrium equations. Note that these reactions will be used in the analysis of base later.

$$\sum F_x = 0$$
$$-F_{axial} + F_{base}^x = 0$$
$$F_{base}^x = F_{axial} = 1020\ N$$
$$\sum F_y = 0$$
$$-F_{humerus} - F_{humerus} + F_{base}^y = 0$$
$$F_{base}^y = 2 \cdot F_{humerus} = 24.5\ N$$
$$\sum M_z = 0$$
$$F_{humerus} \cdot (L_2 + L_3) + F_{humerus} \cdot L_3 - M_{base} = 0$$
$$M_{base} = 392\ N \cdot mm$$

Shear and moment diagrams can be seen in Figure 48 and Figure 49.

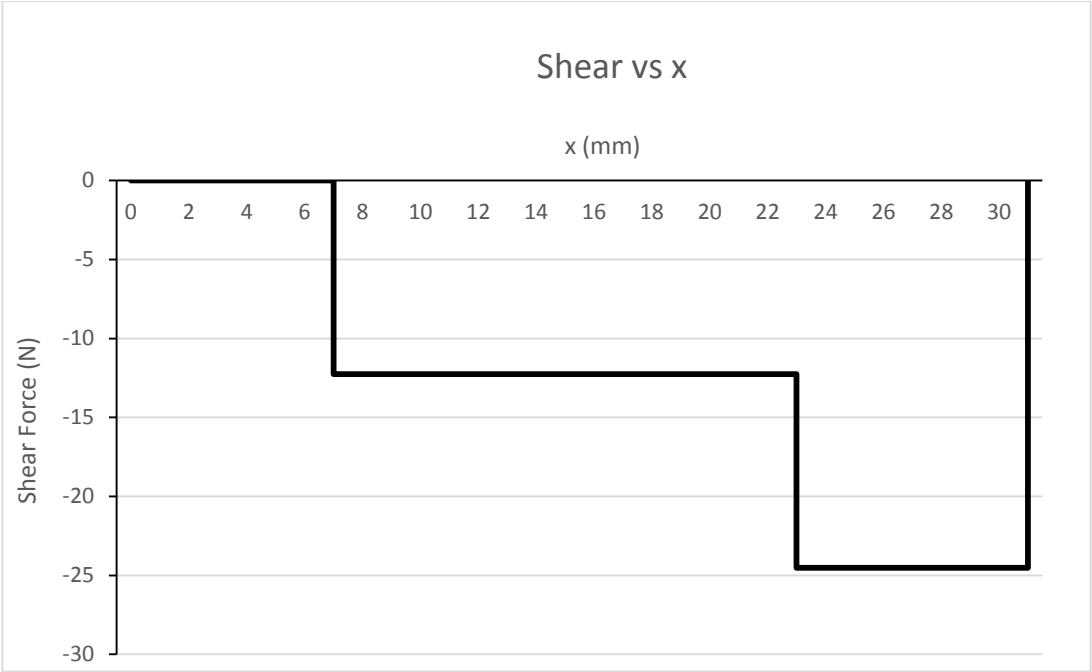

Figure 48: Shear Force Diagram

Figure 49: Bending Moment Diagram

As expected, the portion of the screw near the support is critical. Bending moment will cause tensile stress in the upper portion of the cross section and compressive stress in the lower one. Since the axial force causes tensile stress, tensile stress is critical in terms of normal stress.

$$\sigma_x = \sigma_{bending} + \sigma_{axial}$$

$$\sigma_x = \frac{M_{base} \cdot c}{I} + \frac{F_{base}^x}{A}$$

$$\sigma_x = \frac{M_{base} \cdot \frac{d_r}{2}}{\pi \frac{d_r^4}{64}} + \frac{F_{base}^x}{\pi \frac{d_r^2}{4}}$$

$$\sigma_x = 644\ MPa$$

$$\sigma_y = 0$$

Shear stress equation is simplified for circular cross sections in Shigley's Mechanical Engineering Design Table 3.2 as: (Budynas & Nisbett, 2008)

$$\tau_{xy} = \frac{4V}{3A} \qquad (4.1)$$

$$\tau_{xy} = \frac{4 \cdot F_{base}^y}{3 \cdot \pi \frac{d_r^2}{4}}$$

$$\tau_{xy} = 8.60\ MPa$$

Maximum normal and shear stresses occur at different portions of the cross section, on the outer surface and at the neutral axis, respectively. Obviously normal stress is the critical one, hence it will be used to determine the factor of safety. Using Maximum Shear Stress Theory, as suggested in Shigley's Mechanical Engineering (Budynas & Nisbett, 2008)

$$\sigma_x = \frac{S_y}{n}$$

$$S_y = 930\ \text{MPa}$$

$$n = 1.444$$

Stress and safety factor will be compared with finite element analysis using ANSYS.

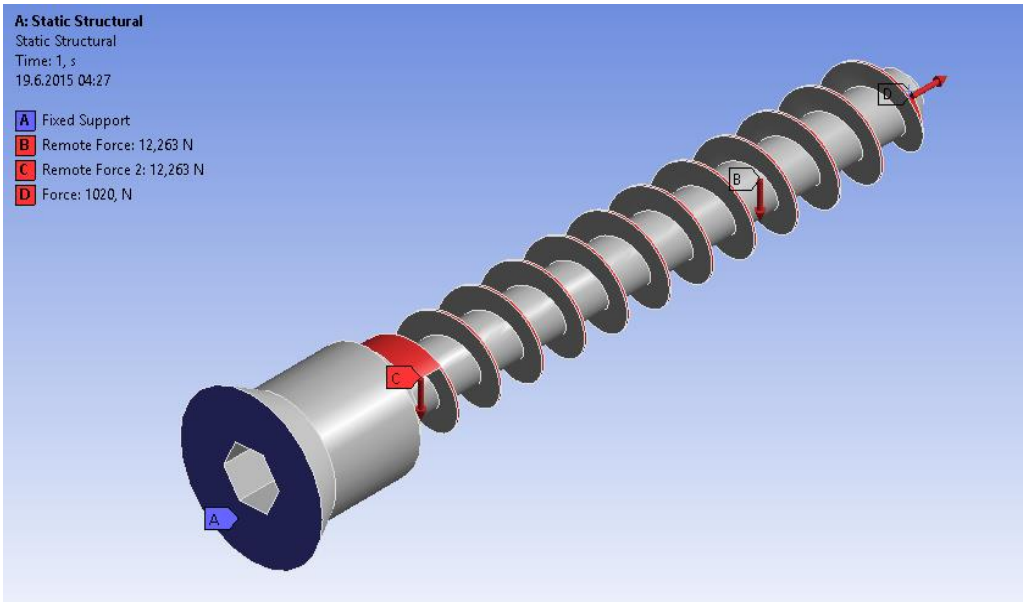

Figure 50: Bone Screw Stress Analysis Boundary Conditions

As can be seen in Figure 50, the head of the screw is assumed as a fixed support similar to the analytical method. Forces applied by the humerus are modeled as remote forces and axial force is applied at the tip of the screw.

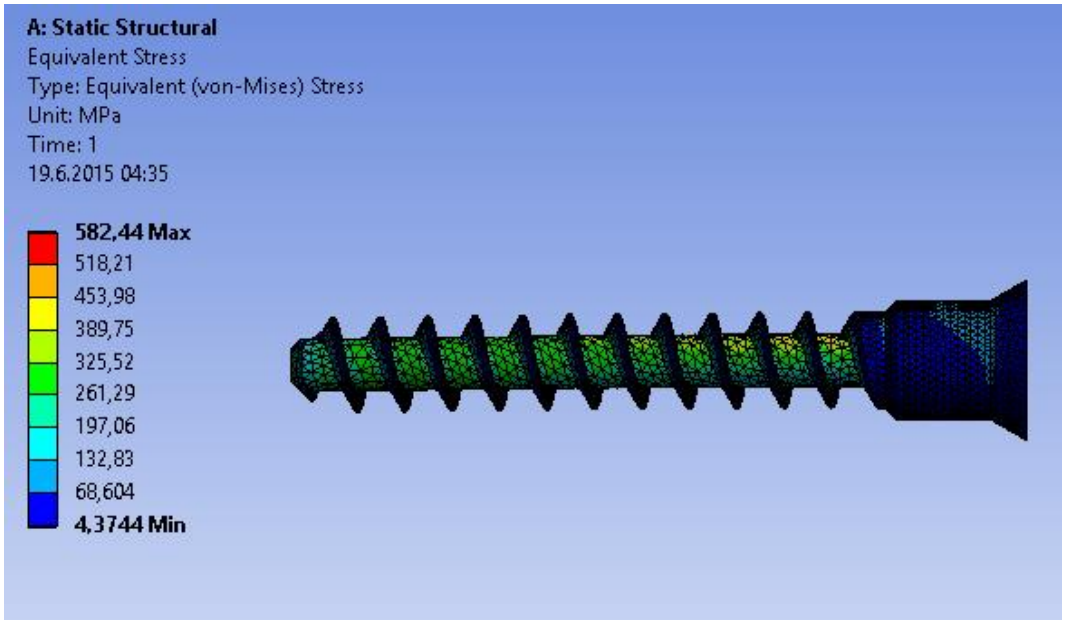

Figure 51: Bone Screw Stress Results

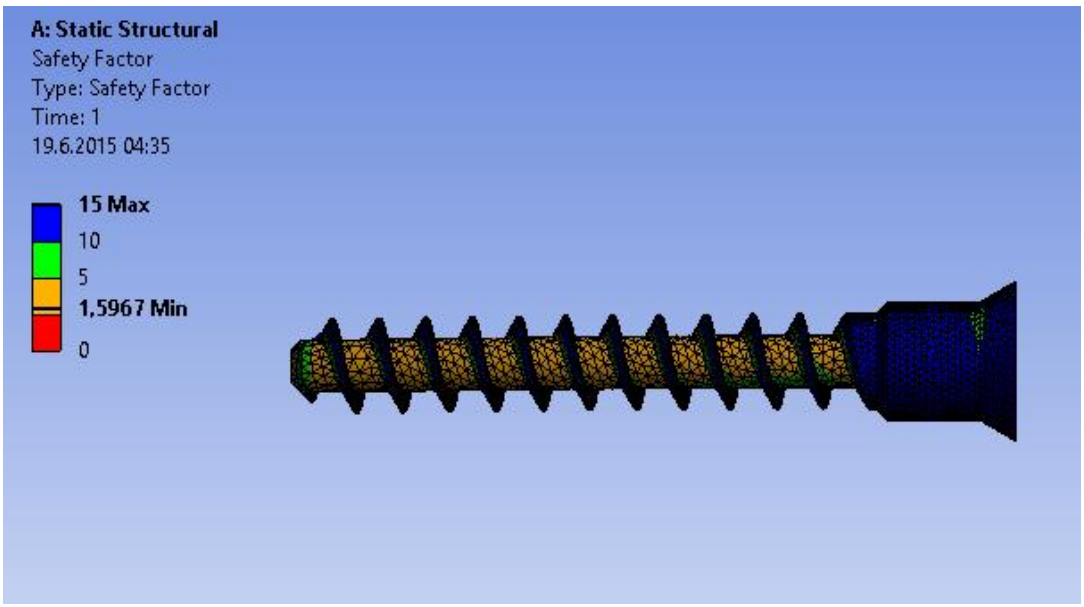

Figure 52: Bone Screw Safety Factor Results

Maximum stress calculated in finite element analysis is 582 MPa leading to a minimum safety factor of 1.597. In the analytical they are 644 MPa and 1.444 respectively. Results are not in perfect agreement but they are in the same order of magnitude. Possible reasons for this difference was stated earlier. To sum up, the design of the bone screw is safe with about 1.5 safety factor. Mesh statistics of the finite element analysis can be seen in Table 15.

Table 15: Bone Screw FEA Mesh Statistics

Nodes	37071
Elements	21256
Mesh Metric	Element Quality
Min	0.1062
Max	1
Average	0.7524
Standard Deviation	0.1529
Element Type	10 Noded Tetrahedral

4.1.4. Stress Analysis of Base

Stress analysis on the base will be performed only using finite element analysis, due to unorthodox shape of the base whose 3D model can be seen in Figure 38. Axial screw forces which are in the neighborhood of 1000 N cause plastic deformations in the base. In fact providing force closed fixation using plastic deformations is the working principle of the system. However, ANSYS Static Structural system outputs accurate stress results in the elastic range only. Therefore, the axial forces in the screws due to torque applied by the surgeon are excluded in this analysis. Clamping force analysis will be conducted later to have at least an educated guess, both bone screw and clamping screw performance will be evaluated mainly with the help of mechanical experiments. Force and moment due to external load of 147.15 N, which were

determined as F_{base}^{y} and M_{base} earlier, will be applied to the base in the analysis. The base is assumed rigidly fixed to the rod, hence a fixed support boundary condition is applied to the surface contacting the rod. Boundary conditions can be seen in Figure 53.

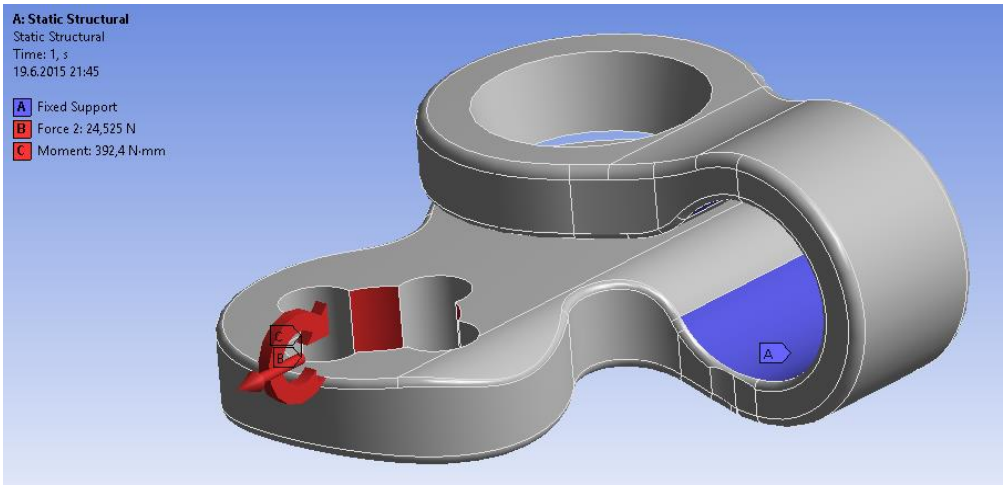

Figure 53: Base Stress Analysis Boundary Conditions

Stress and safety factor results are presented in Figure 54 and Figure 55.

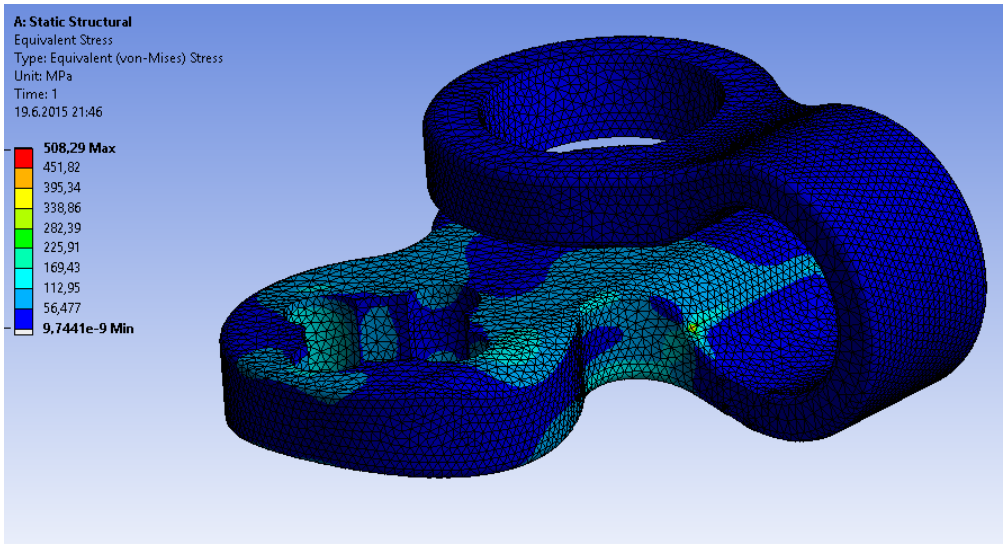

Figure 54: Base Stress Results

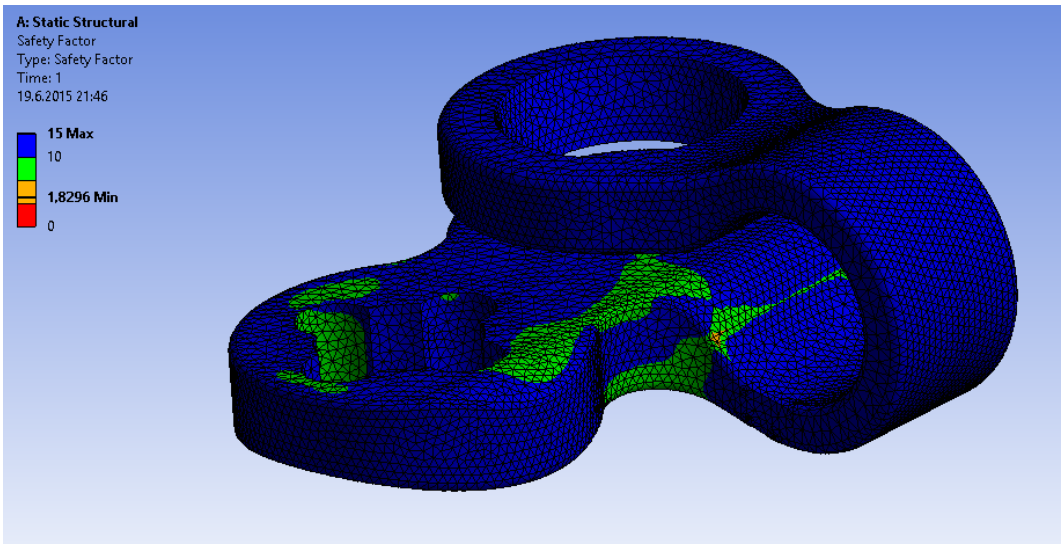

Figure 55: Base Safety Factor Results

Maximum stress in the base is 508 MPa leading to a safety factor of 1.83. So design of the base is safe in terms of the external load. Force, moment in x direction and moment in z direction reactions are also obtained, 24.5 N, 417 N·mm and 184 N·mm, respectively. These reactions will be used in the analysis of the rod. Mesh details of the analysis can be seen in Table 16.

Table 16: Base FEA Mesh Statistics

Nodes	128135
Elements	78078
Mesh Metric	Element Quality
Min	0.1174
Max	1
Average	0.7793
Standard Deviation	0.1167
Element Type	10 Noded Tetrahedral

4.1.5. Stress Analysis of Rod

Stress analysis of the rod will be conducted analytically first, then finite element method will be used and the results will be compared. In the analytical method, axis system of ANSYS will be used for convenience. The loads on the rod are compression by the external load and bending moment in two directions. Six base parts are assumed to be fixed on the rod with equal spacing. The free body diagrams can be seen in Figure 56 and Figure 57.

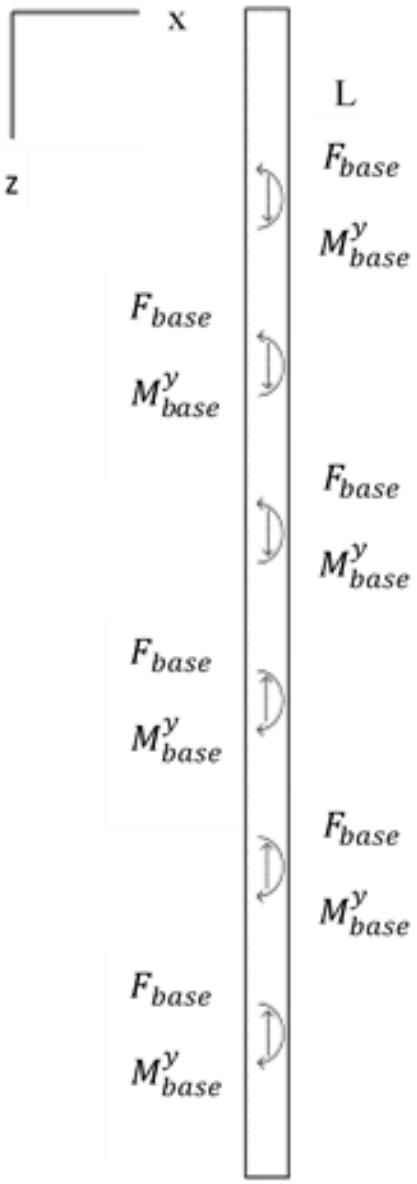

Figure 56: FBD of Rod on x-z Plane

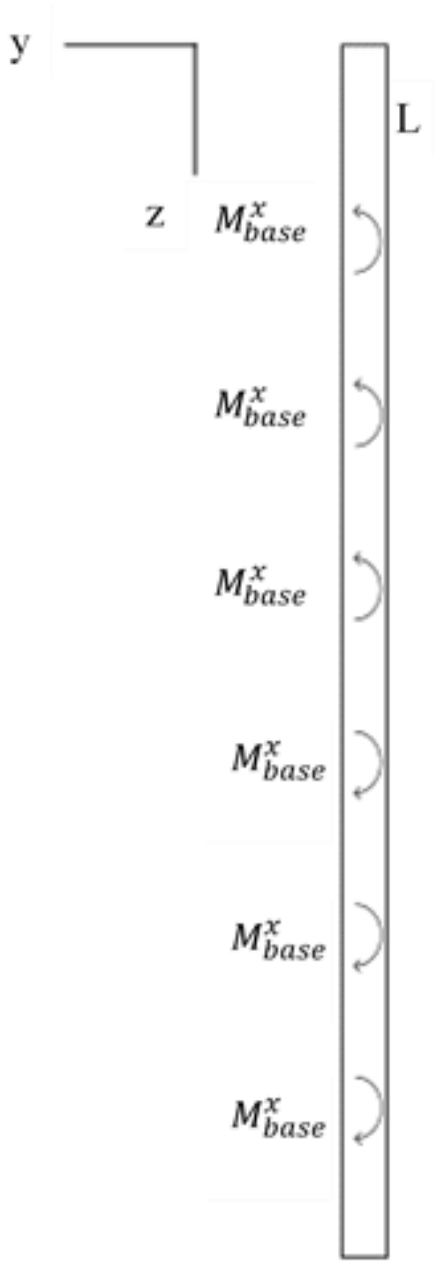

Figure 57: FBD of Rod on y-z Plane

The most critical portion of the rod is obviously the middle section in terms of stress. To find the internal forces, assuming a cut through the middle section of the rod, equilibrium equations will be used:

$$\sum F_z = 0$$
$$F^z_{internal} - 3 \cdot F_{base} = 0$$
$$F^z_{internal} = 3 \cdot F_{base}$$
$$F^z_{internal} = 73.6\ N$$
$$\sum M^y = 0$$
$$M^y_{internal} - 3 \cdot M^y_{base} = 0$$
$$M^y_{internal} = 3 \cdot M^y_{base}$$
$$M^y_{internal} = 1251\ N \cdot mm$$
$$\sum M^x = 0$$
$$-M^x_{internal} + 3 \cdot M^x_{base} = 0$$
$$M^x_{internal} = 3 \cdot M^x_{base}$$
$$M^x_{internal} = 551\ N \cdot mm$$

Stresses in the body will be found to determine safety factor for yielding. For solid circular cross sections, the plane containing the moment corresponding to the vector sum of two moments contains the maximum bending stress. The normal stress due to axial forces will be added to the bending stress due to superposition. Since the forces cause compression, maximum stress will be compressive.

$$\sigma_m = \frac{Mc}{I}$$
$$\sigma_m = \frac{\left({M^y_{internal}}^2 + {M^x_{internal}}^2\right)^{\frac{1}{2}} \left(\frac{d}{2}\right)}{\frac{\pi d^4}{64}}$$
$$\sigma_m = 111.4\ MPa$$
$$\sigma_{axial} = \frac{F_{rod}}{A}$$
$$\sigma_{axial} = 3.8\ MPa$$

$$\sigma = \sigma_m + \sigma_{axial}$$
$$\sigma = 115.2\ MPa$$

There is no other stress component, so this critical stress will be used to determine the safety factor, with a yield stress of 930 MPa.

$$n = \frac{S_y}{\sigma}$$
$$n = 8.07$$

So the design is safe according to analytical calculations. It should be noted that stresses due to clamping are neglected. Boundary conditions and results of the analysis can be seen in Figure 58, Figure 59 and Figure 60. Forces are applied at the corresponding points but the location of the moment does not change the result, so twelve moments are lumped into four moments bending the rod.

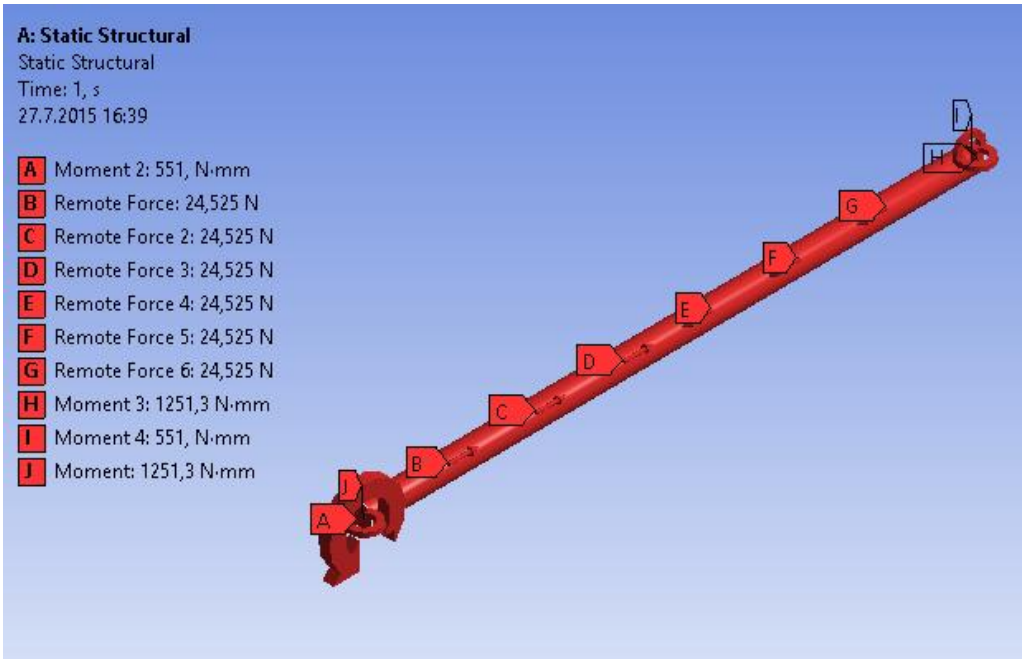

Figure 58: Rod Finite Element Analysis Boundary Conditions

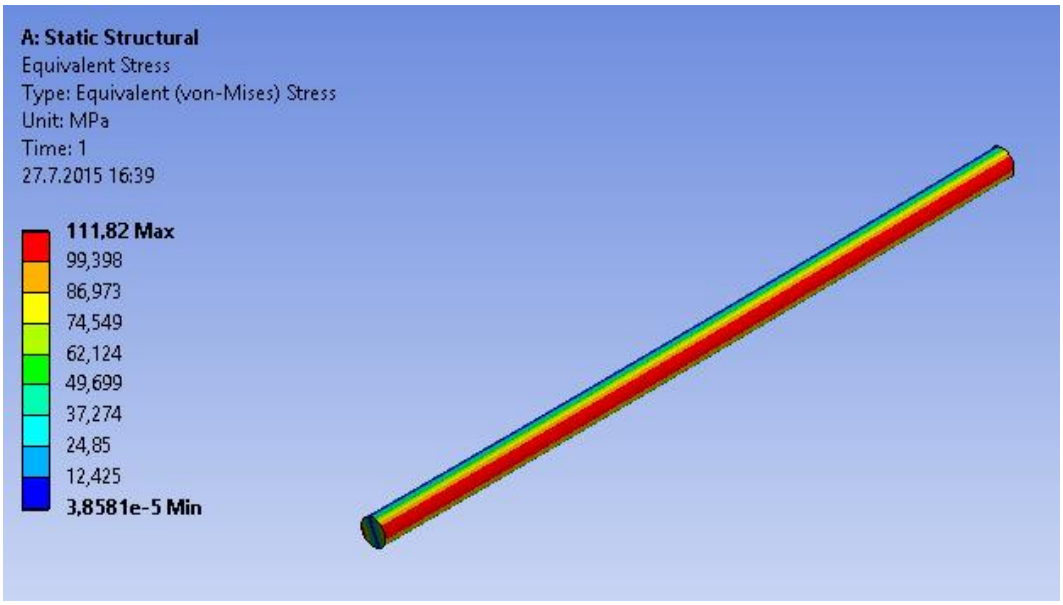

Figure 59: Rod Finite Element Analysis Stress Results

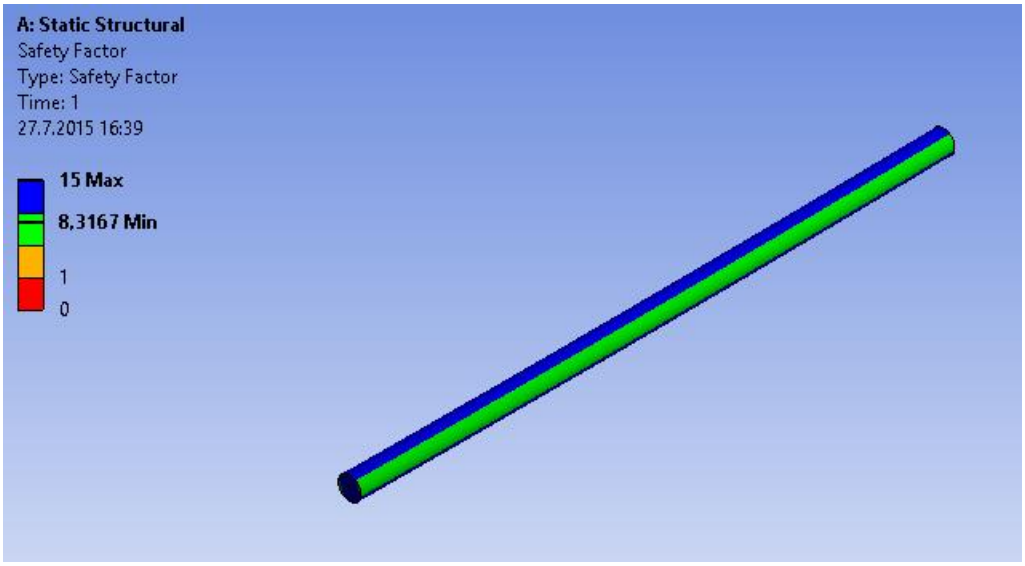

Figure 60: Rod Finite Element Analysis Safety Factor Results

Maximum stress is calculated as 111.82 MPa leading to minimum safety factor of 8.32. The results are in almost perfect agreement with the analytical method results. The mesh details of the finite element analysis can be seen in Table 17.

Table 17: Rod FEA Mesh Statistics

Nodes	203519
Elements	137789
Mesh Metric	Element Quality
Min	0.3034
Max	1
Average	0.8453
Standard Deviation	9.299E-02
Element Type	20 Noded Hexahedral

4.1.6. Stress Analysis of Clamping Screw

Clamping screw is under axial load only. Hence normal stress will be calculated using a similar approach to the stress analysis of the bone screw. The stress will be determined with the smallest diameter of the screw, root diameter which is 3.2 mm. The force on the screw will be decided using equations 3.2 and 3.3 with the following geometry:

$$d = 4\ mm$$
$$d_r = 3.2\ mm$$
$$l = 2.3\ mm$$

Leading to K and F results, with assumed 2000 N·mm applied torque:

$$K = 0.26$$
$$F_{axial} = 2087\ N$$

Normal stress:

$$\sigma = \frac{F_{axial}}{\frac{\pi d^2}{4}}$$
$$\sigma = 259.5\ MPa$$

The bending stress at the root of the thread will also be calculated using Equation 8.11 from Shigley's Mechanical Engineering Design (Budynas & Nisbett, 2008) assuming equal distribution of the load over the thread:

$$\sigma_b = \frac{6F}{\pi d_r n_t p} \qquad (4.2)$$
$$\sigma_b = 830.4\ MPa$$

Bending stress is critical so safety factor is:

$$n = \frac{S_y}{\sigma_b}$$
$$n = 1.072$$

So the clamping screw is just safe, hence assumed torque of 2000 N·mm is strongly not recommended. Since both modes of failure are considered, finite element analysis will not be conducted for the clamping screw.

4.1.7. Assembly Sliding Analysis

Assembly sliding analysis will be conducted similarly to the analysis in the earlier designs. Screw force will be calculated first, it will be applied to the base part using finite element analysis to decide the force on the rod and this force will be multiplied with the coefficient of friction. Obviously some harsh assumptions are made, but the result will provide an educated guess and will then be compared to the experiment results. The axial force calculated earlier is applied to the base using finite element analysis. Boundary conditions are presented in Figure 61.

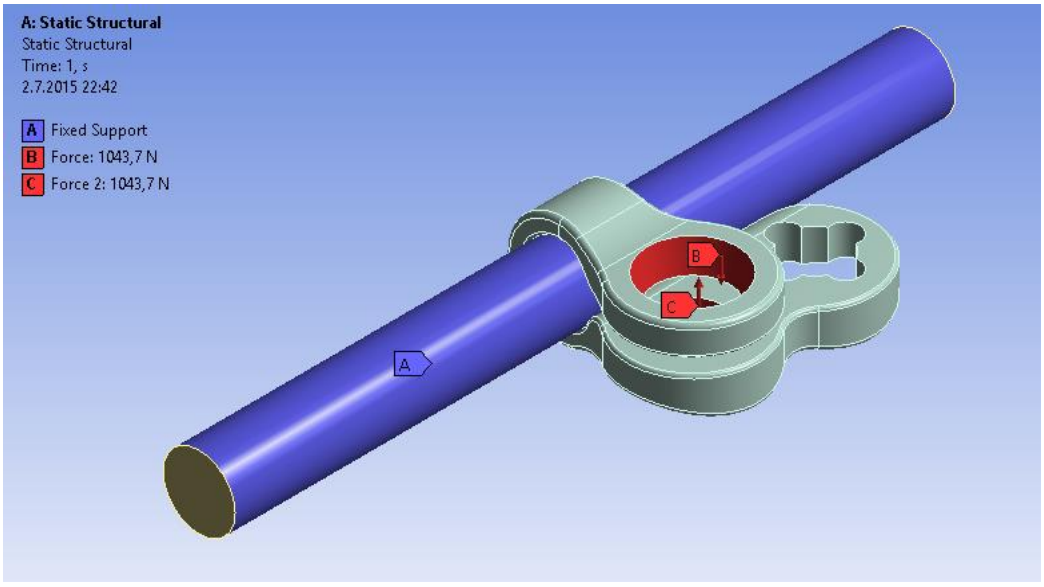

Figure 61: Clamping Analysis Boundary Conditions

Force reaction is obtained as 1218.7 N. Mesh details of the analysis can be seen in Table 18.

Table 18: Clamping FEA Mesh Statistics

Nodes	77544	
Elements	28437	
Mesh Metric	Element Quality	
Min	0.1162	
Max	0.9999	
Average	0.8	
Standard Deviation	0.1453	
Element Type	Rod	20 Noded Hexahedral
	Base	10 Noded Tetrahedral

In addition to force created by the clamping screw, the eccentricity of the base creates a moment. This moment causes reaction moment on the base, due to contact with the rod. To obtain friction force, the reaction moment will be replaced with two forces, i.e. two point contact between the rod and the base will be assumed. These forces will be calculated by static analysis for which the free body diagram is presented in Figure 62.

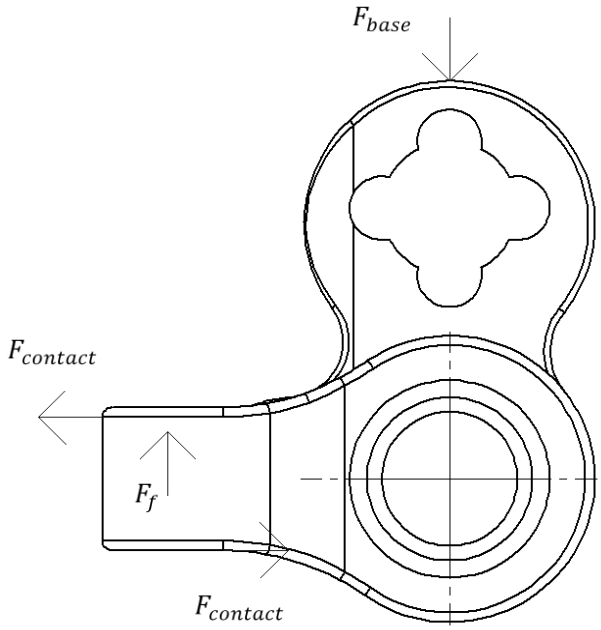

Figure 62: FBD of Sliding Analysis

$$\sum M = 0$$

$$-7 \times F_{base} + 2.25 \times F_{contact} + 2.25 \times F_{contact} = 0$$

$$F_{contact} = \frac{7 \times F_{base}}{4.5}$$

$$F_f = \mu(2F_{contact} + F_{reaction})$$

$$F_f = 388.5\ N$$

It should be noted that this is the maximum friction force for this case of loading. Since applied force 24.5 N is less than the maximum friction force, the assembly will not slide. Another point worth mentioning is that the friction force available increases with the load applied to the base. Therefore the design is safe in terms of sliding. Same procedure will be used with different values after the experiments are completed and the results will be compared.

4.1.8. Assembly Rolling Analysis

In this section the frictional moment between the base and the rod will be calculated. A target value is not specified by the medical doctors. Therefore the frictional moment will be decided considering the mechanical experiments. In Figure 63, free body diagram can be seen. Pressure due to clamping is assumed uniform and obtained with the help of finite element analysis as 110 MPa. As previously mentioned for earlier designs, the distribution is actually not uniform but for the sake of simplicity the average value from the finite element analysis is assumed to be acting uniformly.

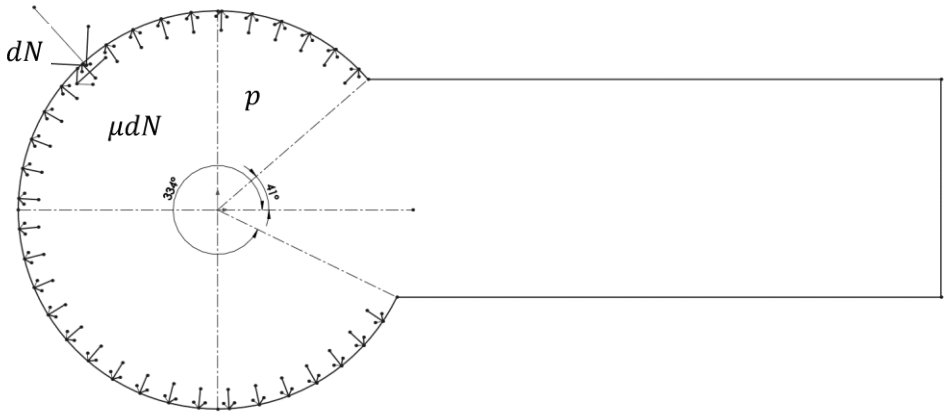

Figure 63: Free Body Diagram for Rolling Analysis

$$dN = pbrd\theta$$

$$M_f = \int_{41°}^{334°} \mu r dN$$

$$M_f = \int_{41°}^{334°} \mu r^2 pbd\theta$$

$$M_f = r^2 \mu pb(5.823 - 0.716)$$

$$M_f = 2715\ N \cdot mm$$

As stated earlier there is no target value available, so the frictional moment is calculated for reference. The same procedure will be used with different values after the experiments results will be compared.

4.1.9. Conclusion

Throughout the analysis, the performance of the design is evaluated considering all aspects. First of all, load sharing is inspected and the design is predicted to carry 60% of the axial load when the bone is healed. Under the safe loading condition suggested by the medical doctors, this leads to bone carrying 59.5 N of load, which is safe in terms of yielding of the bone. After that, stress analyses of each part are conducted. Under aforementioned assumptions, all parts are observed to be safe. However, under the assumed torque of 2000 N·mm, the clamping screw is just safe enough. The applied torque should be kept less than this value. Finally, sliding and rolling analyses are conducted on the assembly. The relations developed in these stages will be compared to the experimental results.

4.2 Mechanical Experiments

Mechanical experiments are conducted in Middle East Technical University Mechanical Engineering Department Biomechanics Laboratory using Shimadzu Universal Test Machine and Mark-10 Torque Meter. Universal test machine covers the whole area of interest in terms of loading capacity. On the other hand torque meter available has a limit of 135 N·cm, which is below the assumed torque in the analysis section. Hence when necessary, analysis is repeated with the corresponding torque values for comparison. Resolution of torque meter is 0.1 N·cm. Mechanical experiments on sliding, rolling and bone screw performance are conducted.

4.2.1. Sliding Experiments

Two types of sliding experiments are performed: increasing clamping torque to observe relationship between torque and frictional resistance; constant clamping torque to observe repeatability of the frictional resistance. Methods are similar in both experiments. The base is fixed on the rod with a known torque. Torque meter and the implant fixed on the rod which is fixed on the universal test machine are presented in Figure 64 and Figure 65, respectively.

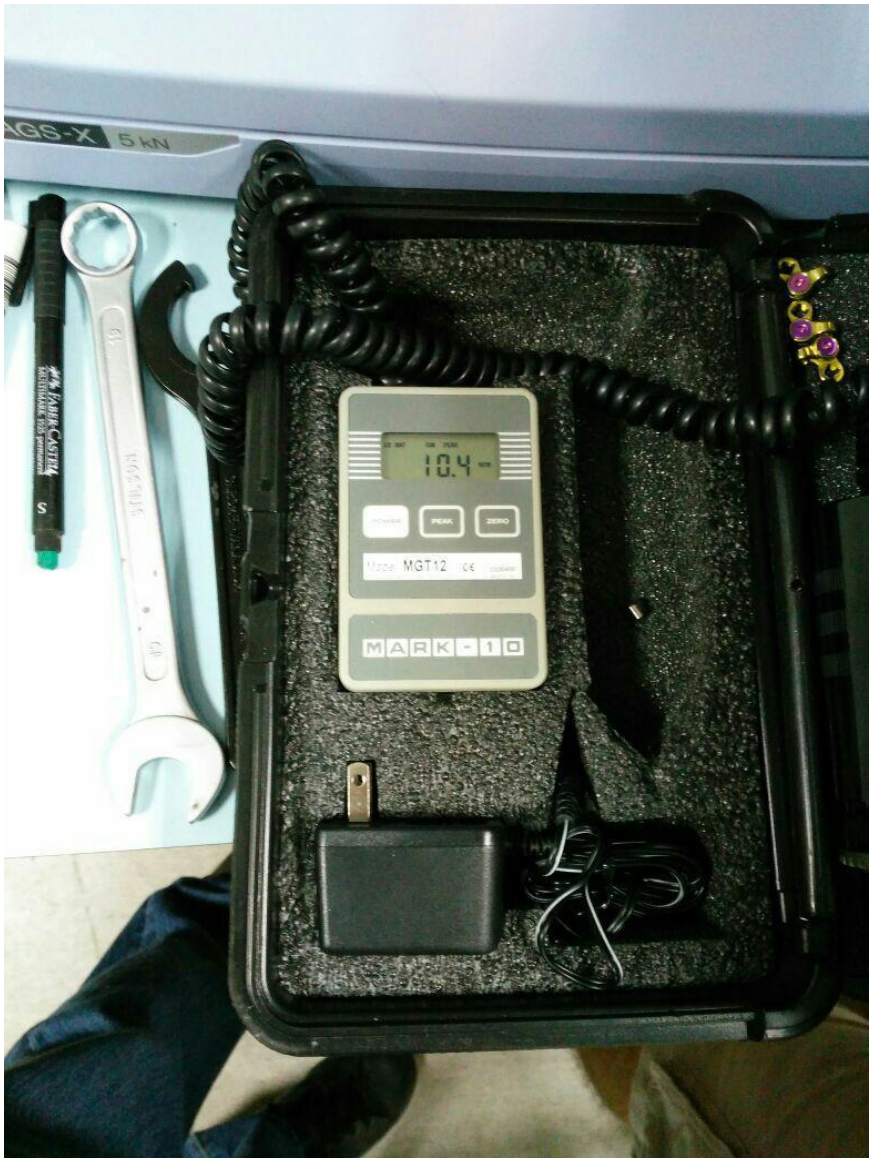

Figure 64: Image of Torque Meter after 10.4 N·cm Torque is Applied

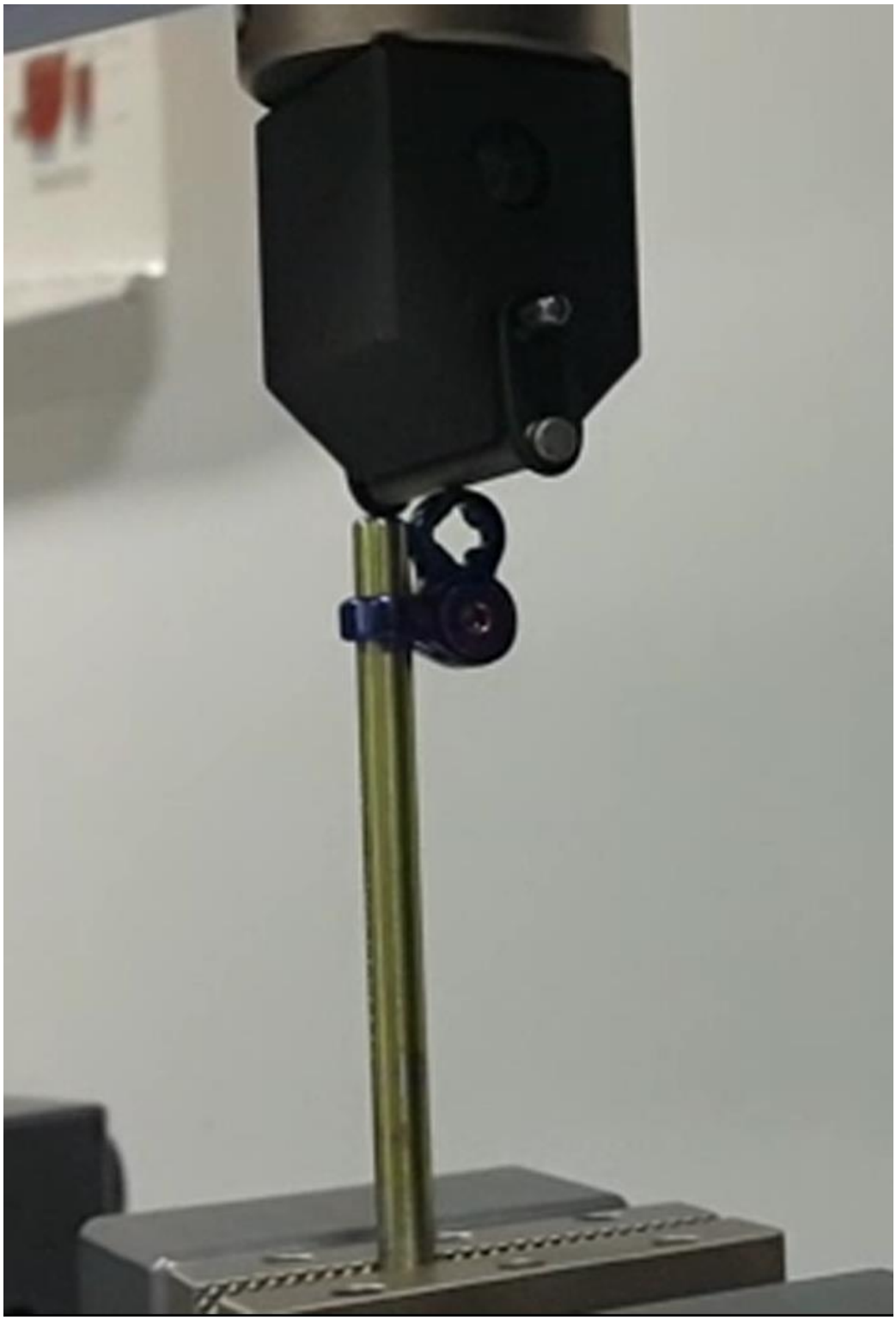

Figure 65: Sliding Experiment Set-up

In the increasing clamping torque experiments, five experiments are performed at 10, 20, 50, 75 and 100 N·cm torque values. Note that the torque meter is manually controlled hence the torque values are not rounded up numbers. Universal test machine outputs force vs displacement data and the experiment is stopped manually when a rapid increase in the displacement is detected, i.e. when the sliding occurs. Raw data from the machine can be seen in Figure 66:

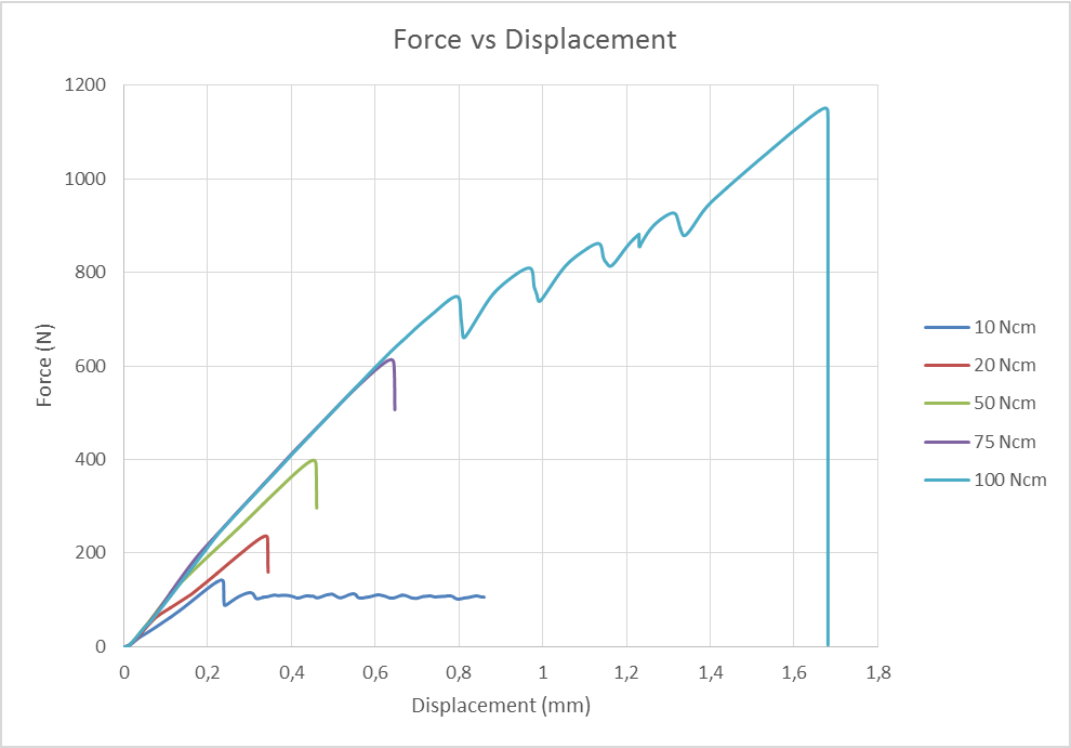

Figure 66: Raw Data of Increasing Torque Sliding Experiment

As can be observed in Figure 66, 10 and 100 N·cm torque experiments were not stopped at the right time, continuing after the slipping. Hence this data is modified to obtain more meaningful results. The data after the first steep drop of the force is excluded.

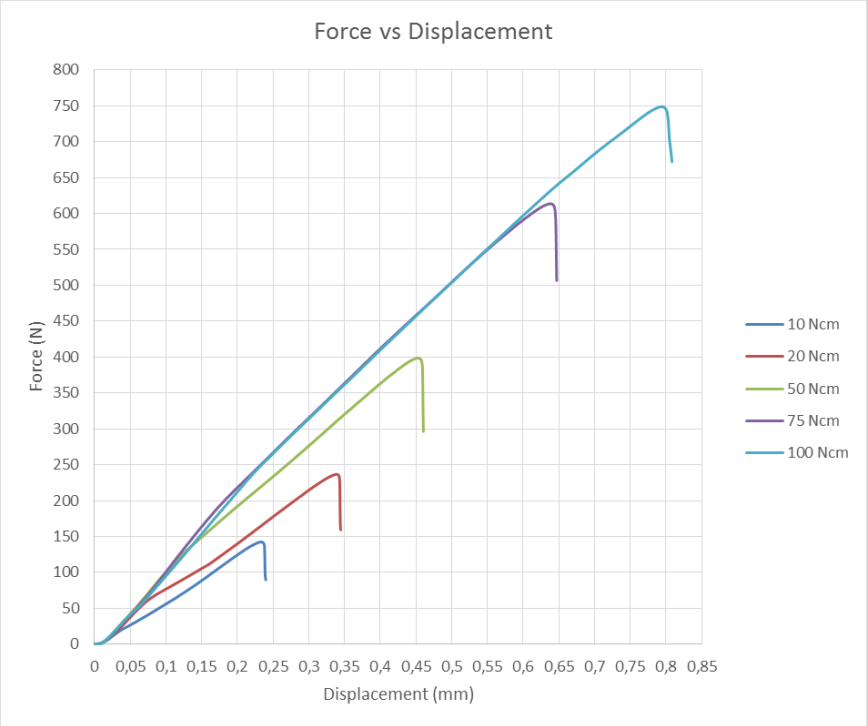

Figure 67: Modified Data of Increasing Torque Sliding Experiment

The maximum values of each test will provide the point that sliding occurs, i.e. the frictional resistance will be obtained for each torque value. Results are presented in Table 19 and Figure 68.

Table 19: Increasing Torque Sliding Experimental vs Analytic Results

Torque (N·mm)	Experimental Force (N)	Analytic Force (N)	Percent Error
101	142.5	151.3	6.2
202	236.7	257.5	8.8
500	398.6	463.5	16.3
758	613.6	711.2	15.9
1009	748.8	883.5	18.0

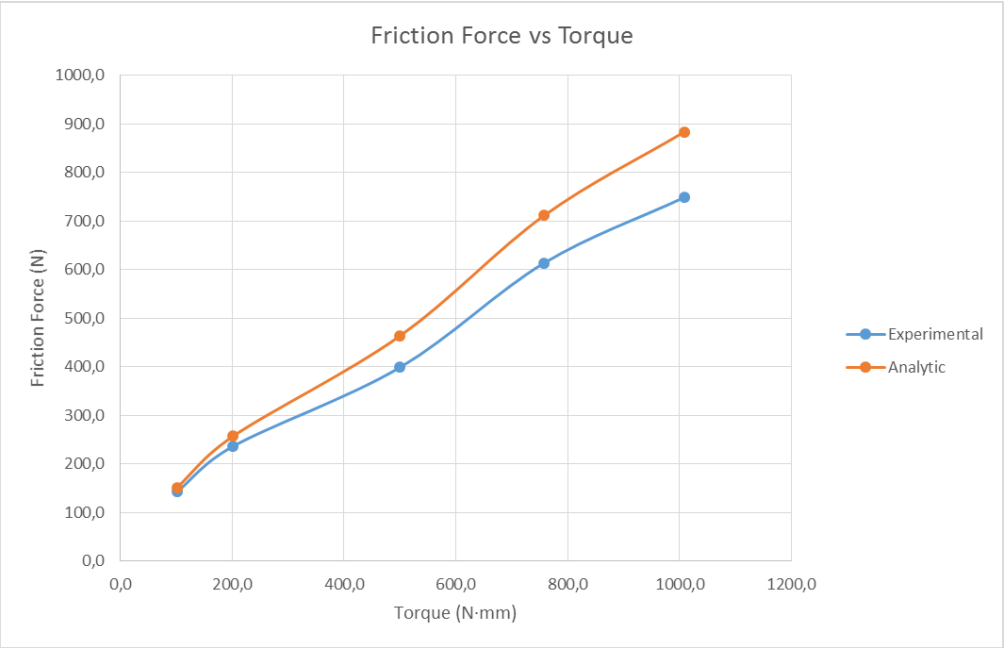

Figure 68: Increasing Torque Sliding Analysis Experimental and Analytic Results

As can be seen from Table 19 and Figure 68, analytic results agree with the experimental to some extent, with the worst error being 18%. For prediction purposes a line will be fitted to experimental data using Least Squares Method. Since the method is very widely known, details of the process will be excluded and only the results will be provided.

$$F_f = 0.667T + 85.1$$

$$R^2 = 0.995$$

Constant clamping torque sliding tests are conducted with the same method, only this time 100 N·cm torque is applied to the clamping screw in all five experiments.

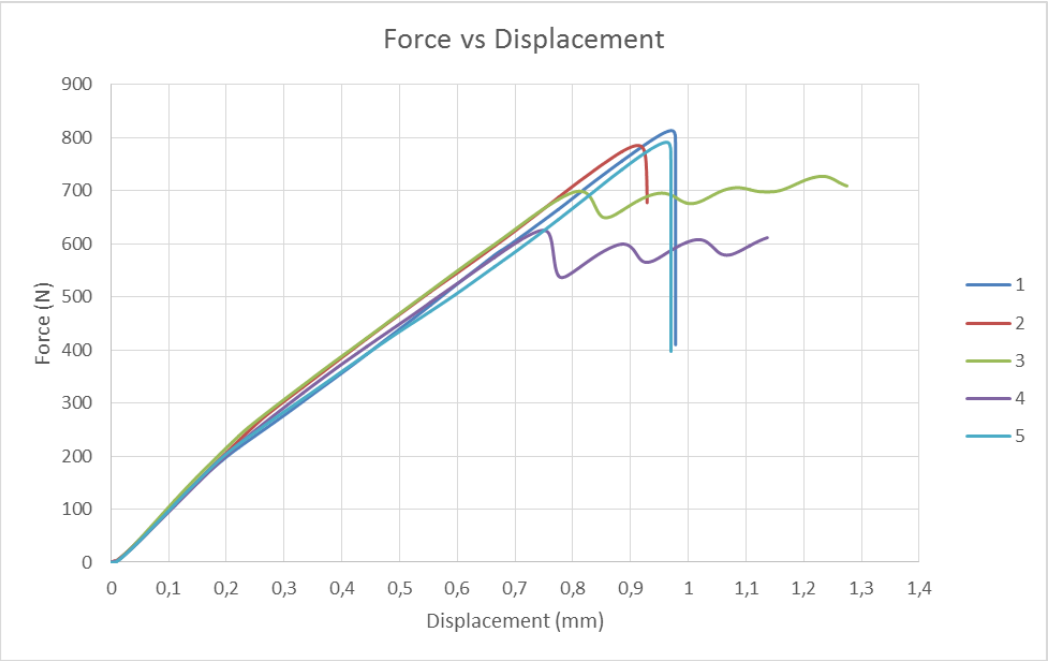

Figure 69: Constant Torque Sliding Experiment Raw Data

As can be seen in Figure 69, two of the experiments were not stopped at the right time. Data be modified for experiments number 3 and 4, excluding the data after the first steep drop of force.

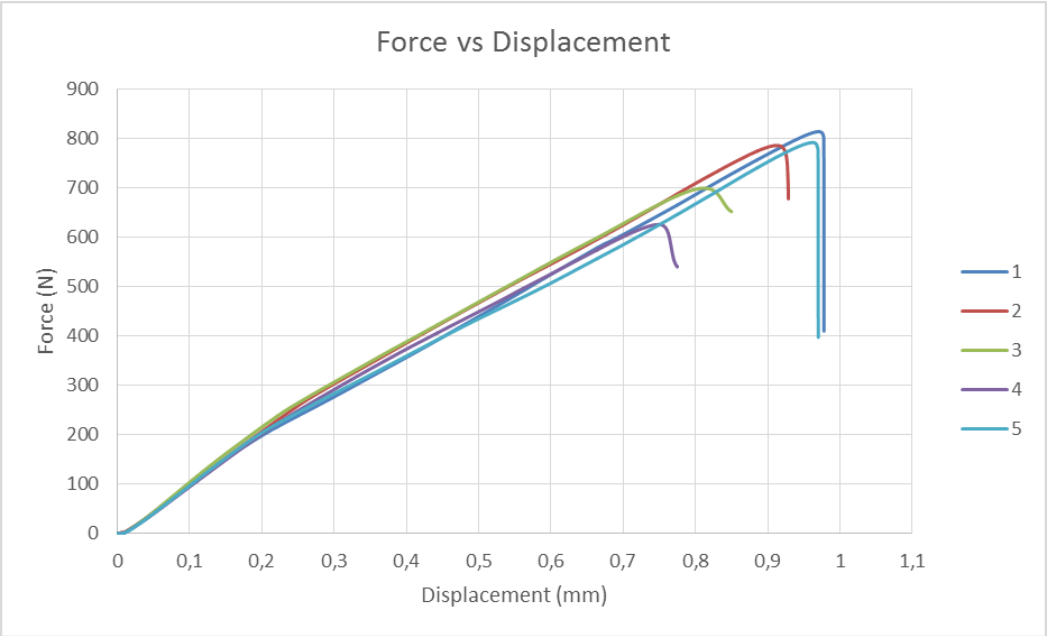

Figure 70: Constant Torque Sliding Experiment Modified Data

Maximum force, i.e. the force when sliding occurs is obtained for each experiment. Results are presented in Table 20.

Table 20: Constant Torque Sliding Analysis Maximum Forces

Experiment #	Torque (N·mm)	Maximum Force (N)
1	1003	813.4
2	1013	785.6
3	1055	699.2
4	1001	625.6
5	1008	791.6

Standard deviation of the experiments are calculated as 70.5 N while mean of the data is 743 N. Leading to coefficient of variation of 0.0949 which is an acceptable value. The most outlying experiment is number 4. The possible reasons of deviation are due to set-up being prepared by inspection. The rod was fixed vertically and the load was

applied at the middle of the base for each experiment, but the human eye is accurate to some extent in terms of angular and linear positioning.

4.2.2. Rolling Experiments

Rolling experiments to observe how much torsional gripping the design can achieve are conducted by fixing the base on the rod with a known torque applied to clamping screw and fixing the rod on the universal test machine, as seen in Figure 71. When the experiment starts, the machine applies and measures force on the clamping screw, by multiplying the force with the eccentricity of the clamping screw with respect to the rod, moment to cause rolling is obtained. Similar to sliding experiments, increasing torque and constant torque experiments are conducted, for observing the effect of torque and observing the repeatability, respectively.

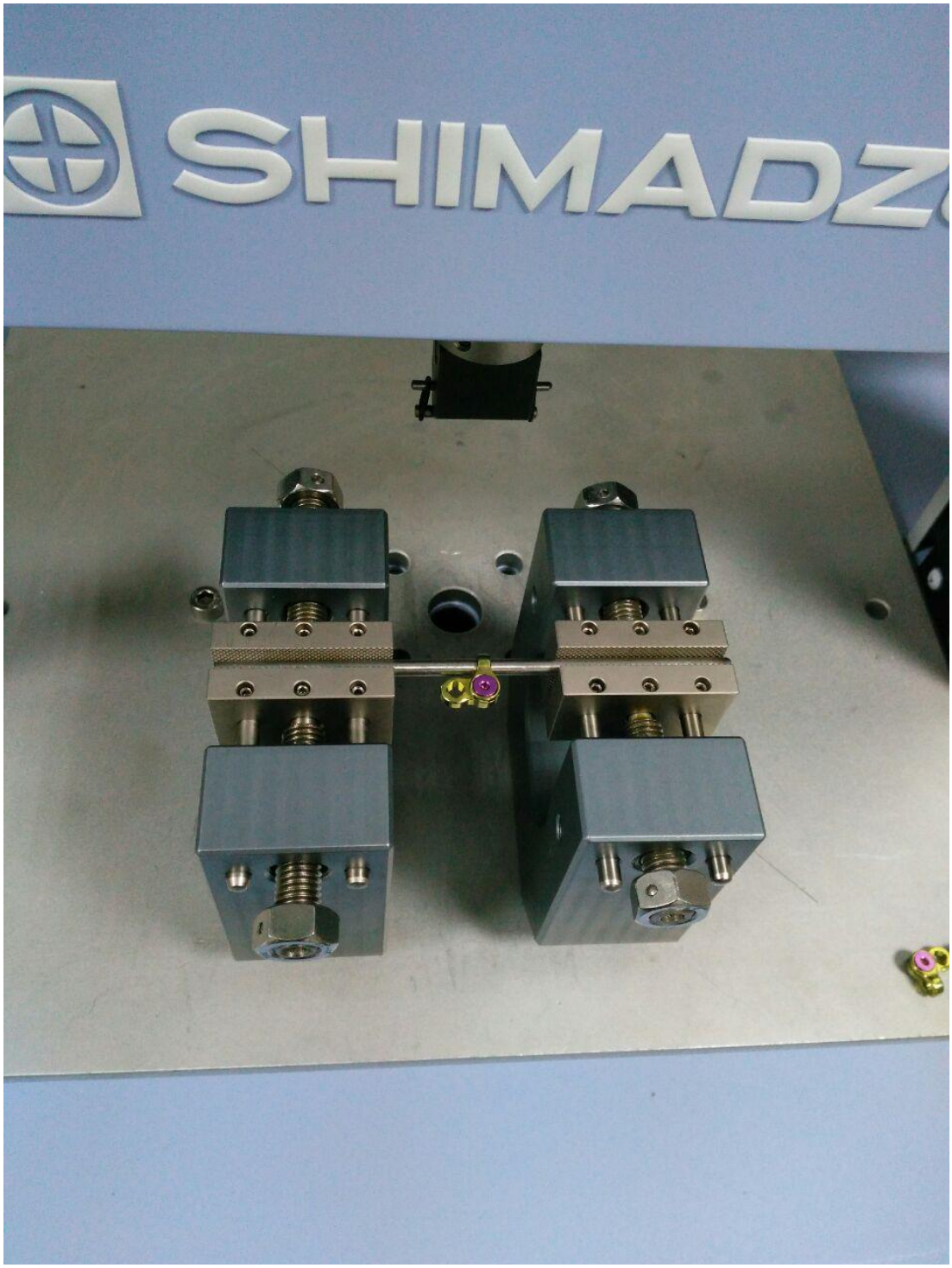

Figure 71: Rolling Experiment Set-up

In the increasing torque experiments, applied torque values are chosen as 10, 20, 50, 75 and 100 N·cm. Raw force vs. displacement results are presented in Figure 72.

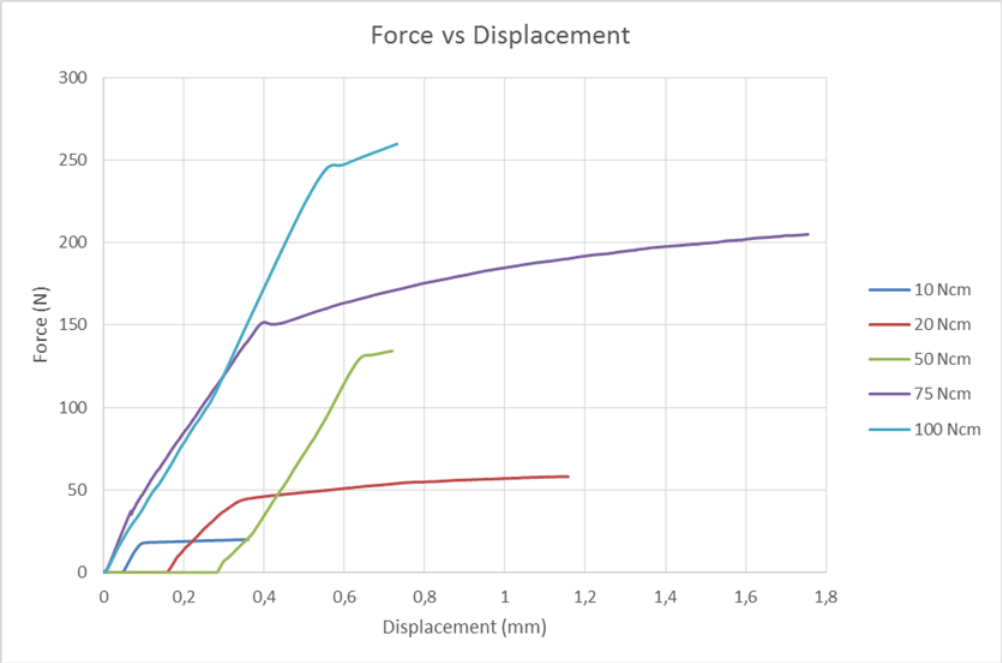

Figure 72: Raw Data of Increasing Torque Rolling Experiments

In all experiments, the point that slope changes is the point of interest, i.e. the point that rolling occurs. Hence all the data after those points will be removed. Also, in first three experiments, there are regions of zero force at the beginning, indicating a gap. Therefore the modified results are presented in Figure 73.

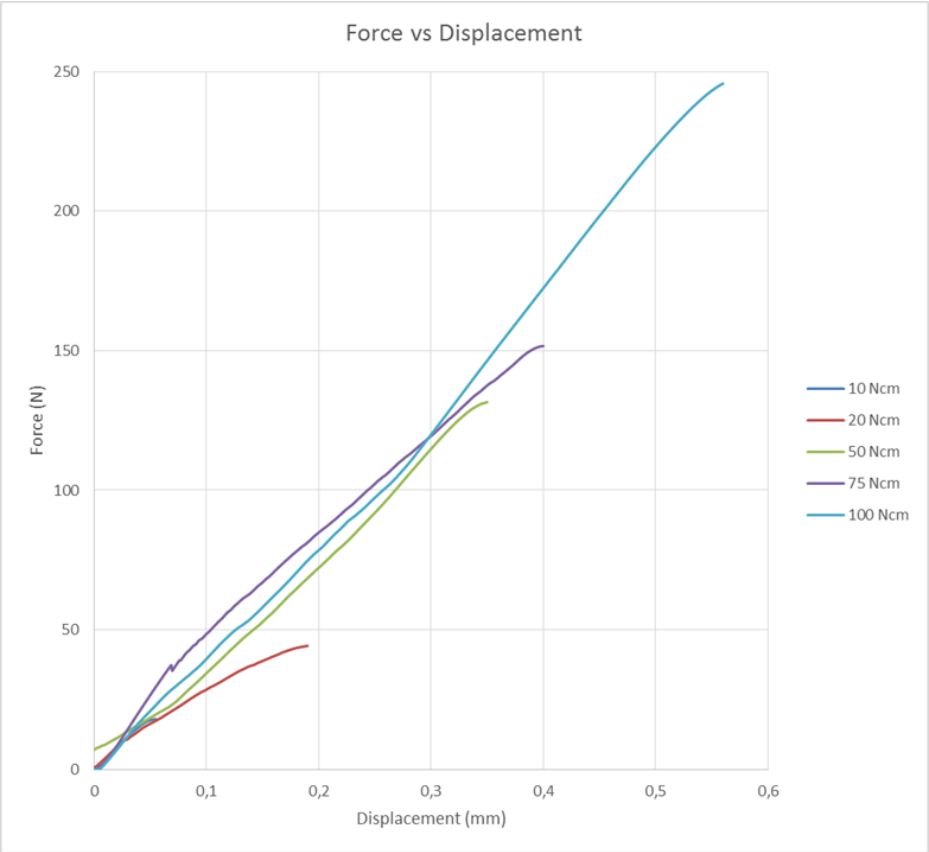

Figure 73: Modified Data of Increasing Torque Rolling Experiments

Maximum forces of these curves represent the point that rolling occurs. Hence maximum forces and corresponding moments are calculated, which then are compared to the results of the analytical method, presented earlier in Section 4.1.8. Results are presented in Table 21 and Figure 74.

Table 21: Increasing Torque Rolling Experimental vs Analytic Results

Torque (N·mm)	Experimental Force (N)	Experimental Moment (N·mm)	Analytic Moment (N·mm)	Percent Error
104	18.0	126.1	131.4	4.2
203	44.3	309.8	262.8	15.2
506	128.2	897.4	650.5	27.5
751	151.7	1061.6	986.1	7.1
1019	245.7	1719.8	1312.7	23.7

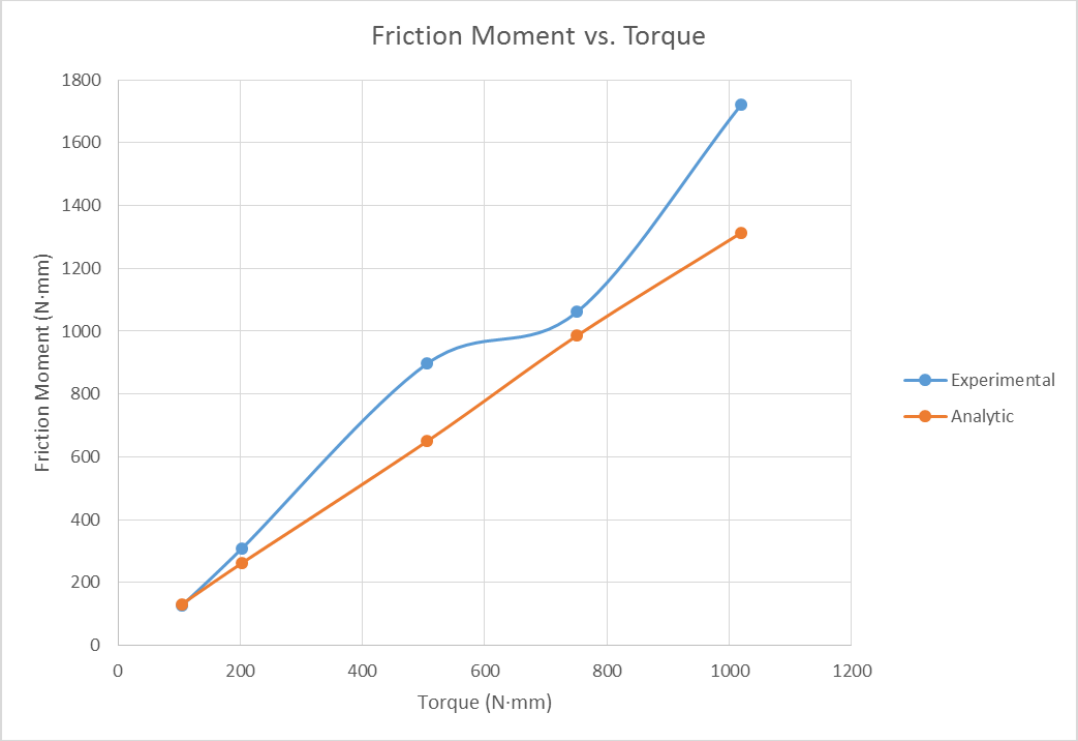

Figure 74: Increasing Torque Rolling Analysis Experimental and Analytic Results

As seen in the results, three of the experiments are in good agreement with the analytical results while two of them are not quite so. However, for the experimental data, it is reasonable to believe that 4th data point, 75 N·cm experiment is the outlying one most likely due to aforementioned possible positioning differences due to accuracy of human eye. This observation also implies that the analytic method underestimates

the friction torque, especially in high torque regions. A line will be fitted to the experimental results for prediction purposes using the Least Squares Method whose results are:

$$M_f = 1.656T - 32.8$$
$$R^2 = 0.978$$

In constant torque experiments, exactly the same method is employed, except that 100 N·cm is applied to clamping screws in all five experiments. Since the reasons to modify the data are previously discussed, raw and modified experiment results are presented directly in Figure 75 and Figure 76, respectively.

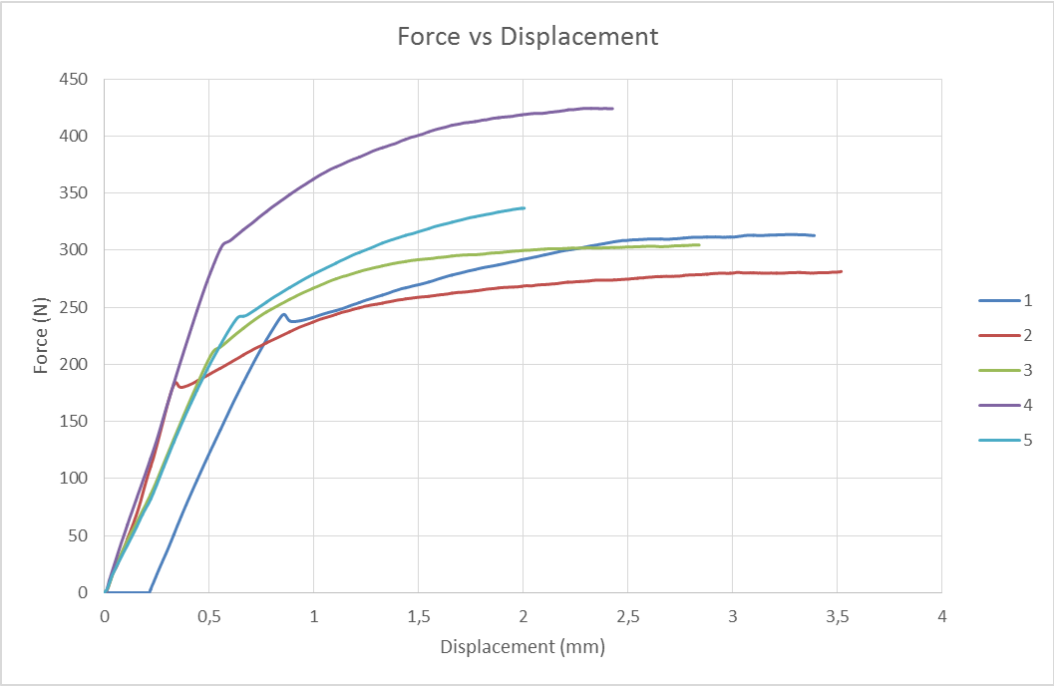

Figure 75: Constant Torque Rolling Experiment Raw Data

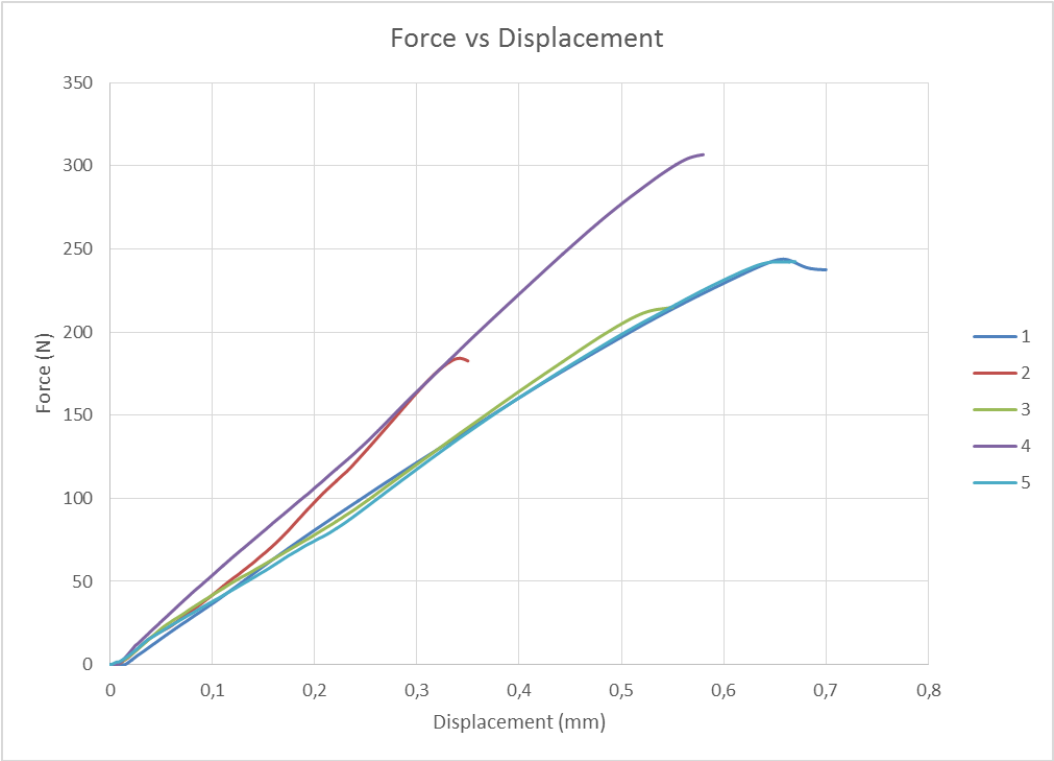

Figure 76: Constant Torque Rolling Experiments Modified Data

The maximum forces of the experiments correspond to the point that rolling occurs. The results are presented in Table 22.

Table 22: Constant Torque Rolling Experiments Results

Experiment #	Maximum Force (N)	Maximum Moment (N·mm)
1	243.8	1706.6
2	184.2	1289.5
3	214.8	1503.8
4	306.7	2146.7
5	242.4	1696.6

Standard deviation of the data is 40.5 N whereas the mean is 238.4 N, leading to coefficient of variation of 0.170. Three experiments agree quite well, experiments number 2 and 4 however disturb the repeatability of the experiments. As previously mentioned, positioning imperfections might have caused increases or decreases in applied moment. Another possible reason of the deviations is the overuse of the rods. There were only four rods available and each experiment damages the surface quality of the rod.

4.2.3. Bone Screw Experiments

In the bone screw experiments, base is fixed on the rod with the clamping screw and the bone screw is fixed on the base horizontally. In all five experiments, same torque values are applied to the clamping screw and bone screw, 100 N·cm and 120 N·cm respectively. Moreover, the location of line of contact between the universal test machine and the screw is the same in all experiments, 10 mm from the screw head. Therefore the torque applied and the moment caused by the external load are not factors in the experiments and repeatability is observed successfully.

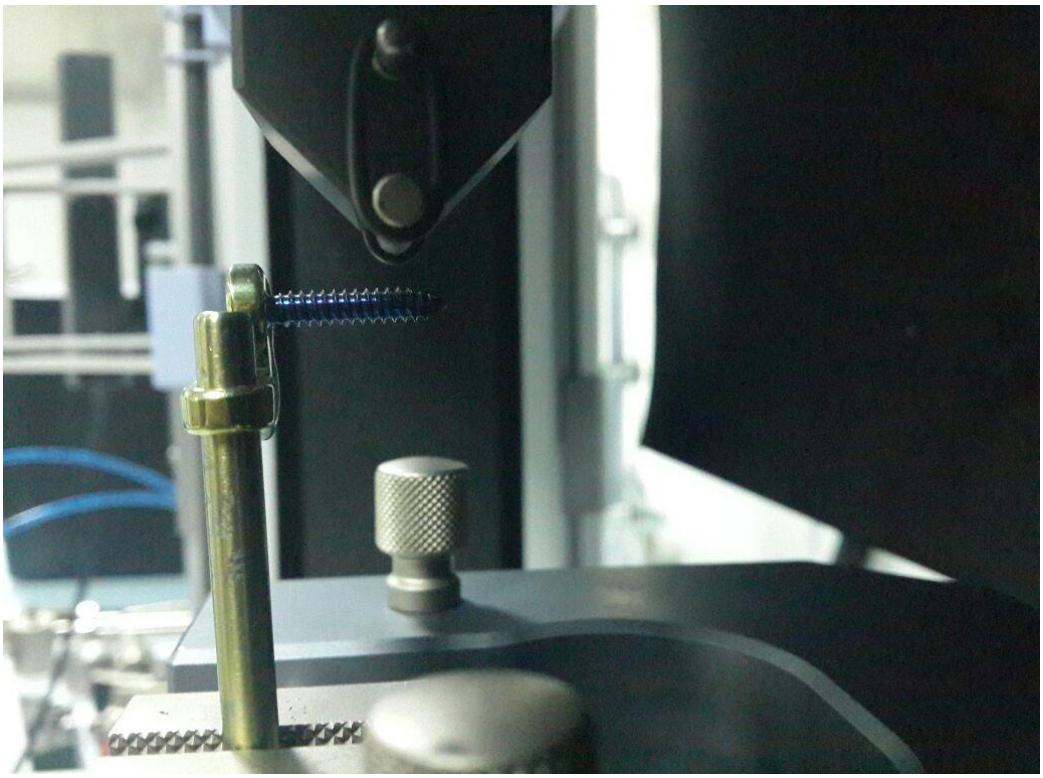

Figure 77: Bone Screw Experiment Set-up

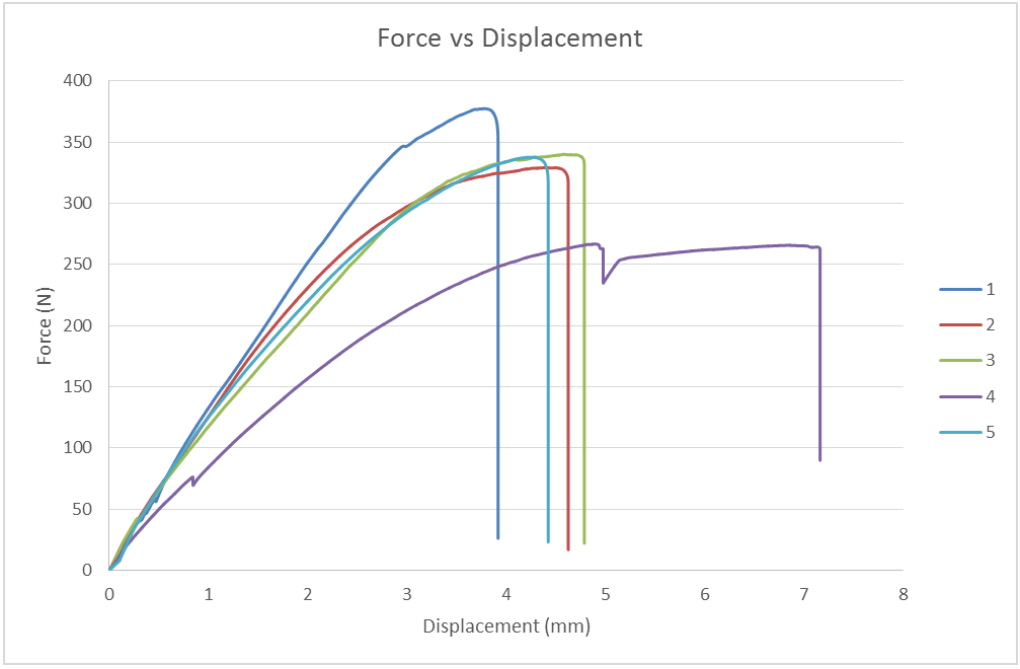

Figure 78: Bone Screw Experiments Raw Data

Similar to experiments mentioned earlier, the raw data of experiment number 4 is erroneous and should be modified. The data after the first drastic fall of force will be excluded.

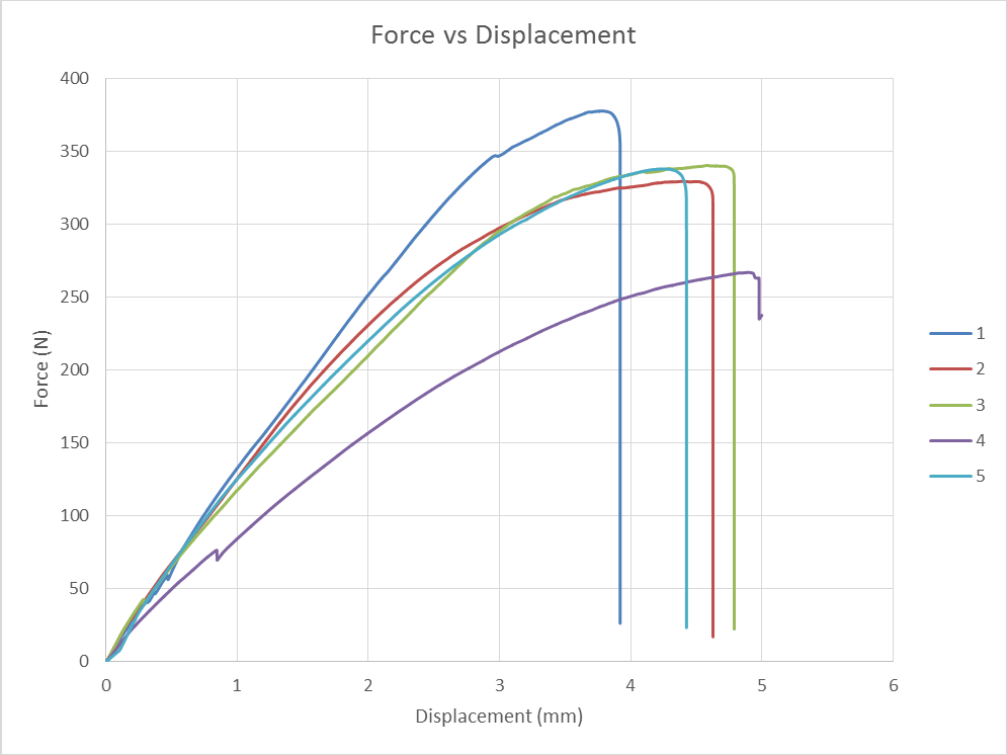

Figure 79: Bone Screw Experiments Modified Data

The point where the bone screw failed are presented in Table 23.

Table 23: Maximum Force in Bone Screw Experiments

Experiment #	Maximum Force (N)
1	377.4
2	329.1
3	340.1
4	266.7
5	337.7

The standard deviation of the experiments is 35.8 N while the mean is 330.2 N, leading to coefficient of variation 0.11. As can be seen from figures and the table, the result in experiment number 4 is considerably lower than the others. The reason is that while all other screws failed by yielding, the screw number 4 was released loose from the base. Figure 80 shows the state of the screws after the experiments, in the order of the experiment numbers from left to right.

Figure 80: Bone Screws after the Experiment

4.2.4. Conclusion

Experiments to assess the performance of the design are conducted focusing on where the analytical assumptions are debatable due to nonlinearities caused by friction and plastic deformation. However analytical and experimental results are found to be in agreement mostly. Experimental errors are mostly due to human eye lacking precision, hence leading to increase or decrease in moments applied. Another possible error is due to overuse of rods throughout the experiments. Only four rods were available for

experiments and each experiment caused some damage to surface properties. Finally, manufacturing tolerances in base parts resulted in some of them to be too tightly fit to the rod, leading to increased friction forces. The dimensions were not measured for each part but difficulty in assembly for some parts was clearly felt. Therefore the tolerance limits for manufacturing is crucial. To sum up, putting errors aside, mechanical experiments indicate that the design is successful in terms of medical doctors' loading expectations.

CHAPTER 5

CONCLUSION

In this study, first of all field knowledge was necessary since the author is a mechanical engineer. The nature of bone, fractures and healing were all crucial to be learned. This field knowledge was obtained and briefly presented in this study. Then the design problem was introduced along with the requirements to be met by the design. Unfortunately, most of the requirements were not numerical targets, due to lack of information provided by the medical doctors. Secondly literature review was conducted so that the various fracture treatment techniques, along with their historical development was grasped. Additionally, studies evaluating performance of treatment techniques were reviewed, focusing on plates and pedical screws. Information on modern biomaterials, with the attention concentrated on metals was also gained.

Next, conceptual designs were presented, with the aim of introducing the progress of the design. Some of the designs were successful mechanically but were eliminated due to medical reasons. The concept of polyaxial screw especially deserves further attention and development, provided that a wider time span and resources are available.

The main question to be answered in this study was “Can the novel design fix a bone fracture properly?” leading to strength concerns and rigidity ones due to consisting of an assembly rather than a solid part. Both these issues were handled in the analysis section. Stress analyses were conducted on each part with the use of external loading suggested by the medical doctors and an assumed torque applied on screws. All parts were proven to be safe, however clamping screw was found to be just safe enough, indicating the assumed torque throughout the analyses was excessive. Moreover, to assess the rigidity of the design friction force and moment were calculated. The results were satisfactory in terms of both sliding and rolling resistance. One drawback of these

analyses is the decision of clamping force or pressure created by the clamping screw. The force calculated by finite element analysis was the reaction force on the rod and was assumed to be net normal force. The net normal force is then multiplied with the coefficient of friction. Another approach was the assumption of uniform pressure distribution as an average of the finite element analysis pressure results. Although the analysis results agreed with the experiment results later, a better way of deciding the clamping force may improve the analysis.

In the next section of the study, experiments were presented. The prototypes used in the experiments were manufactured by Hipokrat Tıbbi Malzemeler İmalat ve Pazarlama A.Ş. using CNC cutting operations. The mechanical experiments indicated that the design is successful in terms of fixation. One drawback of the experiments was overuse of rods. A possible improvement over the mechanical experiments may be the use of a solution to imitate the behavior of bodily fluids, in which the system will actually work. Moreover, the use of an actual bone or a bone imitating material in mechanical experiments may improve them.

The future work for the design to be a product is firstly conducting the mechanical experiments in an accredited laboratory with enough number of experiments when compared to this study. Later, the animal experiments will take place according to proper ethical regulations. Since the design is novel, it is not possible to compare the findings of the study to the findings of another one. However, the claim of the design, becoming an alternative to modern treatment techniques, was assessed and the novel design is a candidate to compete with the commercially available designs.

REFERENCES

ANSYS Inc. (2013). *ANSYS Meshing User's Guide.*

Apley, A., & Noorden, M. (2000). A History of External Fixation. In G. De Bastiani, A. Apley, & A. Goldberg, *Orthofix External Fixation in Trauma and Orthopaedics.* Springer-Verlag London.

Bartonicek, J. (2010). Early History of Operative Treatment of Fractures. *Arh. Orthop Trauma Surgery*.

Biomet. (2015). *Biomet Plates.* Retrieved from Biomet: http://www.biomet.com/wps/wcm/connect/internet/0cdc63e7-00d2-400f-9a8e-1d36ea5c0996/OptiLock+Upper+Extremity+Plating+System+Proximal+Humeral+Plates.pdf?MOD=AJPERES&CACHEID=0cdc63e7-00d2-400f-9a8e-1d36ea5c0996

Bong, M., Koval, K., & Egol, K. (2006). The History of Intramedullary Nailing. *Bulletin of the NYU Hospital for Joint Diseases*.

Budynas, R. G., & Nisbett, J. K. (2008). *Shigley's Mechanical Engineering Design* (8th ed.). McGraw- Hill.

Cannada, L. (2011). *Fracture Classification.* Retrieved August 2014, from Orthopedic Trauma Association: http://ota.org/media/29245/G06-FX-classification-JTG-rev-2-3-10.ppt

Cervantes , T., Slocum Jr, A., & Seldin, E. (2011). Design and Experimental Evaluation of Adjustable Bone Plates for Mandibular Fracture Fixation. *Journal of Biomechanics*.

Christensen, N. O. (1973). Küntscher Intramedullary Reaming and Nail Fixation for Non-Union of Fracture of the Femur and Tibia. *The Journal of Bone and Joint Surgery*.

Desai, R., Malkani, A., Hitt, K., Jaffe , F., Schurman, J., & Shen, J. (2012). Revision Total Hip Arthroplasty Using a Modular Femoral Implant in Paprosky Type 3 and 4 Femoral Bone Loss. *The Journal of Arthroplasty*.

Dickinson, A., Browne, M., Roques, A., & Taylor, A. (2013). A Fatigue Assesment Technique for Modular and Prestressed Orthopaedic Implants. *Medical Engineering & Physics*.

El Sawy, A., & Shaarawy, M. (2013). Evaluation of Metal Ion Release from Ti6Al4V and Co-Cr-Mo Casting Alloys: In Vivo and In-Vitro Study. *Journal of Prosthodontics*.

Faraz, A., & Payandeh, S. (2001). Towards Approximate Models of Coulomb Frictional Moments in: (1) Revolute Pin Joints and (2) Spherical-Socket Ball Joints. *Journal of Engineering Mathematics*.

Greenough, C. (2000). *Finite Element Library*. Retrieved from Software Engineering Support Center : http://www.softeng.rl.ac.uk/st/projects/felib4/Docs/html/Level-0/Level-0.html#Contents

Kalfas, I. H. (2001). Principles of Bone Healing. *Journal of Neurosurgery*.

Kang, D. G., Lehman, Jr., R. A., Wagner, S. C., Bevevino, A. J., Tracey, R. W., Gaume, R. E., & Dmitriev, A. E. (2014). Effects of Rod Reduction on Pedicle Screw Fixation Strength in the Setting of Ponte Osteotomies. *The Spine Journal*.

Liu, G.-y., Mao, L., Xu, R.-m., & Ma, W.-h. (2014). Biomechanical Comparison of Pedicle Screws versus Spinous Process Screws in C2 Vertebra. *Indian Journal of Orthopaedics*.

Liu, L.-h., Guo, C.-t., Zhou, Q., Pu, X.-b., Song, L., Wang, H.-m., . . . Liu, L. (2014). Biomechanical Comparison of Anterior Lumbar Screw-Plate Fixation versus Posterior Lumbar Pedicle Screw Fixation. *Journal of Huazhong University Science and Technology (Medical Science)*.

Lokanadham, S., Khaleel, N., & Raj, P. (2013). Morphometric Analysis of Humerus Bone in Indian Population. *Scholar Hournal of Applied Medical Sciences*.

Ma, X. Q. (1992). Morphological Effects of Mechanical Forces on the Human Humerus. *British Journal of Sports Medicine*.

Malekani, J., Schmutz, B., Gu, Y., Schuetz, M., & Yarlagadda, P. (2012). Orthopedic Bone Plates: Evolution in Structure, Implementation Technique and Biomaterial. *International Journal of Engineering Technology*.

Marshall, S. T., & Browner, B. D. (2012). *Sabiston Textbook of Surgery: The Biological Basis of Modern Surgical Practice.* Elsevier.

McCarthy , J., & Lee, J. (2007). Complex Revision Total Hip Arthroplasty with Modular Stems at a Mean of 14 Years. *Clin Orthop Relat Res*.

Merriam-Webster Medical Dictionary. (2015). Retrieved from Merriam-Webster Medical Dictionary: http://www.merriam-webster.com/

Piero, A. (2013, July 9). *Body Building Anatomy.* Retrieved from Slideshare: http://image.slidesharecdn.com/bodybuildinganatomy-130709104732-phpapp01/95/bodybuilding-anatomy-19-638.jpg?cb=1373368130

Pruitt, L., & Chakravartula, A. (2011). *Mechanics of Biomaterials: Fundamental Principles for Implant Design.*

Sakellariou, V., Mavrogenis, A., Babis, G., Soucacos, P., Magnissalis, E., & Papagelopoulos, P. (2012). Comparison of Four Reconstructive Methods for Diaphyseal Defects of the Humerus After Tumor Resection. *Journal of Applied Biomechanics*.

Samiezadeh, S., Avval, P. T., Fawaz, Z., & Bougherara, H. (2014). On Optimization of a Composite Bone Plate Using the Selective Stress Shielding Approach. *Journal of the Mechanical Behavior of Biomedical Materials*.

Shahrokni, M., Zhu, Q., Liu, J., Tetzlaff, W., & Oxland, T. (2012). Design and Biomechanical Evaluation of a Rodent Spinal Fixation Device. *Spinal Cord*.

Stryker. (2015). *Stryker Trauma.* Retrieved from Stryker: https://www.stryker.com/en-us/products/Trauma/LowerExtremities/PlatingSystems/AxSOSLockingPlates/index.htm

Şen, B., Çakmak , M., Seyhan, F., Göğüş, A., & Taşer, Ö. (1991). Kırık Sonrası Oluşan Kallusun Devamlı Kompresyonu Tekniği ile Primer Kırık İyileşmesi (Deneysel Araştırma). *Acta Orthop Traum Turc*.

Talu, U., Kaya, İ., Dikici, F., & Şar, C. (2000). Pedicle Screw Salvage: The Effect of Depth and Diameter on Pull-out Strength: A Biomechanical Study. *Acta Orpthopaedica et Traumotologica Turcica*.

Tarnita, D., Tarnita , D., Tarnita , R., Berceanu, C., & Cismaru, F. (2010). Modular Adaptive Bone Plate Connected by Nitinol Staple. *Materialwissenschaft und Wekstofftechnik.*

TST. (2015). Retrieved January 2015, from http://www.tstsan.com/?Urunler&scid=185

Universal Medical Device Nomenclature System. (1999).

Yalnız, E., Çiftdemir, M., Eşkin, D., & Dülger, H. (2009). The Safety of Pedicle Screw Fixation in the Thoracic Spine. *Acta Orthopaedica et Traumatologica Turcica*.

Zimmer. (2015). Retrieved from http://www.zimmer.com/medical-professionals/products/spine/sequoia-pedicle-screw-system.html

Zimmer. (2015). *Zimmer Products.* Retrieved from Zimmer: http://www.zimmer.com/medical-professionals/products/trauma/zimmer-distal-radius-plating-system.html

APPENDIX A

MEDICAL GLOSSARY

Acetabulum: The cup-shaped socket of the hip joint which is a key feature of the pelvis. The head (upper end) of the femur (the thigh bone) fits into the acetabulum and articulates with it, forming a ball-and-socket joint. *Adj*. acetabular

Bicortical: Connected to two cortical plates.

Cancellous Bone: Also known as spongy or trabecular bone, is one of the two types of bone tissue found in the human body. Cancellous bone is found at the ends of long bones, as well as in the pelvic bones, ribs, skull, and the vertebrae in the spinal column. It is very porous and contains red bone marrow, where blood cells are made. It is weaker and easier to fracture than cortical bone, which makes up the shafts of long bones.

Cortical Bone: Superficial thin layer of compact bone.

Diaphysis: The shaft of a long bone. *Adj. diaphyseal*

Distal: Situated away from the point of attachment or origin or a central point e.g. distal femur is the portion of the femur close to the knee.

Endosteum: The layer of vascular connective tissue lining the medullary cavities of bone. *Adj*. endosteal

Femur: The proximal bone of the hind or lower limb that is the longest and largest bone in the human body, extends from the hip to the knee. Also called thigh bone. *Adj*. femoral

Humerus: The longest bone of the upper arm or forelimb extending from the shoulder to the elbow. *Adj*. humeral

Intramedullar: Situated or occurring within a medulla.

Medulla: The inner or deep part of an organ or structure.

Monocortical: Connected to a single cortical plate.

Osteoblast: A bone-forming cell.

Osteoclast: Any of the large multinucleate cells closely associated with areas of bone resorption.

Osteocyte: A cell that is characteristic of adult bone.

Osteogenesis: Development and formation of bone. *Adj*. osteogenic

Pedicle: The basal part of each side of the neural arch of a vertebra connecting the laminae with the centrum.

Percutaneous: Effected or performed through the skin.

Periosteum: The membrane of connective tissue that closely invests all bones except at the articular surfaces. *Adj*. periosteal

Proximal: Situated next to or near the point of attachment or origin or a central point e.g. proximal femur is the portion of the femur close to the hip.

Radius: The bone on the thumb side of the human forearm.

Trauma: An injury (as a wound) to living tissue caused by an extrinsic agent.

Vertebra: Any of the bony or cartilaginous segments that make up the spinal column and that have a short more or less cylindrical body whose ends articulate by pads of elastic or cartilaginous tissue with those of adjacent vertebrae and a bony arch that encloses the spinal cord. *Adj*. vertebral

Woven Bone: Bony tissue characteristic of the embryonic skeleton in which the collagen fibers of the matrix are arranged irregularly in the form of interlacing networks. Also called nonlamellar bone, reticulated bone.

(Merriam-Webster Medical Dictionary, 2015)

APPENDIX B

TECHNICAL DRAWINGS OF THE FINAL DESIGN

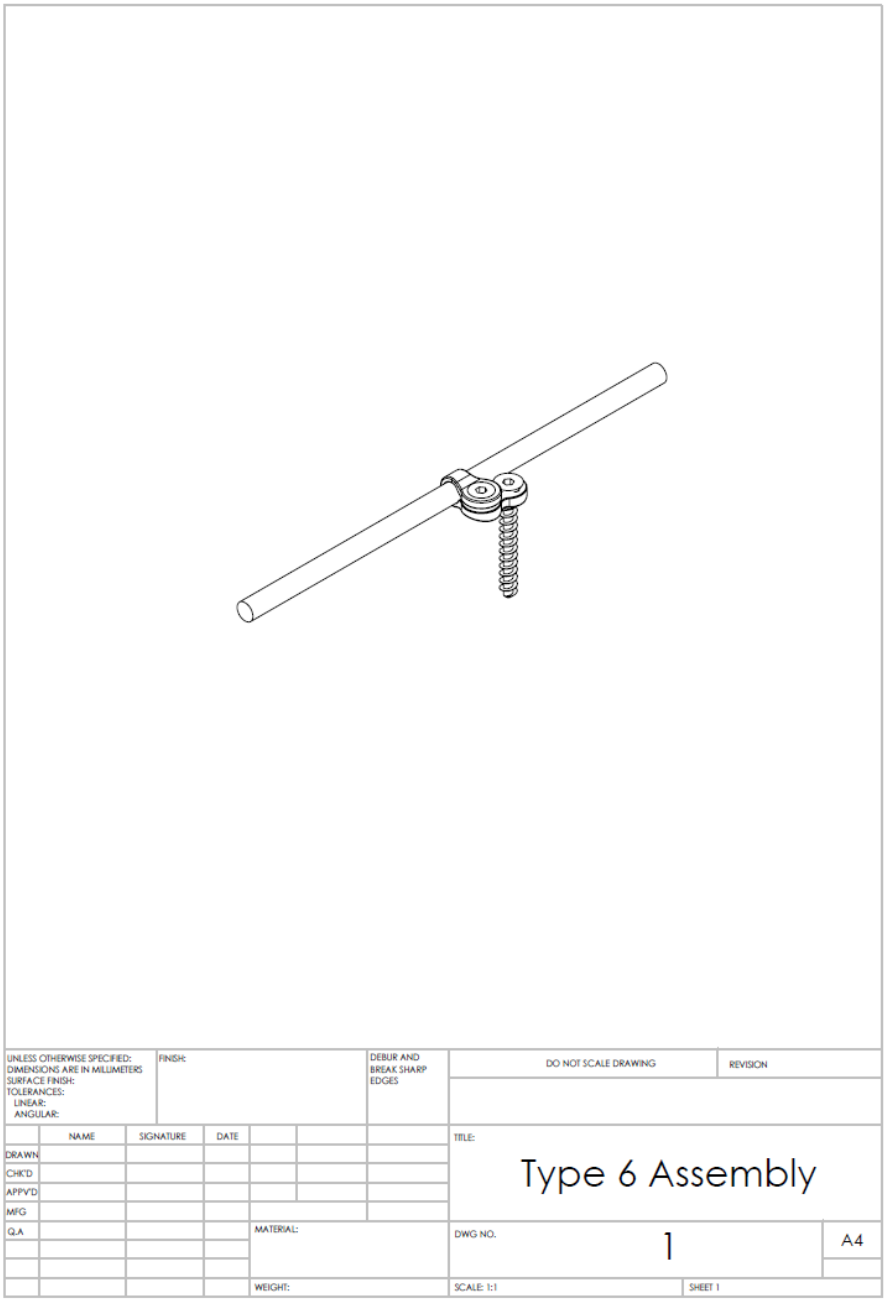

Figure 81: Assembly

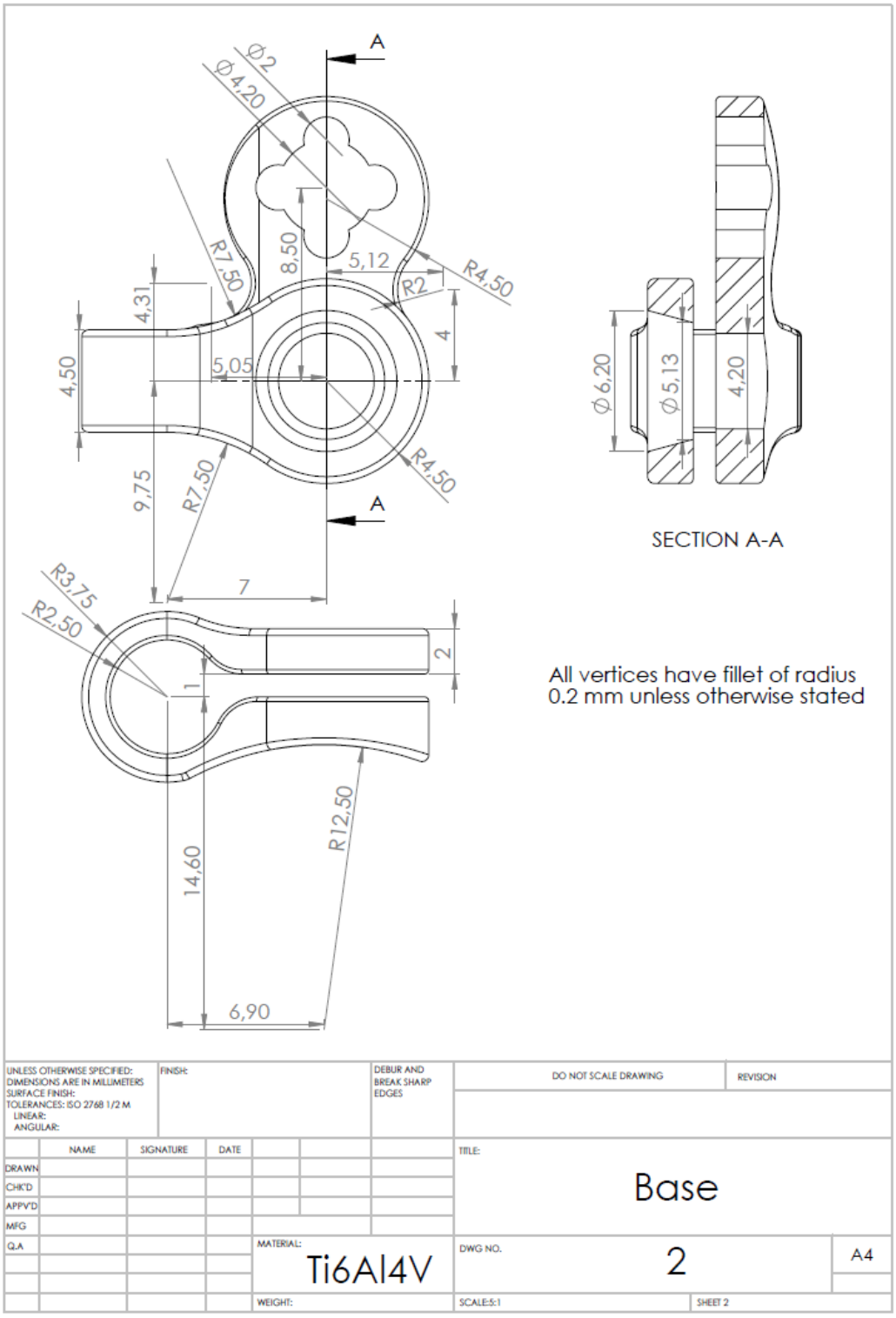

Figure 82: Technical Drawing of Base

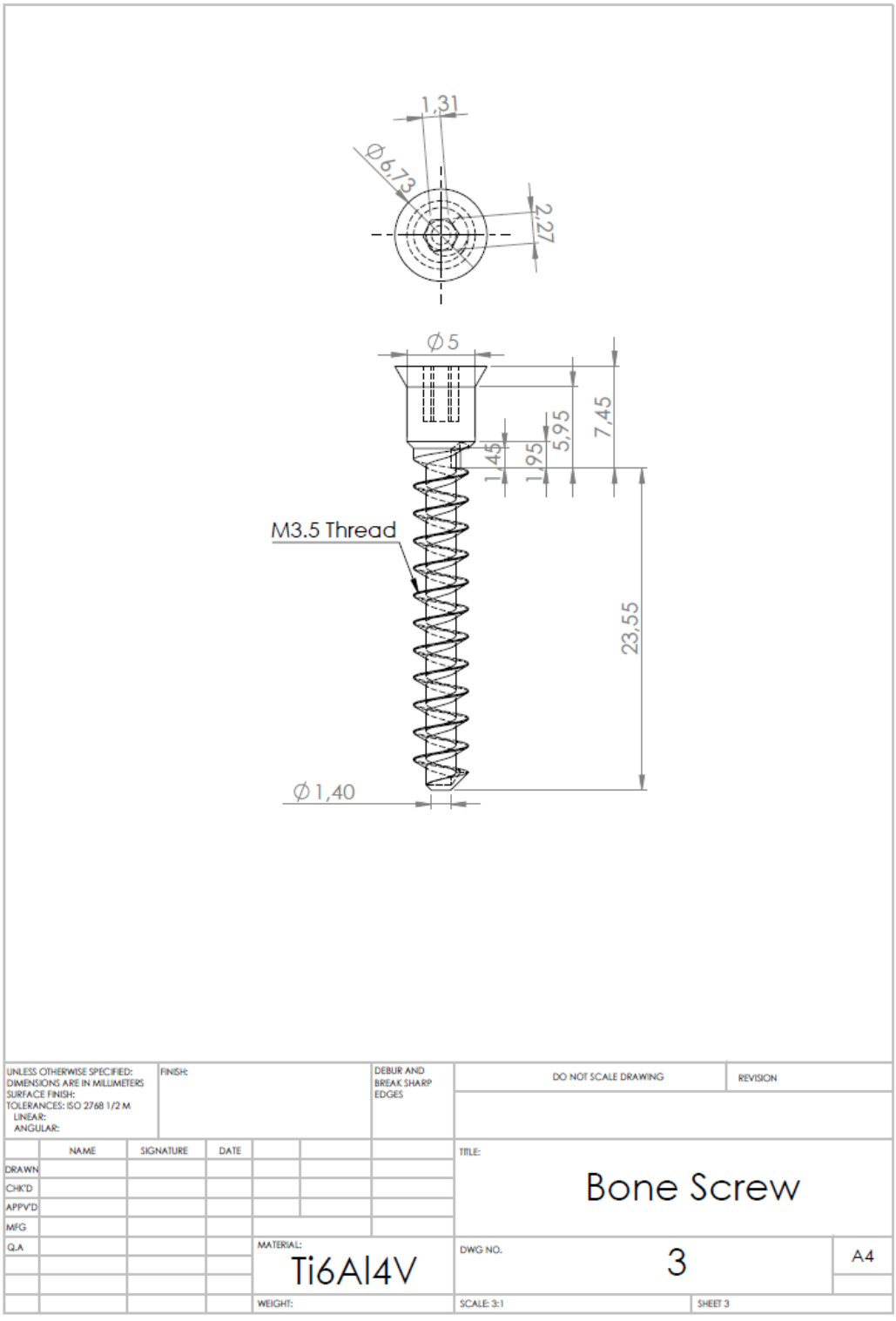

Figure 83: Technical Drawing of Bone Screw

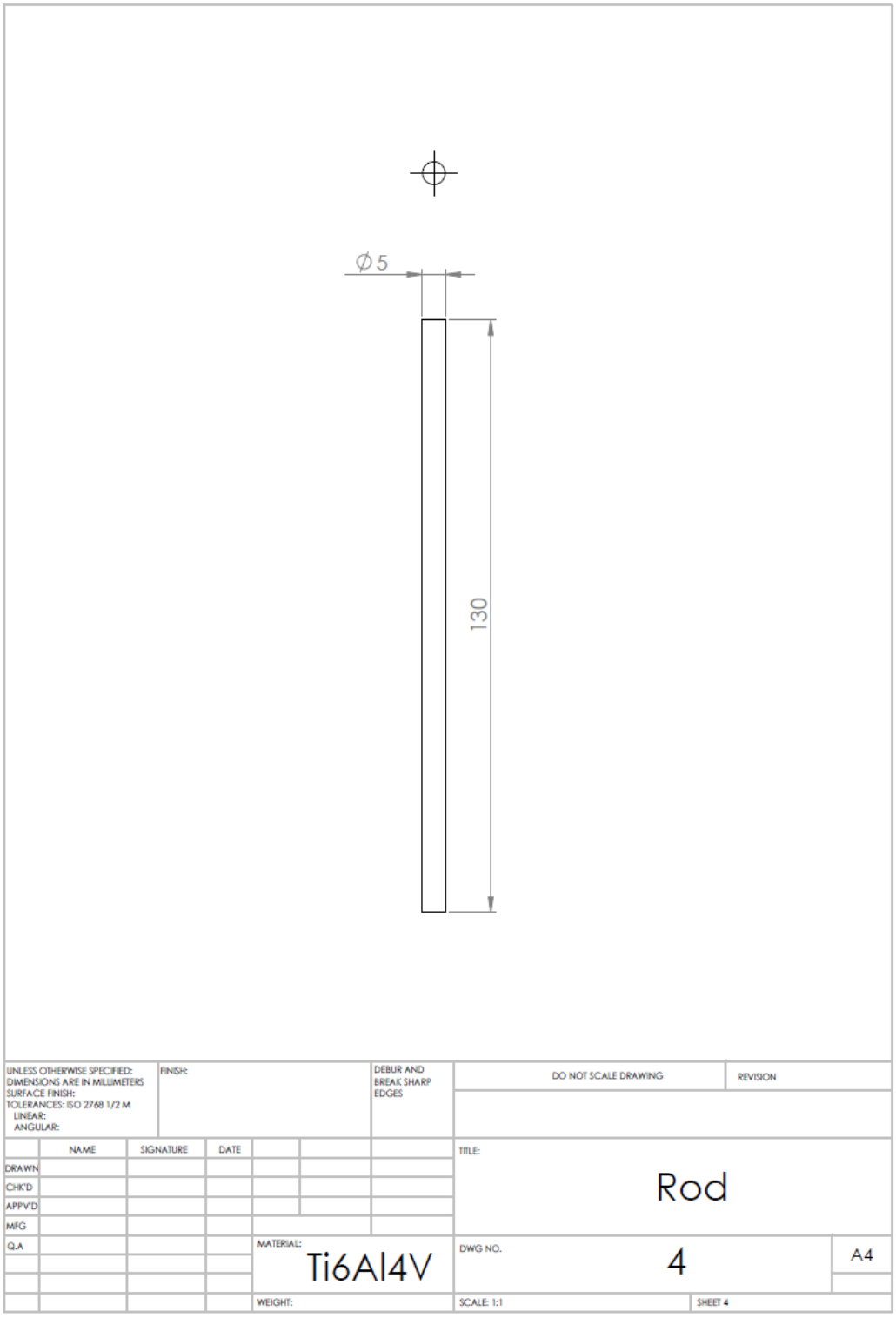

Figure 84: Technical Drawing of Rod

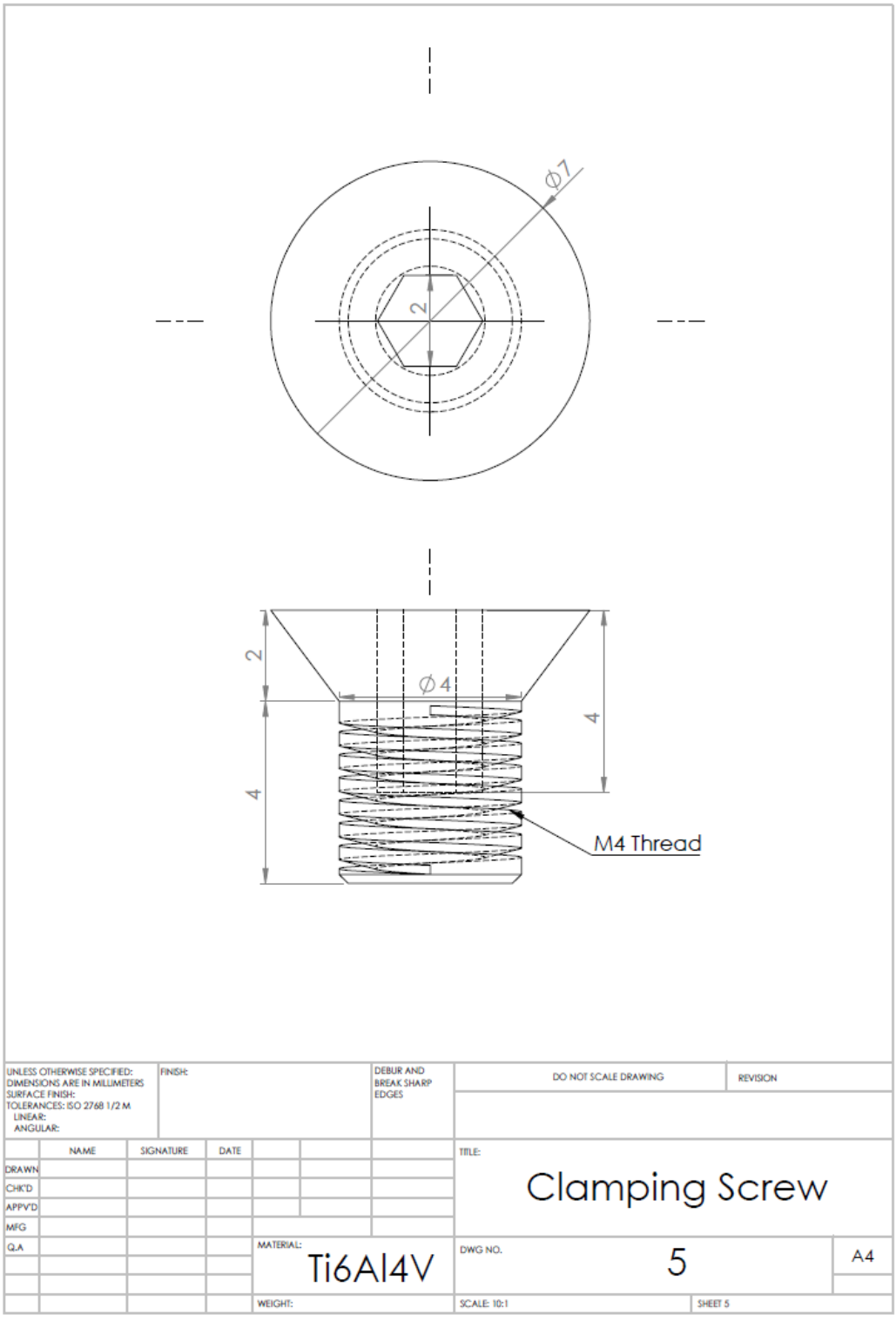

Figure 85: Technical Drawing of Clamping Screw